Revised stratigraphic framework for the lower Anti-Atlas Supergroup based on U–Pb geochronology of magmatic and detrital zircons (Zenaga and Bou Azzer-El Graara inliers, Anti-Atlas Belt, Morocco)

Abdelhak Ait Lahna, Nasrrddine Youbi, Colombo Celso Gaeta Tassinari, Miguel Angelo Stipp Basei, Richard Ernst, Latifa Chaib, Abdelhafed Barzouk, João Mata, Andreas Gärtner, Hassan Admou, et al.

Journal Pre-proof

Revised stratigraphic framework for the lower Anti-Atlas supergroup based on U–Pb geochronology of magmatic and detrital zircons (Zenaga and Bou Azzer-El Graara inliers, Anti-Atlas Belt, Morocco)

Abdelhak Ait Lahna, Nasrrddine Youbi, Colombo Celso Gaeta Tassinari, Miguel Angelo Stipp Basei, Richard E. Ernst, Latifa Chaib, Abdelhafed Barzouk, João Mata, Andreas Gärtner, Hassan Admou, Moulay Ahmed Boumehdi, Ulf Söderlund, Mohamed Khalil Bensalah, Jean-Louis Bodinier, Lhou Maacha, Andrey Bekker

PII: S1464-343X(20)30197-7

DOI: https://doi.org/10.1016/j.jafrearsci.2020.103946

Reference: AES 103946

To appear in: *Journal of African Earth Sciences*

Received Date: 11 December 2019

Revised Date: 28 June 2020

Accepted Date: 30 June 2020

Please cite this article as: Lahna, A.A., Youbi, N., Gaeta Tassinari, C.C., Stipp Basei, M.A., Ernst, R.E., Chaib, L., Barzouk, A., Mata, Joã., Gärtner, A., Admou, H., Boumehdi, M.A., Söderlund, U., Bensalah, M.K., Bodinier, J.-L., Maacha, L., Bekker, A., Revised stratigraphic framework for the lower Anti-Atlas supergroup based on U–Pb geochronology of magmatic and detrital zircons (Zenaga and Bou Azzer-El Graara inliers, Anti-Atlas Belt, Morocco), *Journal of African Earth Sciences* (2020), doi: https://doi.org/10.1016/j.jafrearsci.2020.103946.

Revised stratigraphic framework for the lower Anti-Atlas Supergroup based on U-Pb geochronology of magmatic and detrital zircons (Zenaga and Bou Azzer-El Graara inliers, Anti-Atlas Belt, Morocco)

Abdelhak Ait Lahna[1]*, Nasrrddine Youbi[1,2], Colombo Celso Gaeta Tassinari[3], Miguel Angelo Stipp Basei[4], Richard E. Ernst[5,6], Latifa Chaib[1], Abdelhafed Barzouk[1], João Mata[2], Andreas Gärtner[7], Hassan Admou[1], Moulay Ahmed Boumehdi[1,2], Ulf Söderlund[8,9], Mohamed Khalil Bensalah[1,2], Jean-Louis Bodinier[10,11], Lhou Maacha[12], Andrey Bekker[13,14]

[1]Department of Geology, Faculty of Sciences-Semlalia, Cadi Ayyad University, Prince Moulay Abdellah Boulevard, P.O. Box 2390, Marrakech, Morocco: aitlahna.abdelhak@gmail.com; youbi@uca.ac.ma; latifa_918@yahoo.fr; barzoukabdelhafed@gmail.com; admou@uca.ac.ma; boumehdi@uca.ac.ma; bensalah@uca.ac.ma.

[2]Instituto Dom Luiz, Faculdade de Ciências, Universidade de Lisboa, 1749-016 Lisboa, Portugal: jmata@fc.ul.pt

[3]Centro de Pesquisas Geocronológicas (CPGeo), Instituto de Geociências (IG), Universidade de São Paulo-USP, Caixa Postal 11348, CEP 05422-970, São Paulo, SP, Brazil: ccgtassi@usp.br.

[4]Instituto de Geociências (IG), Departamento de Mineralogia e Geotectônica (GMG), Universidade de São Paulo-USP, Rua do Lago, 562 Cidade Universitária 05508-080 São Paulo, SP, Brazil: baseimas@usp.br

[5]Department of Earth Sciences, Carleton University, 1125 Colonel By Drive, Ottawa, Canada K1S 5B6: Richard.Ernst@carleton.ca

[6]Faculty of Geology and Geography, Tomsk State University, 36 Lenin Ave, Tomsk 634050, Russia: Richard.Ernst@ernstgeosciences.com

[7]Senckenberg Naturhistorische Sammlungen Dresden, Museum für Mineralogie und Geologie, Sektion Geochronologie, GeoPlasma Lab, Königsbrücker Landstraße 159, 01109 Dresden, Germany: Andreas.Gaertner@senckenberg.de

[8]Department of Geology, Lund University, Sölvegatan 12, SE-223 62 Lund, Sweden: Ulf.Soderlund@geol.lu.se

[9]The Swedish Museum of Natural History, SE-114 18 Stockholm, Sweden

[10]Mohammed VI Polytechnic University, Geology and Sustainable Mining Department, Hay Moulay Rachid, Ben Guerir, 43150, Morocco: JeanLouis.Bodinier@um6p.ma

[11]Géosciences Montpellier, Université de Montpellier 2, CNRS, Cc 60, Place Eugène Bataillon, 34095 Montpellier Cedex 05, France: bodin@gm.univ-montp2.fr

[12]Managem Group, Twin Center, Tour A, Angle Boulevards Zerktouni & Al Massira Al Khadra, P.O. Box 5199, Casablanca, Morocco: L.maacha@managemgroup.com

[13] Department of Earth and Planetary Sciences, University of California, Riverside, CA 92521, USA: andrey.bekker@ucr.edu

[14] Department of Geology, University of Johannesburg, Auckland Park 2006, South Africa

*Corresponding author: aitlahna.abdelhak@gmail.com

Revised for Journal of African Earth Sciences

Running Title “Revised stratigraphic framework for the lower Anti-Atlas Supergroup” by Ait Lahna et al., 2020.

23959 words

18 figures & 2 tables

10 supplementary data tables and figures

Abstract

U-Pb geochronology of magmatic and detrital zircons (Zenaga and Bou Azzer-El Graara inliers, Anti-Atlas Belt, Morocco) and a reassessment of the published constraints suggest a revised stratigraphic framework for the lower Anti-Atlas Supergroup. Five, major unconformity-bounded lithostratigraphic packages are here distinguished: the two lower units of Paleoproterozoic age are named the Tasserda-Taghatine Group (2030-1706 Ma) and the Oumoula (Mimount) Formation (ca. 1745-1650 Ma); the third unit of Paleoproterozoic to Neoproterozoic age (ca. 1650 to > 883 Ma) is the Tizi n'Taghatine Group; the fourth and fifth units of Neoproterozoic age are the ca. 883 Ma Tachdamt and the ca. 700 Ma Bleida formations. Implications of this revised stratigraphic framework include: 1) the Tasserda-Taghatine Group might be linked to the post-orogenic collapse after the Eburnean Orogeny; 2) the Tizi n'Taghatine Group might be ca. 1.1 Ga in age based on proposed correlation with the Taoudeni Basin succession in Mauritania; 3) the Bleida Formation likely reflects deposition in the foreland basin at the early stage of the Pan-African Orogeny; 4) the Oumoula (Mimount) Formation, Tizi n'Taghatine Group, and Tachdamt Formation potentially record extensional events within the Nuna/Columbia and Rodinia supercontinents; 5) the provenance of the lower Anti-Atlas Supergroup (based on our new detrital zircon dating) is mainly from the West African craton along with possible contributions from other cratons such as Amazonia and the Sahara Metacraton; 6) the flood basalt sequence of the Tachdamt Formation likely belongs to the ca. 885-883 Ma intraplate Iguerda-Taïfast Large Igneous Province (LIP) event defined by previously dated dykes in the Iguerda and Taïfast inliers; and 7) the 1650 Ma Zenaga LIP can be potentially linked with LIP magmatism in Baltica and Laurentia.

Key Words: Morocco; Anti-Atlas Belt; Proterozoic; lower Anti-Atlas Supergroup; U-Pb geochronology

Highlights

►The Taghdout mafic sill of the Ifzwane Suite yielded an age of 1676 ± 37 Ma

77 ►The maximum depositional age of the lower Anti-Atlas Supergroup ranges from 2049 Ma
78 (bottom) to 700 Ma (top) and the provenance is mainly from the WAC
79 ►A new 5-part lithostratigraphic framework for the Proterozoic lower Anti-Atlas Supergroup of
80 the Anti-Atlas Belt is proposed
81 ►The 1650-1640 Ma Zenaga and 885-883 Ma Iguerda-Taïfast LIPs provide important stratigraphic
82 constraints
83 ► Correlation between the lower Anti-Atlas Supergroup and the Taoudeni Basin succession in
84 Mauritania
85

1. Introduction

Substantial advances in the understanding of the geological evolution of several major Precambrian accretionary orogens of North America and Baltica (Hoffman, 1988; Chacko et al., 2000; Corrigan et al., 2005, 2009; Pehrsson et al., 2013; Bogdanova et al., 2008; 2016) have been made in recent years. However, there is still a fundamental gap in the knowledge of Precambrian orogenic belts in Africa. Much of the uncertainty about the accretionary history of the Precambrian African orogens stems from the limited database of reliable radiometric ages on structurally important units, combined with a lack of detailed studies using modern kinematic analysis in these deformed regions as well as of cutting-edge research using sedimentology and sequence stratigraphy.

One of the crucial Neoproterozoic African orogens is exposed in the Anti-Atlas Belt of Morocco located in the northern part of the West African Craton (WAC, Fig. 1). Extensive outcrops of the Neoproterozoic Pan-African Belt and underlying Paleoproterozoic foreland (Michard et al., 2008; Gasquet et al., 2008; Soulaimani et al., 2018 and references therein) are well exposed and have been studied for a long time (e.g. Choubert, 1963). Traditionally, the Precambrian of the Anti-Atlas Belt has been divided into three broad lithosomes (e.g. Choubert, 1963): the P I (Archean to Paleoproterozoic), P II (early and middle Neoproterozoic), and P III (late Neoproterozoic) (Fig. 2). This lithostratigraphic subdivision has recently been challenged (Walsh et al., 2002; 2012; Thomas et al., 2002; 2004; Michard et al., 2008; Gasquet et al., 2008; Youbi et al., 2013). In the conventional interpretation, the oldest, Paleoproterozoic rocks (PI) of the Anti-Atlas Belt are subdivided into a series of complexes (e.g. the Zenaga and Kerdous complexes in the Siroua and Kerdous basement inliers, respectively). The rocks of the P II lithosome deposited on this basement have collectively been called the *Anti-Atlas Supergroup*, within which there are four groups of volcano-sedimentary units (e.g. Lkest-Taghdout, Bou Azzer, Iriri, and Saghro groups) and they are conventionally inferred to be Neoproterozoic in age. Various intrusive suites are also recognized (e.g. Ifzwane and Toudma Suites). These volcano-sedimentary units have been related to the earliest passive margin, oceanic, and island-arc settings with inferred ages between ca. 800 and 660-640

Ma. The earliest Pan-African deformation at 660-640 Ma resulted from closure of the ocean basin, SW-directed thrusting, and accretion of the island-arc remnants.

Recent studies provided new structural, geochronological, and geochemical data, however many critical questions about the accretionary history of the Anti-Atlas Belt are still debated (e.g. Soulaimani et al., 2018 and references therein). Such questions include the age of obducted oceanic crust segments (Siroua and Bou Azzer El Graara ophiolites), relationship between arc terranes to the north with ophiolites and an associated blueschist facies belt to the south, the age and nature of the basement in these terranes, the degree of interaction of Neoproterozoic magmas with the basement, and the timing of accretion of these terranes to the West African Craton. Finally, discrimination between the post-Eburnean sedimentary succession, recently dated to be late Paleoproterozoic in age (Ikenne et al., 2017; Soulaimani et al., 2019; Youbi et al., 2019; this work), and the Neoproterozoic sedimentary sequence (Leblanc and Moussine-Pouchkine, 1994; Bouougri and Saquaque, 2004; Blein et al., 2014a,b; Soulaimani et al., 2018; Youbi et al., 2018) remains uncertain.

The lower Anti-Atlas Supergroup of the Anti-Atlas Belt (Lkest-Taghdout Group *sensu* Thomas et al., 2004; Figs. 1D, 2 and 3) is one of the most important Proterozoic lithostratigraphic units on the WAC, yet with poor age constraints. It consists essentially of basalts, quartzites, and stromatolitic/oolitic carbonates, intruded by dolerite dyke swarms and sill complexes (Ifzwane and Toudma Suites). The lower Anti-Atlas Supergroup was previously thought to be ca. 1000-800 Ma in age on the basis of (1) stromatolites characteristic for the Neoproterozoic carbonate successions (Choubert, 1962), and (2) the Rb/Sr age of the contact-metamorphosed host rocks associated with mafic dykes (789 ± 10 Ma) in the Tachdamt Subinlier of the Bou Azzer El Graara Inlier (Clauer, 1976; Cahen et al., 1984).

The present study is based on field observations and new U-Pb ages for igneous zircons from dolerite sill intruding carbonates from the lower Anti-Atlas Supergroup in the Zenaga Inlier and detrital zircon grains from four samples from the lower, middle, and upper parts of the lower Anti-

Atlas Supergroup in the Zenaga and Bou Azzer El Graara inliers. We propose a new lithostratigraphy for the Proterorozoic lower Anti-Atlas Supergroup of the Anti-Atlas Belt based on a discussion of our data in combination with the previously published data (Abati et al., 2010; Walsh et al., 2012; Letsch, 2018; Bouougri et al., 2020) and constrain the provenance for the five, major unconformity-bounded packages of the supergroup.

2. Geological background

2.1. The West African Craton

The West African Craton (WAC, Fig. 1) extends across northwestern Africa, and consists of two Archean basement shields, the Reguibat Shield to the north and the Leo-Man Shield to the south. The Archean nuclei (3.5-2.7 Ga in age) of these shields are juxtaposed against an array of Paleoproterozoic domains (2.35-2.00 Ga in age) made up of greenstone belts and regions of extensive tonalite-trondhjemite-granodiorite (TTG) plutons, which are overlain by Meso- to Neoproterozoic and younger sedimentary basins. Smaller basement inliers are composed of Paleoproterozoic rocks: the Kayes and Kedougou-Kenieba inliers to the west, and those of the Anti-Atlas Belt to the north (Ennih and Liégeois, 2008; Abati et al., 2012). The WAC remained largely stable since 2 Ga (Schofield et al., 2006; Jessell et al., 2016). The basement of the WAC has evolved through several major orogenic cycles: the Paleoarchean Leonian cycle (several episodes between 3.40 and 3.10 Ga with uncertain chronology, related to continental accretion; e.g. Thiéblemont et al., 2004; Koffi et al., 2020), the Liberian cycle (2.85-2.70 Ga; Key et al., 2008; Koffi et al., 2020), the Paleoproterozoic Eburnean and Birimian cycles (2.15-2.07 Ga and 2.27-1.96 Ga, respectively; Abouchami et al., 1990; Boher et al., 1992; Egal et al., 2002; Schofield et al., 2006; Baratoux et al., 2011; Grenholm et al., 2019; McFarlane et al., 2019) and the late Neoproterozoic Pan-African orogenic event (885-550 Ma; Thomas et al., 2002; 2004; Gasquet et al., 2005; 2008; Walsh et al., 2012; Youbi et al., 2018). The WAC hosts four major intracratonic basins: the large central Taoudeni Basin and the smaller Tindouf and Volta basins, to the north and southwest, respectively, and the Gourma aulacogen to the east (Moussine-Pouchkine and Bertrand-

Sarfati, 1978; Villeneuve, 2005; Deynoux et al., 2006; Lottaroli et al., 2009). These basins comprise mostly Mesoproterozoic-Neoproterozoic to Devonian-Carboniferous sediments. The WAC is surrounded by Pan-African belts, including the Trans-Saharan and Anti-Atlas belts (Ennih and Liégeois, 2008; Liégeois et al., 2013; Toummite et al., 2013; Brahimi et al., 2018).

Early compilations of WAC lithostratigraphy suggested an absence of Mesoproterozoic events or rocks, indicating a tectonically quiescent period between 1.7 and 1.0 Ga (e.g. Ennih and Liégeois, 2008 and references therein). The lack of detrital zircons of that age in the pre-Cryogenian strata is considered characteristic of sediments sourced from the WAC (e.g. Abati et al., 2010; Gärtner et al., 2013; 2017; 2018). However, recent studies in the northern WAC (El Bahat et al., 2013; Kouyaté et al., 2013; Söderlund et al., 2013; Youbi et al., 2013; Ikenne et al., 2017) demonstrated important intraplate magmatic events based on dating of mafic dykes by the U-Pb method on baddeleyite and zircon. Six distinct events are distinguished throughout the inliers: ca. 2040 Ma Tagragra of Tata, 1750 Ma Tagragra of Akka, 1650 Ma Zenaga, 1416–1380 Ma Bas Drâa, and 885-883 Ma Iguerda-Taïfast events, and 612-600 Ma pulse of the Central Iapetus Magmatic Province (CIMP; Walsh et al., 2002; Gasquet et al., 2004; El Bahat et al., 2013; Kouyaté et al., 2013; Söderlund et al., 2013; Youbi et al., 2013; El Bahat et al., 2017; Ikenne et al., 2017; Bouougri et al., 2020 ; Youbi et al., 2020). Re-Os geochronology of the sedimentary succession of the Atar Group in the Taoudeni Basin of Mauritania indicated depositional ages ranging from 1109 ± 22 to 1105 ± 37 Ma (Rooney et al., 2010). These Mesoproterozoic ages are confirmed by the study of microfossils (Beghin et al., 2017) and chemostratigraphy (Kah et al., 2012). Recently, Baratoux et al. (2019) identified four new magmatic events 1.79-1.76, 1.58, 1.53, and 0.91-0.87 Ga in the southern WAC that add additional evidence for Mesoproterozoic mafic intrusive activity on this craton. Ar-Ar ages of ca. 1.24 Ga for the 1575 and 1520 Ma dyke swarms are considered to record a thermal overprint (Tapsoba et al., 2018).

2.2. The Anti-Atlas Belt

The ENE-WSW trending Anti-Atlas Belt (800 km long and 200 km wide) of Morocco is the most important segment of the Neoproterozoic Pan-African Orogen in the northern part of the WAC (Fig. 1D). The Precambrian basement crops out in several erosional inliers ("boutonnières" in French), containing Late Ediacaran and younger units (Bas Drâa, Ifni, Kerdous, Tagragra of Akka, Tagragra of Tata, Igherm, Siroua, Zenaga, Bou Azzer, Saghro, and Ougnat; Fig. 1D) and distributed along two major fault systems (South Atlas Fault, SAF and Anti-Atlas Major Fault, AAMF; Fig. 1D).

The Anti-Atlas Belt contains the Paleoproterozoic basement (affected by the Eburnean Orogeny) unconformably overlain by the lower Anti-Atlas Supergroup (= Lkest-Taghdout Group *sensu* Thomas et al., 2004; = Tizi n'Taghatine Group *sensu* Bouougri and Saquaque, 2004), which is in turn unconformably overlain by the Ouarzazate Supergroup related to the Pan-African Orogeny. The two major periods of tectonothermal activity, associated with crustal accretion, have been recognized during the Proterozoic (Fig. 2) in the Anti-Atlas Belt and are described below.

(i)The Paleoproterozoic Eburnean Orogeny (2.20-2.07 Ga; Abouchami et al., 1990; Boher et al., 1992; Egal et al., 2002; Schofield et al., 2006; Baratoux et al., 2011; McFarlane et al., 2019*)*. The Paleoproterozoic basement rocks are found exclusively SW of the AAMF (Choubert, 1963), but they may also constitute the basement to the Pan-African Orogen to the NE (Ennih and Liégeois, 2001; Liégeois et al., 2006; Gasquet et al., 2008). The Paleoproterozoic basement is composed of metasedimentary rocks, granites, paragneisses, and migmatites, with U-Pb zircon ages ranging from 2200 to 2030 Ma (e.g. Aït Malek et al., 1998; Walsh et al., 2002; Thomas et al., 2002; Gasquet et al., 2004, 2008; O'Connor, 2010).

(ii) The Neoproterozoic Pan-African Orogeny (885–550 Ma). The Neoproterozoic sequences of the Anti-Atlas Belt are composed of units that were involved in the Pan-African Orogeny and the unconformably overlying post-collisional volcano-sedimentary rocks of the Ouarzazate Supergroup, which are a part of the Central Iapetus Magmatic Province (CIMP; Doblas et al., 2002; Maloof et al., 2005; Gasquet et al., 2005, 2008; Ernst and Youbi, 2017; Tuduri et al., 2018; Youbi et al., 2020). The Neoproterozoic rocks underlying the Ouarzazate Supergroup are subdivided into the

lower units (Lkest-Taghdout, Bou-Azzer, and Iriri groups), affected by all Pan-African orogenic events, and the upper units (Saghro and Bou Salda groups), only affected by the latest stage of the Pan-African Orogeny (e.g. Walsh et al., 2002; Thomas et al., 2004; Gasquet et al., 2005; 2008; Alvaro et al., 2014).

The lower Anti-Atlas Supergroup consists essentially of basalt, quartzite, and stromatolitic/oolitic carbonate, cut by undated dolerite dyke swarms and sill complexes (Thomas et al., 2004; Bouougri and Saquaque, 2004). It marks the onset of a period of rifting at the northern portion of the WAC during the late Neoproterozoic. The rifting culminated with the opening of an oceanic basin on the northern edge of the WAC. The relics of the oceanic crust (Bou-Azzer Group) are preserved in the Bou-Azzer and Siroua inliers as highly sheared allochthonous ophiolite complexes (El Hadi et al., 2010; Blein et al., 2014a and references therein). The ophiolitic assemblage is mainly made up of ultramafic rocks (serpentinites with few chromite pods), but also includes mafic meta-cumulates, meta-basaltic sheeted dykes, and, to a smaller extent, pillow lavas (Leblanc, 1975, 1981; Admou and Juteau, 1998). Their geochemical signatures point to emplacement in a supra-subduction zone (Bodinier et al., 1984; Naidoo et al., 1991; Ahmed et al., 2005; Hodel et al., 2017; Triantafyllou et al., 2019; 2020). Dating of plagiogranite intrusions in the Siroua Inlier indicated formation of an oceanic crust at ca. 760 Ma (U-Pb zircon age; Samson et al., 2004). Given the absence of reliable radiometric data on the age of the lower Anti-Atlas Supergroup, ca. 760 Ma was considered as the minimum age of its formation. The rifting might be associated with the late Neoproterozoic extension within the supercontinent Rodinia (Gasquet et al., 2008). Following the opening of the ocean basin, a subduction phase was initiated with island-arc development (the Iriri Group in the Siroua Inlier; Thomas et al., 2002; Triantafyllou, 2015; 2016). The cores and overgrowths of zircon grains from the Iriri Group migmatite yielded two U–Pb SHRIMP ages at 743 ± 14 and 663 ± 13 Ma, respectively (Thomas et al., 2002). The older age obtained from the cores is interpreted as the age of crystallization and emplacement of the migmatite protolith in an island–arc setting, whereas the younger age is thought to represent the timing of ophiolite obduction and arc accretion to the

241 northern edge of the WAC in association with the regional metamorphism and the main orogenic
242 event in the Anti-Atlas Belt (Thomas et al., 2002).
243 The development of the Anti-Atlas Belt oceanic arc complexes occurred during three magmatic
244 flare-ups at ca. 750, 700, and 650 Ma that were interspersed with an early major tectonic episode
245 between 730-700 Ma (Triantafyllou et al., 2018; 2020). A garnet Sm-Nd date of 647.2 ± 1.7 Ma
246 was recently obtained for the Tasriwine ophiolite complex in the Siroua Inlier (Inglis et al., 2016).
247 This age is more than 15 million years younger than the previous age estimate by Thomas et al.
248 (2002). North of the AAMF in the eastern Anti-Atlas Belt (Figs. 1D and 2), the oldest rocks are
249 thick deposits of basalt and turbidite of the Saghro Group, interpreted as either a distal-slope
250 equivalent of the upper part of the lower Anti-Atlas Supergroup, deposited between the WAC to the
251 south and an island arc (Saquaque et al., 1989; Thomas et al., 2002), or slivers of the stretched
252 Eburnean crust (Hindermeyer, 1953; Ouguir et al., 1996; Fekkak et al., 2001; 2002; Massironi et al.,
253 2007; Schiavo et al., 2007; Michard et al., 2017).
254 Preliminary detrital zircon data reported by Liégeois et al. (2006) and summarized in Gasquet et al.
255 (2008) suggest that the sediments of the Saghro Group in the Kelaa Mgouna section were derived
256 from sources ranging in age from about 880 to 615 Ma. The later post-collisional, extensional stage
257 (605–542 Ma) is characterized by molasse deposition and magmatism of the Ouarzazate
258 Supergroup, which was followed by the foreland development in the Saharan cratonic basin to the
259 south (Taroudant and Tata groups; e.g. Doblas et al., 2002; Maloof et al., 2005; Gasquet et al.,
260 2005, 2008; Hefferan et al., 2014; Karaoui et al., 2014; 2015; Tuduri et al., 2018; Geyer and
261 Landing, 2006; 2020; Youbi et al., 2020).
262
263 **2.3. The lower Anti-Atlas Supergroup**
264 Since our study is focused on the lower Anti-Atlas Supergroup, we will give here an updated review
265 of its lithology, stratigraphy, and nomenclature. The lower Anti-Atlas Supergroup, known in the
266 Anti-Atlas literature as the Taghdout (Lkest/Tizi n'Taghatine) Group, contains a sedimentary

succession deposited along the northern margin of the WAC (e.g. Thomas et al., 2002, 2004; Bouougri and Saquaque, 2004; Alvaro et al., 2014). The lower part of the lower Anti-Atlas Supergroup shows a progressive change of sedimentary facies from SW to NE representing a broad proximal to distal trend: conglomerates, sandstones, and quartz sandstones predominate in the Ifni and Kerdous inliers, while quartz sandstones, carbonates, shales, turbidites, and basaltic lava flows (the so called "Série des Calcaires et Quartzites"; see Choubert, 1962) developed in the Igherm, Siroua, Zenaga, and Bou Azzer El Graara inliers (Bouougri and Saquaque, 2004; Thomas et al., 2004; Alvaro et al., 2014). The scarcity of structural studies combined with modern sedimentology and sequence stratigraphy to test correlations between the groups in different inliers has led to a proliferation of synonymous names in the lithostratigraphic terminology: e.g. the Jbel Lkest Group in the Kerdous Inlier (Hassenforder, 1987; O'Connor, 2010), the Bleida-Tachdamt or Bleida Group in the Bou Azzer El Graara Inlier (Leblanc and Moussine-Pouchkine, 1994; Blein et al., 2014a), and the Taghdout Group (= Tizi n'Taghatine) in the Zenaga Inlier (Thomas et al., 2002, 2004; Bouougri and Saquaque, 2004). Correlation between these groups (recently combined into the Lkest-Taghdout Group, equivalent to the lower Anti-Atlas Supergroup; Gasquet et al., 2008; Álvaro et al., 2014) is both lithostratigraphic and structural. The only lithostratigraphic correlation linking the Siroua-Zenaga and Bou Azzer El Graara inliers was proposed by Bouougri and Saquaque (2004) who considered the section of the Tizi n'Taghatine mountain pass as a stratotype for the group named after this locality. Although their lithostratigraphy requires revision, we will refer to it in this work. Two reasons motivated this choice: (1) the dated samples of this study are from the same area that Bouougri and Saquaque (2004) focused on, and (2) the Siroua-Zenaga and Bou Azzer El Graara inliers are the only areas where modern sedimentology and sequence stratigraphy were applied (Fig. 1D). However, we will use the name of the lower Anti-Atlas Supergroup (an equivalent of the Lkest-Taghdout Group) because, although the latter group is widely known in the literature (Gasquet et al., 2008; Álvaro et al., 2014), it combines genetically unrelated sequences deposited in superimposed sedimentary basins and in different tectonic settings with long-lasted

hiatuses along unconformities. Five, major unconformity-bounded lithostratigraphic packages are further here distinguished: the lower Tasserda-Taghatine Group, the second Oumoula (Mimount) Formation, the third Tizi n'Taghatine Group, the fourth Tachdamt Formation, and the uppermost Bleida Formation.

For a long time, until 2013, available data on the lower Anti-Atlas Supergroup suggested that the continental passive margin developed during the Tonian between about 1000 Ma (based on stromatolite morphology pointing to a Neoproterozoic age; Choubert, 1963) and ca. 787 Ma (Rb-Sr isochron age of contact metamorphism of the host rocks associated with mafic dykes at Tachdamt; Clauer, 1976; Cahen et al., 1984). However, these age constraints are still debated (Gasquet et al., 2008; Alvaro et al., 2014; Ikenne et al., 2017; Soulaimani et al., 2018; 2019; Youbi et al., 2019). There are too few reliable geochronologic age constraints to tightly constrain the age of the lower Anti-Atlas Supergroup. It unconformably overlies the Eburnean basement, including the post-tectonic 2032 ± 5 Ma Azguemerzi granodiorite of the Zenaga Inlier, and in turn is unconformably overlain by the subhorizontal volcanic and sedimentary succession of the Late Ediacaran (ca. 606-541 Ma) Ouarzazate Supergroup (Figs. 6A, B). The lower Anti-Atlas Supergroup records a low-grade tectonometamorphic event related to the Pan-African Orogeny dated at 663 ± 13 Ma (Thomas et al., 2002) and 647.2 ± 1.7 Ma (Inglis et al., 2016) in the Siroua Inlier. Consequently, the depositional age of the lower Anti-Atlas Supergroup can be broadly bracketed between 2032 ± 5 Ma and 663 ± 13 / 647.2 ± 1.7 Ma.

The lower Anti-Atlas Supergroup sediments are intruded by abundant dolerite and gabbro dykes and sills, also found as dyke swarms and sill complexes in the Paleoproterozoic basement of the Zenaga (Fig. 4) and several other inliers (e.g. Igherm, Tagragra of Akka, Tagragra of Tata, Kerdous, and Bas Drâa). These rocks have been collectively called the Ifzwane Suite in the Zenaga and Siroua inliers (Thomas et al., 2004), and the Toudma Suite in the Kerdous Inlier (Thomas et al., 2004; O'Connor, 2010).

Letsch (2018) showed that the quartzites of the Mimount Formation (*sensu* Thomas et al., 2002) and the Oumoula Formation (*sensu* Bouougri and Saquaque, 2004), overlying the basal, carbonate-quartzite-metapelite units near the Town of Taghdout at the northern margin of the Zenaga Inlier (see Thomas et al., 2002), do not contain detrital zircons younger than ca. 1987 Ma (Benziane, 2007; Walsh et al., 2012) and ca. 1809 Ma (Abati et al., 2010), respectively. Neoproterozoic detrital zircon grains only appear in the overlying formations of the Saghro and Bou Salda groups of the Siroua Inlier (Abati et al., 2010). Detrital zircons from the Mimount and Oumoula formations display exclusively Paleoproterozoic ages, suggesting a ca. 1890 Ma maximum depositional age for the upper parts of the formations. In the Ifni Inlier, detrital zircons from quartzites of the upper part of the Lkest Group (the basal group of the lower Anti-Atlas Supergroup) exhibit two main clusters in distribution of SHRIMP $^{207}Pb/^{206}Pb$ ages, 2060-1890 and 1810-1640 Ma (Schulte et al., 2016). The maximum depositional age is given by a weighted average $^{207}Pb/^{206}Pb$ date of 1744 ± 26 Ma based on four youngest concordant grains.

3. Sampling and Analytical Procedures

3.1. Sampling

In order to investigate the maximum depositional age of the lower Anti-Atlas Supergroup of the Anti-Atlas Belt, we collected five samples from two key inliers within the Anti-Atlas Orogen (Zenaga and Bou Azzer El Graara) for geochronological investigation. The Taghdout sill that intruded to the lower part of the lower Anti-Atlas Supergroup in the Zenaga Inlier was sampled for geochemistry and zircon U-Pb geochronology: sample TA1 was collected at the centre of the sill and herein dated at 1676 ± 37 Ma and sample TA2 is from the margin of the sill. Four metasedimentary samples were collected for detrital zircon U-Pb geochronology: one sample from metasiltstones of the Tasserda Formation of the Zenaga Inlier and three samples from the Agoummy, Tachdamt, and Bleida formations of the lower Anti-Atlas Supergroup in the Bou Azzer

343 Inlier (Figs. 3, 4, and 5). Sample site locations, a brief description of the samples, and their ages are
344 provided in Table 1.
345
346 **3.2. Analytical procedures**
347 **3.2.1. Whole-rock geochemistry**
348 Elemental concentrations of whole rocks were obtained at "Service d'Analyse des Roches et des
349 Minéraux" at the Geochemical and Petrographical Research Center in Nancy (SARM laboratory-
350 CRPG-CNRS, Nancy, France). To avoid contamination, crushing and pulverizing were undertaken
351 using agate mills. Powders were treated with $LiBO_2$, dissolved with HNO_3, and analyzed and
352 calibrated with international geostandards (Basalt BE-N, Basalt BR, Dolerite WS-E, Microgabbro
353 PM-S). Major and trace elements were analyzed using inductively coupled plasma atomic emission
354 spectroscopy (ICP-AES) and Inductively Coupled Mass Spectrometry (ICP-MS), respectively. The
355 analytical procedures are described in detail at http://helium.crpg.cnrs-nancy.fr/SARM/.
356
357 **3.2.2. U-Pb Geochronology**
358 Zircon grains from all studied samples were separated from 3-5 kg of crushed rocks using
359 conventional heavy liquid and magnetic separation techniques (jaw crusher, disk grinder, Wilfley
360 table, Frantz isodynamic magnetic separator, and density separation using bromoform and
361 methylene iodide) at the Centro de Pesquisas Geocronológicas, Universidade de São Paulo (CPGeo-
362 USP), Brazil. About 20 to 100 zircon grains from each sample were mounted in epoxy resin,
363 polished to approximately half of mean grain thickness for further imaging with transmitted light
364 and cathodoluminescence to resolve internal grain texture. After coating with Au,
365 cathodoluminescence (CL) images of zircon grains were obtained using a Quanta 250 FEG
366 scanning electron microscope equipped with Mono CL3 + cathodoluminescence spectroscope
367 (Centaurus) at the Centro de Pesquisas Geocronológicas of the University of São Paulo (CPGeo-
368 USP), Brazil. The conditions used in CL analysis were as follows: 60 μA emission current, 15.0 kV

accelerating voltage, 7 μm beam diameter, 200 μs acquisition time, and a resolution of 1024 × 884 pixels.

3.2.2.1 Sensitive High Resolution Ion Microprobe (SHRIMP II) analysis

Igneous zircon grains from the dolerite sample TA 1 and detrital zircon grains from the quartzite samples BA21 and BA24 were analyzed by the U-Pb isotopic technique using a SHRIMP II at CPGeo-USP following the analytical procedures of Williams (1998). The crystals were mounted, together with the TEMORA-2 reference zircon (Black et al., 2004), in epoxy and polished to expose the interior of the grains. Correction for common Pb was made based on ^{204}Pb measured, and the typical error for the ^{206}Pb/^{238}U ratio was less than 2%; uranium abundance and U/Pb ratios were calibrated against the TEMORA-2 reference material, and the ages were calculated using Isoplot® version 3.0 software application (Ludwig, 2003). Errors are reported as 1σ deviations and ages have been calculated at the 95% confidence level.

3.2.2.2 Laser Ablation Inductively Coupled Plasma Mass Spectrometry (LA-ICP-MS) analysis

U-Pb analyses of detrital zircon grains from the samples TG-15-1 and ALBL29 were performed using a Neptune multicollector inductively coupled plasma mass spectrometer (MC-ICP–MS) and an Analyte G2 excimer laser ablation (LA) system at CPGeo-USP, Brazil. The U–Pb analysis was performed in the following order: two blanks, two 612 NIST standard glasses, three external standards, 13 unknown samples, two external standards, and two blanks. An interpolation of the four blank measurement sequences, using the bracketing method with two blanks before and two after the samples, was subtracted from all the seven measured masses (202, 204, 206, 207, 208, 232, and 238). The ^{235}U isotope was not measured, but calculated using the relative abundance ^{238}U/^{235}U=137.88. The ^{204}Hg interference on ^{204}Pb was corrected using ^{202}Hg and assuming ^{204}Hg/^{202}Hg = 4.350360. Using the partially corrected ^{207}Pb/^{206}Pb ratio as an estimate for the age and the equations of Stacey and Kramers (1975), the ^{206}Pb/^{204}Pb, ^{207}Pb/^{204}Pb, and ^{208}Pb/^{204}Pb relative abundances were calculated and corrected for common (non-radiogenic) Pb fraction.

Bracketing measurement of unknowns with NIST-612 standard glasses (two measurement sequences before and after) was used to convert the total Pb, Th, and U signals to ppm concentrations.

A final bracketing (with three measurements before and two after unknown) with the GJ-1 reference zircon (Jackson et al., 2004) was used to correct the effect of the instrumental fractionation on four ratios ($^{206}Pb/^{238}U$, $^{207}Pb/^{235}U$, $^{207}Pb/^{206}Pb$, and $^{208}Pb/^{232}Th$) before they were used to calculate the respective ages. Errors in all arithmetic operations were algebraically propagated. Least squares fitting was used for the best line fit and all the data are reported at the 1σ level calculated with Isoplot 3.70 (Ludwig, 2008). A U-Pb analysis is concordant when it overlaps with the Concordia within uncertainty. So, it seems to be appropriate to exclude results with a low level of concordance ($^{206}Pb/^{238}U$ age / $^{207}Pb/^{206}Pb$ age × 100), but very large errors that overlap with the Concordia from interpretation. Thus, an interpretation with respect to the obtained ages was done for all grains within the concordance interval of 90-110 % ($^{206}Pb/\ ^{238}U$ age / $^{207}Pb/\ ^{206}Pb$ age × 100) which is often used (e.g. Spencer et al., 2016). Discordant analyses were generally interpreted with caution. Analyses with discordance of more than 10% were discarded. For zircons younger than 1300 Ma, $^{206}Pb/^{238}U$ ages were preferred, while for older zircons the $^{207}Pb/^{206}Pb$ ages were used. The detrital zircon age distribution by probability density was performed using the AgeDisplay application (an EXCEL workbook to evaluate and display univariate geochronological data using binned frequency histograms and probability density distributions) (Sircombe, 2004).

4. Results

4.1. The Great Mafic Sill of the Ifzwane Suite at Taghdout Town

4.1.1. Field observations

The Taghdout sill was collected near Taghdout Town, ca. 9 km NW of Tazenakht City (Table 1 and Figs. 3 and 4), from a 227 m thick, well-preserved, massive sill belonging to the Ifzwane Suite (dolerite dyke swarm and sill complex of the Zenaga Inlier, of likely multiple ages as discussed in

section 2.1). The sill intruded into the lower part of the lower Anti-Atlas Supergroup (Fig. 6C), which mainly consists of carbonate and mixed siliciclastic-carbonate sequence of the Ifrane-n-Taghatine Formation (Bouougri and Saquaque, 2004). The sill can be traced in outcrops for more than one km in length and has thick chilled margins of marble grading away from the intrusion into carbonate host rock (Figs. 3, 4, and 6D). The following new samples were used in this study: TA1 (centre of the sill) and TA2 (border of the sill) from the Taghdout sill of the Zenaga Inlier.

4.1.2. Petrographic features

Fresh samples of the Taghdout sill are dark-grey, but due to widespread hematitic alteration the rock appears reddish. However, the original texture and primary igneous mineralogy are usually well preserved. The texture varies from a coarse-grained doleritic texture in the centre of the sill to a fine-grained, microlitic porphyric texture at the border of the sill (Fig. 7).

The primary igneous minerals consist of clinopyroxene (augite and locally pigeonite), very rare orthopyroxene, plagioclase, and oxides. Apatite and zircon are present as accessory minerals; amphibole and, more rarely, biotite are found around pyroxene crystals or as irregular patches in the groundmass. Although tholeiitic mafic rocks are generally characterized by low alkaline content (Na_2O+K_2O), granophyric quartz/K-feldspar mesostasis was observed in coarse-grained portions of the sill, consistent with the examples previously described in literature (e.g. Fodor, 2009; Block et al., 2015). The secondary mineral assemblage includes albite, chlorite, actinolite, epidote, titanite, calcite, and quartz, which is characteristic for the greenschist facies of metamorphism.

4.1.3. Geochronology: U-Pb dating of the Great Taghdout sill

The zircon grains from the sample TA1 range in length from 120 to 150 μm. Cathodoluminescence (CL) images (Figure S1 of supplementary data) show that most zircons are stubby sub-euhedral to euhedral, with a typical oscillatory zoning within a large uniform central zone, followed by much finer, poorly resolvable oscillatory zoned bands. Some grains lack any zoning (Figure S1 of supplementary data). We analyzed 18 spots on 13 zircon grains (Table S1 of supplementary data).

High Th/U ratios (between 1.18 and 3.38) support a magmatic origin for the zircons (Fig. 8) (cf. Möller et al., 2003; Hoskin and Schaltegger 2003; Linnemann et al., 2007). Most of the analyzed spots with high U and Th concentrations show evidence for significant Pb loss. On the Wetherill diagram, these thirteen analyses are aligned along a discordia that shows two intercepts with the concordia (Fig. 9A): an upper intercept with an age of 1639 ± 34 Ma and a lower intercept with an age of 688 ± 65 Ma. The age of 1639 ± 34 Ma is interpreted to reflect the time of magmatic emplacement of the sill, whereas the 688 ± 65 Ma age is thought to correspond to the time of a metamorphic and /or thermal overprint event. However, these intercept ages have a very high Mean Square Weighted Deviation (MSWD = 6.8), making this age poorly constrained. In contrast, analyses with low Th and U concentrations (Th <1000 ppm, spots 2.1, 7.1, and 13.1) produced nearly concordant $^{207}Pb/^{206}Pb$ ages. We therefore calculated the weighted mean average $^{207}Pb/^{206}Pb$ age for those spots characterized by low Th and U concentrations, obtaining a mean $^{207}Pb/^{206}Pb$ age of 1676 ± 37 Ma (n = 3, MSWD = 3.1; Fig. 9B).

4.1.4. Geochemical characteristics

The major and trace element composition of previously studied and new samples (TA1 and TA2) are listed in Table 2. On the total alkali versus silica diagram (Fig. 10A), the studied samples TA1 and TA2 and the ca. 1.6 Ga doleritic dykes and sills previously analyzed by Youbi et al. (2013) plot in the subalkaline basalt field. These additional dolerites are: DZ 36 (dated at 1640 ± 2 Ma and 1641 ± 3 Ma; Kouyaté et al., 2013) and DZ 40 (dated at 1656 ± 9 Ma; Kouyaté et al., 2013) of the Zenaga Inlier (close to Tazenakht City), and doleritic dyke (AMHA069 dated at 1654 ± 16 Ma; Kouyaté et al., 2013) from the Agadir Melloul Inlier. This subalkaline affinity is also evident from Nb/Y ratios that are below 0.67 (cf. Pearce and Cann, 1973; Winchester and Floyd, 1977). Addittionaly, their non-orogenic tholeiitic character is shown in the Ti vs. V diagram of Shervais (1982) (Fig. 10B) with the data plotting exclusively within the Continental Flood Basalt (CFB) and Mid-Ocean Ridge Basalt (MORB) fields (20 < V/Ti < 50). When plotted on a multi-element

variation diagram (spidergram; Fig. 11), the dated dykes display patterns similar to some continental tholeiites such as those of the Central Atlantic Magmatic Province (CAMP) with a moderate enrichment in large-ion lithophile elements (LILE) and distinct positive Pb and negative Nb anomalies (Bertrand et al., 1982; Youbi et al., 2003; Marzoli et al., 2004, 2019; Tegner et al., 2019). Nb anomalies have been related to crustal contamination or the influence of a subduction zone, which was either active during magma generation or earlier metasomatized lithospheric mantle with which asthenospheric magma interacted during ascent (e.g. Thompson et al., 1982; Dupuy and Dostal, 1984; Coish and Sinton, 1992; Dorais et al., 2005). Furthermore, the negative Nb anomaly is accompanied by negative P anomaly; this pattern is similar to some low-Ti CFB tholeiitic magmas contaminated by continental crust. This and the relatively high Ti/V ratios (see Fig. 10B) point to a non-orogenic origin of the mafic magmas, which were contaminated with continental crust during magma ascent/emplacement (Ikenne, 1997; Hafid, 1999; Hafid et al., 2001; El Aouli et al., 2004; 2010; El Bahat et al., 2013; Youbi et al., 2013; El Bahat et al., 2017).

4.2. Geochronology: Detrital Zircon Study of the lower Anti-Atlas Supergroup

4.2.1 Metasiltstone of the Tasserda Formation: sample TG-15-1

The sample TG-15-1 (Table 1) is purple, coarse-grained quartz-rich metasiltstone collected from the Tasserda Formation near the village of Taghadout (Figs. 3 and 4). The Tasserda Formation consists of thick- to medium-bedded quartz arenites with few channels filled with conglomerates. The main mineral components of siltstone are quartz and feldspar embedded in a sericite-rich matrix (Fig. 12A).

The zircon grains of this sample exhibit mean lengths and widths of 120 and 60 µm, respectively. In most cases, they are sub-euhedral to euhedral in shape. The internal texture of zircon grains shows oscillatory concentric, sector, and banded zoning (Figure S2 of supplementary data). The Th/U ratio ranges from 0.03 to 1.15 (Fig. 8). About 83 % of the analyzed zircons have Th/U ratios larger than 0.1, potentially indicating that they were derived from intermediate to felsic igneous rocks (cf. Möller et al., 2003; Hoskin and Schaltegger 2003; Linnemann et al., 2007). The other 17 % have a

Th/U ratio below 0.1 and could be of metamorphic origin. From the total of 99 measured spots, 74 yielded less than 10 % discordant ages (Table S2 of supplementary data). About 99 % of the zircon population is of Paleoproterozoic age (26 % are Rhyacian and 73 % are Orosirian), ranging from 2294 ± 32 Ma to 1831 ± 35 Ma, with a prominent peak at around 2022 Ma and three minor peaks at about 2294, 2142, and 1870 Ma. One remaining analysis, representing 1% of the concordant ages of this sample, yielded an age of 2653 ± 32 Ma (Fig. 13A, B). The dominance of the Paleoproterozoic ages indicates that almost all of the detrital zircon grains were derived from the Paleoproterozoic (Eburnean) crust. The seven youngest zircon grains yielded a concordia age of 2049.3 ± 4.6 Ma, which constrains the maximum depositional age of the Tasserda Formation (Fig. 13A, B).

4.2.2. Quartzites of the Agoummy Formation: sample BA21

The sample BA21 (Table 1) is a medium-grained quartzite collected from the Agoummy Formation at the Tachdamt section (Figs. 3 and 5). The Agoummy Formation consists of thick- to medium-bedded quartzites with few conglomerates nested in channels.

The quartzites are dominated by quartz that is mainly subrounded. Some quartz grains show overgrowth rims. The rock is moderately sorted with a matrix that consists of silt-sized quartz and mica minerals such as sericite. Intergranular voids are filled with secondary Fe-Ti oxides (Fig. 12B).

Zircons from this sample have a mean length and width of 110 and 70 µm, respectively. Zircon grains are mainly sub-rounded to rounded in shape with some euhedral crystals (Figure S3 of supplementary data). Most of them show oscillatory zoning, suggesting that they are of igneous origin. This is corroborated by their Th/U ratios ranging from 0.19 to 1.50 (Fig. 8). The internal textures include oscillatory zoning, planar zoning, banded zoning, and a minor portion with sector zoning. A total of 55 spots have been analysed (Table S3 of supplementary data), of which 50 yielded 90 to 110% concordant ages. About 84% are Paleoproterozoic (Statherian - 4%, Orosirian - 24%, Rhyacian - 54%, and Siderian - 2%), 12% of all ages are Neoarchean and 4% are Mesoarchean (2869 ± 8 Ma and 2857 ± 32 Ma). The Neoarchean ages range from 2735 ± 11 to

2531 ± 18 Ma, while the Paleoproterozoic ages range from 2498 ± 14 to 1786 ± 20 Ma. The probability-density plot is dominated by peaks at ca. 2205, 2080, 2035, and 1812 Ma. The six youngest grains, ranging from 1834 ± 24 Ma to 1786 ± 20 Ma, combined yield a concordia age of 1818 ± 6.4 Ma (MSWD = 1.5; probability = 0.22), which likely represents the maximum depositional age for the Agoummy Formation (Fig. 13C, D).

4.2.3. Quartzites of the Tachdamt Formation: sample ALBL29

The sample ALBL29 (Table 1) is a medium- to coarse-grained, poorly sorted quartz arenite from the lowermost part of the Tachdamt Formation at the Bleida section (Figs. 3 and 5). This formation consists of basaltic lava flows and interbedded volcanic breccias, lapilli tuffs, and volcanoclastic sediments. The mineral assemblage mainly consists of quartz with a small amount of feldspar and a matrix of silt-sized quartz and mica minerals (Fig. 12C).

Zircon grains from this sample exhibit a mean length and width of 160 and 90 µm, respectively. The grains are sub-rounded and euhedral (Figure S4 of supplementary data). The internal textures predominantly show concentric zoning, with few grains lacking any zoning. The Th/U ratio ranges from 0.01 to 1.26, with a dominant population of likely igneous origin (98%; 0.1 to 1.26) and a minor population with a potentially metamorphic origin (2%; 0.01 to 0.1; Fig. 8). Out of 96 measured spots (Table S4 of supplementary data), 92 yielded less than 10% discordant ages (Fig. 14A, B). About 54% of the ages are Mesoproterozoic (Calymmian - 22%, Ectasian - 17%, and Stenian - 17%), 41.3% of the ages are Paleoproterozoic (Siderian - 4%, Rhyacian - 8%, Orosirian - 18%, and Statherian - 11%), 2% of the ages are Neoproterozoic (Tonian), 1% of the ages are Mesoarchean, and 1% of the ages are Neoarchean. Neoarchean and Mesoarchean ages are each represented by one analysis at 2577 ± 53 and 2969 ± 48 Ma, respectively. Paleoproterozoic ages range from 2482 ± 66 to 1603 ± 175 Ma with two prominent peaks at ca. 1978 and 1752 Ma. The Mesoproterozoic ages range from 1572 ± 55 to 1043 ± 12 Ma with four prominent peaks at ca. 1525, 1280, 1208, and 1060 Ma. The Neoproterozoic age at 822 ± 6 Ma is only 92% concordant and has a very low Th/U ratio of 0.01 indicating some overprint of the zircon grain. This grain is

551 therefore not used to calculate a maximum depositonal age. The inferred maximum age of
552 deposition is set by a concordia age derived from the youngest population of concordant grains at
553 1060 ± 5.5 Ma (four grains), and 930 ± 12 Ma, a 100% concordant single grain analysis with a
554 Th/U ratio of 1.10 (Fig.14A, B).

555 **4.2.4. Metasandstone of the Bleida Formation: sample BA24**

556 The sample BA24 (Table 1) is a fine-grained, moderately sorted metasandstone from the middle
557 part of the Bleida Formation (Figs. 3 and 5) at the Bleida section. The Bleida Formation consists of
558 up to 600 m thick siliciclastic deposits interbedded with volcanoclastics. The sample contains
559 quartz, plagioclase, and lithic fragments with matrix bearing clays, sericite, muscovite, and chlorite.
560 The grains are subangular to subrounded indicating that the sediment is immature (Fig. 12D).
561 The zircon grains of this sample exhibit a mean length and width of 125 and 85 µm, respectively,
562 and most of them are sub-rounded to sub-angular in shape. The internal texture of the zircons
563 revealed by CL images comprise concentric and sector zoning, and some unzoned grains (Figure S5
564 of supplementary data). The Th/U ratio ranges from 0.18 to 1.31, indicating a magmatic origin of
565 the zircon grains (Fig. 8). Of 44 measured spots (Table S5 of supplementary data), 40 yielded less
566 than 10% discordant ages. A total of 93% exhibits Paleoproterozoic ages (Siderian - 7%, Rhyacian -
567 49%, and Orosirian - 37%), Mesoarchean, Mesoproterozoic, and Neoproterozoic populations are
568 each 2%. The Mesoarchean is represented by one age of 2852 ± 7 Ma, while the Paleoproterozoic
569 ages range from 2487 ± 6 to 1841 ± 12 Ma with one prominent peak at ca. 2075 Ma and three minor
570 peaks at ca. 2158, 1960, and 1852 Ma. The only Mesoproterozoic age is 1276 ± 14 Ma and the
571 Neoproterozoic age is 977 ± 10 Ma. Two youngest grains, overlapping within errors, give a
572 concordia age of 1855 ± 6.5 Ma (Fig. 14C, D).
573 In summary, the inferred maximum depositional ages based on concordia diagrams for the
574 sedimentary succcesion of the lower Anti-Atlas Supergroup are 2049.3 ± 4.6 Ma Ma for the
575 Tasserda Formation, 1818 ± 6.4 Ma for the Agoummy Formation, 1060 ± 5.5 Ma for the Tachdamt

Formation, and 1855 ± 6.5 Ma for the Bleida Formation (Table 1). However, the latter formations could be younger (see Section 5.3)

5. Discussion

5.1 The 1.68-1.64 Ga Zenaga Event

The SHRIMP U-Pb geochronologic data for the Great Taghdout sill presented here shows a weighted mean average $^{207}Pb/^{206}Pb$ age of 1676 ± 37 Ma interpreted to date the magmatic emplacement of the sill (Fig. 9B). This age is similar within error to those obtained for other dolerite dykes and sills in the studied area (Zenaga Inlier), as well as in other inliers of the Anti-Atlas Belt (e.g. Agadir Melloul Inlier). Kouyaté et al. (2013) obtained ages of 1640 ± 2 Ma and 1641 ± 3 Ma (U-Pb baddeleyite) on the sill (DZ 36), which intrudes the Eburnean basement in the Zenaga Inlier (Fig. 4). They also obtained an age of 1656 ± 9 Ma (U-Pb baddeleyite) on another sill (DZ40), which is connected to a sill intruding the lowermost part of the lower Anti-Atlas Supergroup of the Zenaga Inlier (the Tasserda-Taghatine Group) and an age of 1654 ± 16 Ma (U-Pb baddeleyite) on a large NE-trending dyke, which crosscuts the Eburnean basement of the Agadir Melloul Inlier. More recently, Youbi et al. (2019) dated two sills intruding quartzites of the Lkest Group (equivalent of the Oumoula Formation) in the Kerdous Inlier. One of the sills yielded an upper intercept date of ca. 1640 Ma, constrained with ID-TIMS data for three zircon grains. LA-ICP-MS data for the same sample yielded a weighted mean average $^{207}Pb/^{206}Pb$ age of ca. 1650 Ma, identical within analytical uncertainties to the ID-TIMS date. Only a single baddeleyite grain has been analyzed from the second sill, producing a similar crystallization age of ca. 1650 Ma. All of these ages overlap within error with the newly obtained age from this study.

These ca. 1.68-1.64 Ga ages match the Rb-Sr dates, which were obtained for granitic rocks from the Anti-Atlas Belt; the Timrharbine granite (Zenaga Inlier), Tasserhert granite (Kerdous Inlier), and Oued Chaiba granite (Bas Drâa Inlier) dated at 1650 ± 50, 1680 ± 35, and 1640 ± 32 Ma, respectively (Charlot, 1976; 1982). This suggests an event of bimodal magmatism during the late

Paleoproterozoic, post-dating the ca. 2.04 Ga Tagragra of Tata LIP extensional event (Kouyaté et al., 2013; Youbi et al., 2013), and confirms the polycyclic character of magmatism in the Anti-Atlas Belt, previously inferred in Kerdous and Tagragra of Akka inliers (Gasquet et al., 2004; Barbey et al., 2004). These ca. 1650 Ma ages are interpreted to belong to a single LIP event, which is termed the Zenaga Event (Kouyaté et al., 2013; Youbi et al., 2013; Ernst, 2014).

Globally, magmatism at ca. 1640-1656 Ma is also observed on other cratons (Fig. 15). In eastern and southwestern Greenland, the Melville Bugt dyke swarm extends for about 1000 km and is precisely dated at 1622-1635 Ma by the U-Pb method (1622 ± 3, 1629 ± 1, 1632 ± 1, and 1635 ± 3 Ma; Halls et al., 2011). Following upon previous work on the ca. 1630 Ma Melville Bugt dyke swarm along the NW coast of Greenland, Klausen and Nilsson (2019) confirmed its proposed continuation to the SE Greenland, indicating an extraordinary >2000 km long Trans-Greenlandic dyke swarm of Laurentia. This correlation was not only based on the swarm's continuous pattern, but also on a matching 1630 ± 4 Ma U-Pb baddeleyite age determination (Klausen and Nilsson, 2019) and similar whole-rock compositions as well as distinctive outcrop characteristics. In Laurentia, the bimodal Narakay Volcanic Complex in the Dease Arm of the Great Bear Lake, associated with deposition in the intracontinental Hornby Bay Basin, NWT, Canada, yielded TIMS U-Pb zircon age of 1663 ± 8 Ma (Bowring and Ross, 1985).

Corresponding magmatism on Baltica includes the ca. 1.64 Ga NW-trending dyke swarms of Häme, Sipoo, and Suomenniemi and the related rapakivi granite complexes exposed in the Svecofennian Domain of the Fennoscandian Shield in southeast Finland (Vaasjoki et al., 1991; Salminen et al., 2017). The most extensive of these dyke swarms is the 1642 ± 2 Ma Häme diabase dyke swarm (U-Pb ID-TIMS baddelleyite age; Salminen et al., 2017).

In Southern Siberia, the Nersa Sill Complex from the Biryusa Block of the Irkutsk Promontary has a 1641 ± 8 Ma U-Pb baddeleyite age (Ernst et al., 2016). Other potential matches are rejected. The Khibelen dykes of the Baikal Uplift, Siberia have a 1674 ± 29 Ma Sm-Nd pyroxene, plagioclase, and whole-rock isochron age (Gladkochub et al., 2010). However, the Khiblelen dykes are on a

trend from the SW-trending Chaya dyke subswarm, which has a 1752 ± 3 Ma U-Pb baddeleyite age (Gladkochub et al. 2010; Ernst et al. 2016), and so the Chaya and Khibelen dykes likely represent a single ca. 1750 Ma swarm. The type section for the Early Riphean, a major Russian stratigraphical division, in the South Urals Mountains, southeast Baltica, contains poorly-dated trachybasalts of the Navysh Subformation of the Ai Formation, which was were originally thought to be of similar age. However, based on more recent high-precision SHRIMP U-Pb zircon dating these volcanics are 1752 ± 11 Ma in age (Krasnobaev et al., 2013a, b; Puchkov et al. 2014).

5.2. Stratigraphic Implications Arising From the U-Pb Dating of the Great Taghdout Sill

Based on the previously published data, the age of the lower Anti-Atlas Supergroup is bracketed between ca. 2032 and 647 Ma (see section 2.3.). The new U-Pb SHRIMP zircon age of 1676 ± 37 Ma obtained for the herein named Taghdout sill provides a new constraint on the minimum age for the lowermost part of the lower Anti-Atlas Supergroup in the Zenaga Inlier. The Taghdout sill intrudes into the lower Anti-Atlas Supergroup and is consequently younger than the intruded sedimentary rocks (that is the Tasserda and Ifrane-n-Taghatine formations) and most likely older than the unconformably overlying Oumoula Formation. The new age indicates that the lowermost part of the lower Anti-Atlas Supergroup was likely deposited during the late Paleoproterozoic (2.03-1.64 Ga). It could potentially be related to extension during the post-Eburnean orogenic collapse and if so should be close in age to ca. 2.0 Ga. In contrast, the much younger ca. 1.67 Ga Taghdout sill, likely related to the ca. 1.65 Ga Zenaga LIP, is a part of the mantle plume event/s that occurred at the late stage of the Nuna / Columbia supercontinent assembly (Fig. 15).

The new 1676 ± 37 Ma age for the sill in the Zenga Inlier is equivalent within uncertainty to the ca. 1706 ± 7 Ma age obtained for mafic intrusions crosscutting basal quartzites in the Igherm Inlier (Ikenne et al., 2017) and the ca. 1650 Ma age of the thick sills intruding the basal part of the lower Anti-Atlas Supergroup in the Kerdous Inlier (Youbi et al., 2019). Together, these ages indicate associated extension. Therefore, the post-Eburnean hiatus of one billion years on the WAC is no longer valid and the pre-Pan-African sediments and magmatic events are preserved along the

654 northern margin of the craton. The 1640-1680 Ma (this study; Youbi et al., 2019) and the ca. 1706
655 Ma (Ikenne et al., 2017) magmatic events indicate that extension predated deposition of the thick
656 quartzites of the Oumoula Formation, but postdated accumulation of the Tasserda and Ifrane-n-
657 Taghatine formations. Further geochronological work is required to determine whether the ca. 1650
658 Ma, ca. 1676 Ma, and ca. 1706 Ma intrusions represent separate intraplate events on the WAC or
659 belong to a single long-lived 1.70-1.65 Ga LIP event across the WAC and potentially representing
660 an event extending into Baltica and Laurentia (Fig. 15). Regardless, all these ages for mafic sills are
661 additional evidence that the lower part of the lower Anti-Atlas Supergroup has an upper
662 Paleoproterozoic age and, therefore, nearly one billion years older than previously thought.
663
664 **5.3. Constraints From Detrital Zircons on the Depositional Age of the Lower Anti-Atlas**
665 **Supergroup**
666 The youngest detrial zircons from the sample TG-15-1 (the Tasserda Formation) are ca. 2049 Ma
667 old (Fig. 13A, B), providing a maximum depositional age for the formation. This is in agreement
668 with the geological context of the lower Anti-Atlas Supergroup: (i) the age of the succession is
669 bracketed between 2032 ± 5 Ma and 647 ± 2 Ma; (ii) the 1676 ± 37 Ma Taghdout sill indicates that
670 the intruded sedimentary rocks (that is the Tasserda and Ifrane-n-Taghatine formations) are older
671 than 1676 ± 37 Ma, consistent with the minimum age constraints of ca. 1650 Ma in the Kerdous
672 Inlier (Youbi et al., 2019) and ca. 1710 Ma in the Igherm Inlier (Ikenne et al., 2017).
673 The six youngest zircon grains in the sample BA21 (the Agoummy Formation) yielded a late
674 Paleoproterozoic concordia age of 1818 ± 6.4 Ma (Fig. 13C, D), providing the maximum age for
675 deposition of this formation. The U-Pb detrital zircon data obtained from this sample are consistent
676 with the U-Pb zircon data for quartzites of the Mimount Formation in the Siroua Inlier (*sensu*
677 Thomas et al., 2002), which is the stratigraphic equivalent of the Oumoula Formation (*sensu*
678 Bouougri and Saquaque, 2004) of the lower Anti-Atlas Supergroup. For the Mimount Formation,
679 Abati et al. (2010) obtained LA-ICP-MS $^{207}Pb/^{206}Pb$ zircon ages from ca. 2936 to ca. 1809 Ma, with

major peaks at ca. 2200 and 2086 Ma and a number of minor peaks (ca. 2005, 1950, and 1818 Ma). The youngest zircon in the Oumoula Formation gave a concordant age of 1809 ± 15 Ma (Abati et al., 2010), while the youngest population age is ca. 1818 Ma, providing a maximum age for deposition of the Oumoula Formation. For the Mimount Formation, Walsh et al. (2012) obtained a range of SHRIMP $^{207}Pb/^{206}Pb$ zircon ages from about 2182 to 1987 Ma, with a major peak at ca. 2050 Ma. The similarity between detrital zircon age distribution in our sample BA21 from the Agoummy Formation and that of the Mimount Formation in Abati et al. (2010) and Walsh et al. (2012) indicates a similar provenance for the Mimount (= Oumoula) and Agoummy formations.

The lack of ca. 1.67 Ga zircon grains in samples from the Mimount and Agoummy formations is worth a note given the prominence of the 1650 Ma Zenaga event (see Section 5.1). However, mafic melts are usually poor in zircons; this may explain their relative absence in these formations.

The youngest detrital zircon grains from the Tachdamt Formation which overlap within errors are ca. 1060 Ma old (Fig. 14A, B). However, there are two younger single zircon grains with ages at 930 ± 12 and 822 ± 6 Ma. The latter age has a concordance of only 92% and a very low Th/U ratio, therefore the maximum age of sedimentation is constrained by ca. 1060 Ma and ca. 930 dates, consistent with ca. 883 Ma U-Pb SHRIMP zircon ages for two tuff horizons interbedded in the basal part of the Tachdamt Formation in the Siroua Inlier (Youbi et al., 2018, Bouougri et al., 2020). The youngest concordant zircon dates that overlap within errors in the sample BA24 from the Bleida Formation yield a concordia age of 1855 ± 6.5 Ma. The two youngest zircon grains provide dates at 1276 ± 14 Ma and 977 ± 10 Ma (Fig. 14C, D). However, Letsch (2018) reported a pronounced bimodal age distribution for a greywacke from the Bleida Formation in the Bou Azzer Inlier with a major Paleoproterozoic population (peaked at ca. 2060 Ma) and a minor Neoproterozoic one (with a prominent mode at ca. 690 Ma); the latter defines, along with the 697.3 ± 2.2 Ma maximum depositional age of the metasiltstone from the most basal part of the Bleida Formation (Bouougri et al., 2020), a Cryogenian maximum depositional age for this formation

(although the minimum depositional age is younger than 883 Ma). These data imply a significant hiatus (697 to <883 Ma) in time of deposition between the Tachdamt and Bleida formations.

Both the Bleida and Tachdamt formations contain Mesoproterozoic detrital zircon ages (Fig. 14), however these ages are less abundant in the Bleida Formation, suggesting a change in the provenance consistent with a major hiatus in the time of deposition for these units. Importantly, detrital zircon ages indicate that the provenance for the lower Anti-Atlas Supergroup was overhelmingly Paleoproterozoic and Mesoproterozoic in age with a much smaller contribution from Archean and Neoproterozoic sources.

5.4. Interpretation of Detrital Zircon Age Clusters

Four major detrital zircon age clusters have been obtained in this study: 3.0-2.4, 2.3-1.74, 1.7-1.4, and 1.25-0.95 Ga (Fig. 16). The few Archean zircon grains, forming a poorly defined cluster, were likely derived from the Reguibat and Leo-Man shields (Rocci et al., 1991; Thiéblemont et al., 2004; Key et al., 2008; Koffi et al., 2020). The second cluster (2.30-1.74 Ga) reflects contribution from mafic and felsic magmatic intrusions emplaced during the Eburnean Orogeny and its aftermath along the northern margin of the WAC (Abouchami et al., 1990; Boher et al., 1992; Egal et al., 2002; Schofield et al., 2006; Kouyaté et al., 2013; Youbi et al., 2013 Baratoux et al., 2011; 2019; McFarlane et al., 2019). The third cluster (1.7-1.4 Ga) is likely linked to the emplacement of dykes and sills accompanying the protracted rifting and the breakup of the Nuna / Columbia supercontinent (Youbi et al., 2013; Evans et al., 2013). Zircons of the fourth cluster (1.25-0.95 Ga) are common in the early Neoproterozoic sedimentary rocks. It is thought that these zircons were derived from the 1.25-0.95 Ga Grenvillian arcs (Rino et al., 2008) that underwent uplift and erosion during and in the aftermath of the amalgamation of the Rodinia supercontinent, and they may have been transported for thousands of kilometres inside the supercontinent by rivers (Rainbird et al., 1997). Interestingly, metamorphic and intrusive units with these ages are common in the Sunsás Orogen (e.g. Sadowski and Bettencourt, 1996; Santos et al., 2008), which borders the Andean side of the Amazonian Craton (Fig. 17), and the Sveconorwegian Orogen of the northwestern part of

Baltica (e.g. Andersson et al., 2007; Christoffel et al., 1999; Cosca et al., 1998) that were adjacent to the WAC in the Rodinia supercontinent configuration.

5.5. Speculations on the Provenance and Paleogeographic Reconstruction

The main feature of our detrital zircon populations is the general absence or scarcity of Mesoproterozoic ages (Figs. 13 and 14), which is consistent with the earlier studies that argued for a tectonomagmatically quiescent period between ca. 1.7 and 1.0 Ga (e.g. Ennih and Liégeois, 2008). The absence or scarcity of Mesoproterozoic ages has been considered diagnostic in distinguishing the WAC provenance as a possible source (e.g. Nance and Murphy, 1994; Friedl et al., 2000; Linnemann et al., 2004; Abati et al., 2010; Bahlburg et al., 2010; Gärtner et al., 2013, 2016, 2017). How could this be reconciled with the U-Pb geochronological evidence for major mafic magmatic events at ca. 1.75, 1.65, and 1.41-1.38 Ga (e.g. Youbi et al., 2013) ? The simplest explanation is that the mafic magmatism does not produce a significant detrital zircon population, and hence these major LIP events are not reflected in the detrital zircon record.

Samples from the upper part of the lower Anti-Atlas Supergroup (the Tachdamt and Bleida formations) contain Mesoproterozoic detrital zircons. Considering that in most reconstructions of the Nuna-Columbia and Rodinia supercontinents, the Amazonian Craton and Baltica were adjacent to the WAC (e.g. Hoffman, 1991; Dalziel, 1991, 1997; Weil et al., 1998; Evans, 2013; Li et al., 2013; Johansson, 2009; 2014; Merdith et al., 2017) and had their sources of Mesoproterozoic zircons far from their borders with the WAC (Fig. 15), both of these cratons could have been potential sources of detrital zircons as long as a long-distance fluvial transport was involved. However, the Amazonian Craton (Tassinari and Macambira, 1999) is characterized by a continuous range of Mesoproterozoic ages since it undergone several late Paleoproterozoic to Mesoproterozoic orogenic events, and igneous and metamorphic units with the ages ranging from 2000 to 1000 Ma are common there (e.g. Santos et al., 2000; Tassinari et al., 2000). While the sample ALB29 is indeed characterized by a continuous range of Mesoproterozoic ages, the sample BA24 has only few Mesoproterozoic zircons. Tantalizingly, similar to the sample ALB29 range of

Mesoproterozoic detrital zircon ages was observed for the ca. 1.1 Ga Polissya Series in the western part of the Ukrainian Shield (SW part of Baltica (Sarmatia); Shumlyanskyy et al., 2015) that was positioned adjacent to the WAC in the configuration of Fig. 15, but equally lacks sources for the Mesoproterozoic detrital zircons. A long-distance transport from NW Baltica has thus been inferred for this mode in detrital zircon ages based on the combined ages and Hf isotope systematics. Mesoproterozoic detrital zircon ages were also found in the Neoproterozoic sedimentary units in the Mauritanides and in the Taoudeni Basin (Straathof, 2011; Nicoll et al., 2010; Bradley et al., 2015; see for compilation Gärtner et al., 2017), indicating long-distance fluvial transport of Mesoproterozoic zircons in the aftermath of the Grenville Orogeny (cf. Rainbird et al., 1997).

5.6. Refining Proterozoic Stratigraphy of the Anti-Atlas Belt

Figure 18 shows a tentative correlation of the lower Anti-Atlas Supergroup (*sensu* Thomas et al., 2004) among the Anti-Atlas inliers. Based on our own geochronologic data and on published U-Pb geochronology, as well as on lithostratigraphy, we propose to abandon the Lkest-Taghdout Group name since it combines genetically unrelated successions deposited in different, superimposed basins recording different tectonic settings and bracketed by long-lasted hiatuses. Instead, we propose to use the lower Anti-Atlas Supergroup as the highest stratigraphic hierarchy unit for the Proterozoic, pre-Pan-African successions of the Anti-Atlas Belt that can be further subdivided in five unconformity-bounded lithostratigraphic units.

(1) The lower lithostratigraphic unit is Paleoproterozoic in age (ca. 2030-1706 Ma) and comprises the Tasserda and Ifrane-n-Taghatine formations, named here the Tasserda-Taghatine Group. Our maximum depositional age for the Tasserda Formation (<2049 Ma) agrees well with the only other detrital zircon study for the Tasserda and Ifrane-n-Taghatine formations by Letsch (2018), who inferred <2038-1975 Ma maximum depositional age for this succession. The lower group is herein related to the Eburnean Orogen collapse at ca. 2.0 Ga and deposition in extensional intracratonic basins.

(2) The second lithostratigraphic unit is also Paleoproterozoic in age (ca. 1745-1650 Ma) and comprises the Oumoula (= Mimount) Formation. In the Ifni Inlier, the stratigraphic equivalent of the lower Anti-Atlas Supergroup, the "Groupe des Quartzites" (Jeannette et al., 1981), consists of quartzites and metasiltstones that have been subdivided into three units that unconformably overlie the Eburnean basement. U-Pb dating of the Eburnean basement in this inlier yielded 2042 ± 5 Ma and 2026 ± 7 Ma ages for the Alouzad and Sahel granites, respectively (Schulte et al., 2016). The detrital zircons from the Ifni Inlier quartzites yielded ages ranging between ca. 2020 and 1745 Ma with no evidence of the Mesoproterozoic ages (Benziane et al., 2016). We tentatively correlate the Ifni Inlier succession with the Oumoula Formation based on a similar detrital zircon distribution patterns.

In the Agadir Melloul and south Siroua inliers, the stratigraphic equivalents of the lower Anti-Atlas Supergroup are the Iguiguil-Tizi n'Taghatine and Ahmamad formations, that both unconformably overlie the Eburnean granites and diorites with ca. 2.04-2.03 Ga U-Pb zircon ages (Choubert et al., 1992; Blein et al., 2014b). The Iguiguil-Tizi n'Taghatine Formation (Fig. 18) contains the Jbel Iguiguil quartzites that are sedimentologically similar to the quartzites of the Oumoula Formation (*sensu* Bouougri and Saquaque, 2004) and Mimount Formation (*sensu* Thomas et al., 2002; 2004). The Ahmamad Formation (Fig. 18) consists of quartzites and locally developed carbonate rocks exposed along the strike-slip faults in the southeastern part of the Azaghar-Izazen Inlier (Blein et al., 2014b and references therein). Both the Iguiguil-Tizi n'Taghatine and Ahmamad formations appear to have a similar age, although spatial (and structural) relationships are not clear (Choubert et al., 1992; Blein et al., 2014b). The Ahmamad Formation is similar to the Oumoula Formation in Jbel Iguiguil. The Iguiguil-Tizi n'Taghatine Formation is intruded by 570 ± 7 Ma dyke swarms and sill complexes of dolerites and gabbros (U-Pb zircon age; Blein et al., 2014b).

The Agadir Melloul Inlier has several ridges with nearly vertical conglomeratic quartzite beds sandwiched in Paleoproterozoic granites. Detrital zircon dates from the quartzites yielded the major

peak at ca. 2.0 Ga and the youngest ages at ca. 1.8-1.7 Ga (Soulaimani et al., 2019), similar to the distribution trend shown by detrital zircons from the the Oumoula Formation.

In the Kerdous Inlier, the stratigraphic equivalent of the lower Anti-Atlas Supergroup is the Jbel Lkest Group and includes the whole section of the "PII" quartzites in the Anzi District (Hassenforder, 1987; O'Connor et al., 2010). The thick, hematite-rich quartzite sequence is not subdivided because of its monotonous nature and the lack of preservation of original textures due to extensive recrystallization, however it seems to correspond to the same depositional facies as the Oumoula Formation (*sensu* Bouougri and Saquaque, 2004) and Mimount Formation (*sensu* Thomas et al., 2002; 2004) quartzites. The great thickness of this formation and its homogeneity imply a constant supply of sediment sustained for a long period of time balanced by a continuous subsidence. Letsch (2018) constrained the maximum depositional age for the quartzite to be 1780 Ma based on U-Pb LA-ICP-MS detrital zircon data. As noted above (Section 5.2.), Youbi et al., (2019) recently dated two mafic sills emplaced into the quartzite. One of the sills yielded an upper intercept date of ca. 1640 Ma, constrained by ID-TIMS data on three zircon fractions. LA-ICP-MS data for the same sample yielded a weighted mean average $^{207}Pb/^{206}Pb$ date of ca. 1650 Ma, identical within analytical uncertainties to the ID-TIMS date. Only a single fraction of baddeleyite has been analyzed from the second sill, indicating a similar crystallization age of ca. 1650 Ma.

The unconformably bounded Oumoula Formation is thus bracketed in age between ca. 1745 and 1650 Ma (Fig. 18). The data suggest that there was a pronounced change in the provenance across the unconformity between the Oumoula and the underlying Tasserda-Taghatine Group. Furthermore, the underlying units show a different structural pattern from the Oumoula Formation in the Zenaga Inlier (cf. Choubert et al., 1951; Brabers, 1988; Letsch, 2018), suggesting that they were deposited in different basins. Discontinuous distribution of the lower group formations and the Oumoula Formation, combined with geochemical composition of the 1.75-1.64 Ga mafic dykes and sills akin to continental flood basalts (Section 4.1.4.), indicate deposition of the Oumoula Formation at ca. 1.75-1.64 Ga in the compartmentalized extensional basins (rifts).

(3) The third lithostratigraphic unit is Paleoproterozoic to Neoproterozoic in age (< ca. 1706-1640 Ma to > ca. 883 Ma). It incorporates the Ifarkhs-n-Tirsal, Wanimzi, Tamgarda, Agoummy, and Imi n-Tizi formations. This lithostratigraphic unit is named here the Tizi n'Taghatine Group. Our detrital zircon ages for the Agoummy Formation provide the first maximum depositional age for this succession (<1818 Ma), but unfortunately it does not improve independent age constraints for this group. Ca. 1650 Ma sills and dykes that intrude the underlying Oumoula Formation, but not the Tizi n'Tghatine Group provide the maximum depositional age and ca. 883 volcanics in the unconformably overlying Tachdamt Formation set the minimum depositional age for this succession. The succession was likely deposited in the intracratonic basin related to the rifting within the assembling Rodinia supercontinent.

(4) The fourth lithostratigraphic unit is the ca. 883 Ma Tachdamt Formation. The Tachdamt Formation consists of a succession of basaltic lava flows interbedded with subordinate pyroclastic rocks. Youbi et al. (2018) and Bouougri et al., (2018; 2020) dated two tuff horizons, interbedded in the basal part of the Tachdamt Formation in the Siroua Inlier, at 885 ± 5.9 Ma and 883 ± 2.3 Ma (U-Pb SHRIMP on zircon). The NE30°-trending Iguerda-Taïfast mafic dyke swarm in the Zenaga and Iguerda-Taïfast inliers and the coeval volcanics of the Tachdamt Formation are part of the ca. 885-883 Ma Iguerda-Taïfast Large Igneous Province (LIP) in the Anti-Atlas Belt of Morocco (Kouyaté et al., 2013; Söderlund et al., 2013; Youbi et al., 2013, 2018; Bouougri et al., 2020), related to the rifting within the Rodinia supercontinent. The formation was likely deposited in the rift basin at the late stage in the assembly of the supercontinent Rodinia, but it remains uncertain whether this basin evolved into a passive continental margin setting along the northern margin of the WAC. Similar-age LIP events have been recognized in the southern part of the WAC (Baratoux et al., 2019), and on the Tarim Terrane of North China (Wang et al., 2015; Zhang et al., 2019) and the Congo Craton (Armstrong et al., 2005; Johnson et al., 2007).

(5) The uppermost unit, the ca. 700 Ma Bleida Formation is characterized by fine-grained and thin-bedded siliciclastic turbidites, interbedded with minor basaltic lava flows, exhalative facies (jasper

and ironstone), and black shales. Depositional setting of the Bleida Formation and the minimum age of its detrital zircons point to deposition in a foreland basin developed in the lead of the ca. 660-680 Ma Pan-African Orogeny (Thomas et al., 2004; Bouougri et al., 2020).

5.7. Potential correlation with the Taoudeni Basin succession in Mauritania

Our study indicates that the lower Anti-Atlas Supergroup records Mid-Proterozoic protracted and episodic deposition in intracontinental basins developed in association with extension and LIPs events on the WAC. Considering that these conditions, likely linked to far-distant tectonic stresses and emplacement of mantle plumes, could also have affected other parts of the WAC, we explore here correlation with another Mid-Proterozoic basin on the WAC, the Taoudeni Basin, located approximately 500 km to the south of the Anti-Atlas Belt (Fig. 1). It contains three unconformity-bounded successions in the ascending order: the Char, Atar, and Assabet el Hassiane groups.

The lower part of the sedimentary fill of the Taoudeni Basin, the Hodh Supergroup (Super-groupe du Hodh), is subdivided into the three unconformity-bound groups: the Char, Atar, and de l'Assabet el Hassiane (Moussine-Pouchkine and Bertrand-Sarfati, 1997; Benan and Deynoux, 1998). The mixed carbonate-siliclastic Char Group was deposited in a fault-bounded, compartmentalized basin developed on the deeply weathered Eburnean basement with aeolean and fluvial redbeds grading upsection to tidally influenced, marine siliciclastic and carbonate deposits with some evidence (halite pseudomorphs, mudcracks and mudchips, dessication cracks) for warm and arid climate. The depositional and tectonic setting of the Char Group is similar to that of the Tasserda-Taghatine Group (lithostratigraphic unit 1 in the Anti-Atlas Belt). Similarly, both successions carry detrital zircons with youngest ages corresponding to the Eburnean basement with an additional contribution in case of the Zenaga Inlier of the Anti-Atlas Belt of slightly younger, ca. 2042-1975 Ma provenance (Bradley et al., 2015; Straathof, 2011; Letsch, 2018; this study). We provisionally correlate these successions and link the development of their corresponding basins to the post-Eburnean orogen collapse.

We recognize no correlative stratigraphic interval in the Taoudeni Basin to the ca. 1745-1650 Ma Oumoula Formation (lithostratigraphic unit 2 of the Anti-Atlas Belt), which we link to extension and LIP emplacement on the WAC at the final stage in the assembly of the Nuna supercontinent. Importantly, ca. 1750 and 1650 Ma mafic magmatism, linked with deposition of the Oumoula Formation, was not so far recognized in the Taoudeni Basin and the surrounding Reguibat Craton.

The next potentially correlative stratigraphic intervals in the Anti-Atlas Belt and the Taoudeni Basin are the Tizi n'Tghatine (lithostraigraphic unit 3) and Atar groups, respectively. Both are mixed carbonate-siliciclastic successions deposited in intracratonic basins in warm and arid climate (Leblanc and Moussine-Pouchkine, 1994; Moussine-Pouchkine and Bertrand-Sarfati, 1997). Our youngest detrital zircon ages for the Agoummy Formation (ca. 1818 Ma) correspond well with the youngest detrital zircon ages reported for the Atar Group (1804 ± 33 Ma, Straathof, 2011; Nicoll et al., 2010; Bradley et al., 2015). Re-Os isochron ages for black shales from the Atar Group yielded the late Mesoproterozoic depositional age (1106 ± 12 Ma, 1109 ± 22 Ma, and 1105 ± 37 Ma; Rooney et al., 2010). These Mesoproterozoic ages are confirmed by the study of microfossils (Beghin et al., 2017) and chemostratigraphy (Kah et al., 2012). Carbonates of the the Tizi n'Tghatine Group have highly negative to near zero carbon isotope values (-5.0 to +1.5 ‰; Alvaro et al., 2014). In comparison, carbonates of the Atar Group show large carbon isotope oscillations from -6.0 to +4.0 ‰ (Fairchild et al., 1990; Shields et al., 2007; Kah et al., 2012) that are characteristic of the latest Mesoproterozoic to early Neoproterozoic seawater.

It is uncertain whether there is a stratigraphic equivalent of either the ca. 883 Ma Tachdamt Formation / Bleida formation (lithostratigraphic units 4 and 5) in the Taoudeni Basin, but the siliciclastic Assabel el Hassiane Group yielded youngest ages for detrital zircons of 952 ± 38 Ma and 965 ± 29 Ma (Straathof, 2011; Bradley et al., 2015), which are consistent with the youngest ages for detrital zircons from the Tachdamt Formation (see Fig. 18). More importantly, both the Tachdamt Formation and the Assabel el Hassiane Group show influx of Mesoproterozoic detrital zircons in the aftermath of the Grenville Orogeny. Similar pattern for the Laurentia has been related

to giant fluvial systems that delivered material from the Grenville Orogen inside the Rodinia supercontinent (Rainbird et al., 1997, 2012; Rainbird and Young, 2009). Kuznetsov et al. (2017) suggested the Rodinia supercontinent configuration ringed by continental arcs and with predominantly internal runoff that seems to fit well to the detrital zircon patterns of the WAC.

6. Concluding remarks

The main conclusions of our study are summarized below.

(1) The lower Anti-Atlas Supergroup was considered as a late Neoproterozoic passive continental margin sequence deposited during rifting and breakup on the northern margin of the WAC, culminating with opening of an oceanic basin between the northern edge of the WAC and an unknown terrane at ca. 760 Ma. Based on U-Pb geochronology data (this work and literature data) and lithostratigraphic constraints, we propose a new lithostratigraphic framework for the Proterorozoic lower Anti-Atlas Supergroup of the Anti-Atlas Belt. U-Pb geochronologic data indicate that deposition of the lower Anti-Atlas Supergroup lasted from the middle Paleoproterozoic to late Neoproterozoic with significant hiatuses along unconformities. Five major, unconformity-bounded lithostratigraphic units are distinguished in the lower Anti-Atlas Supergroup. The lower unit is the ca. 2030-1706 Ma Tasserda-Taghatine Group and comprises the Tasserda and Ifrane-n-Taghatine formations. The second unit is the ca. 1745-1650 Ma Oumoula (Mimount) Formation. The third unit is Paleoproterozoic to Neoproterozoic in age (the ca. 1706-1640 Ma to > ca. 883 Ma Tizi ‘n’Taghatine Group that incorporates the Ifarkhs-n-Tirsal, Wanimzi, Tamgarda, Agoummy, and Imi n-Tizi formations. The fourth unit is the ca. 883 Ma Tachdamt Formation and the uppermost unit is the ca. 700 Ma Bleida Formation.

Using this lithostratigraphic framework in combination with ages of LIPs on the WAC and herein developed correlation with the Taoudeni Basin succession highlights protracted and yet episodic mid-Proterozoic sedimentation in intracratonic basins on the WAC in association with extensional events and far-distance plate-boundary stresses that lasted from the early stage in the Nuna / Columbia assembly to the early stage in the breakup of the Rodinia supercontinent. Deposition of

936 the Tasserda-Taghatine Group is potentially linked to the post-Eburnean orogenic collapse. The
937 Oumoula (Mimount) Formation might reflect the intracontinental extension within the Nuna
938 /Columbia supercontinent in response to either ca. 1750 Ma or 1650 Ma LIP event. The Tizi
939 'n'Taghatine Group might be correlative to the ca. 1.1 Ga Atar Group (Taoudeni Basin). The
940 Tachdamt Formation records rifting within the Rodinia supercontinent, but it is uncertain whether
941 this event led to the development of the passive continental margin along the northern boundary of
942 the WAC. Finally, the Bleida Formation deposited in the foreland basin records the early stage in
943 the assembly of the Gondwana supercontinent. The WAC formed the core of the Nuna / Columbia
944 supercontinent and transited to the Rodinia supercontinent directly unaffected by the supercontinent
945 breakup and subsequent assembly.
946 (2) The maximum depositional age and provenance of the lower Anti-Atlas Supergroup are
947 constrained by new detrital zircon ages from the lower, middle, and upper parts of the sedimentary
948 successions at the Zenaga and Bou Azzer El Graara inliers. The inferred maximum depositional
949 ages are: ca. 2049 Ma for the Tasserda Formation, ca. 1818 Ma for the Agoummy Formation, ca.
950 1060 Ma for the Tachdamt Formation, and ca. 700 Ma for the Bleida Formation. Four detrital
951 zircon age clusters have been defined in this study: ca. 3.0-2.4, 2.3-1.74, 1.7-1.4, and 1.25-0.95 Ga.
952 The provenance of detrital zircon was mainly on the WAC (that is the Reguibat and Leo-Man
953 shields), but other cratons such as Amazonia, Baltica, and the Sahara Metacraton (Hoggar, Mali)
954 cannot be excluded as possible subsidiary source areas. Importantly, we find that subsequent to the
955 Grenville Orogeny, long-distance transport by fluvial systems delivered onto the WAC
956 Mesoproterozoic zircons either from Fennoscandia of Baltica or Sunsas Belt of Amazonia (see Fig.
957 15). Transport from either of these two areas requires giant fluvial systems directed inward of the
958 Rodinia supercontinent.
959 (3) The Tachdamt Formation (lithostratigraphic unit 4) consists mainly of a succession of basaltic
960 lava flows. A ca. 885 Ma mafic dyke swarm in the Zenaga and Iguerda-Taïfast inliers and the
961 coeval volcanics of the Tachdamt Formation constitute a LIP in the Anti-Atlas Belt of Morocco,

named the Iguerda-Taïfast LIP. Similarly aged LIPs also occur on other cratons such as the Tarim Terrane (North China) and Congo Craton (Central Africa) and might reflect rifting at the late stage in the assembly of the Rodinia supercontinent.

Acknowledgements

Most of this work was carried out at the Department of Geology of the Faculty of Sciences-Semlalia, Cadi Ayyad University of Marrakech and the "Centro de Pesquisas Geocronológicas (CPGeo), Instituto de Geociências (IG), Universidade de São Paulo-USP, São Paulo (SP), Brazil" within the framework of the scientific and technical agreement between the São Paulo University and the Cadi Ayyad University (responsibles Colombo Celso Gaeta Tassinari and Nasrrddine Youbi). We acknowledge Academy Hassan II for Science and Technology for funding studentship for Abdelhak Ait Lahna in 2016 to 2018. Financial support for this work was also provided by several research projects: (i) Academy Hassan II for Science and Technology (HIIAST/SDU/2016.02) to Nasrrddine Youbi and co-workers; (ii) Medyna; and (iii) FCT (Portugal)-CNRST (Morocco) to Nasrrddine Youbi and João Mata. Richard E. Ernst was partially supported from Mega-Grant 14.Y26.31.0012 of the Russian Federation. João Mata acknowledges the financial FCT support through project UIDB/50019/2020 – IDL. The Editor Prof. Damien Delvaux is gratefully acknowledged for his comments, patience, and support. We greatly appreciate thoughtful comments of reviewers Prof. David Evans and Dr. Shuan-Hong Zhang that helped to improve the manuscript.

Figure captions

Fig. 1. (A) Location of Northwestern Africa; (B) Geological map of Northwestern Africa (after Thiéblemont, 2016 and Brahimi et al., 2018); (C) Distribution of main tectonic elements (after Brahimi et al., 2018); and (D) Geological map of the Anti-Atlas Belt in southern Morocco showing

the studied area in the Zenaga and Bou Azzer El Graara inliers (after Gasquet et al., 2008). Abbreviations: G.- Groups; J.- Jbel; Paleoprot.- Paleoproterozoic; T.-Tizi

Fig. 2. Generalized lithostratigraphic column for the Anti-Atlas Pan-African orogen. After Thomas et al., (2004), modified by Gasquet et al., (2005; 2008) and Youbi et al., (2013), and taken from Youbi et al., (2013). The conventional viewpoint has been that there is a gap in magmatic activity between 1.7 and 1.0 Ga in the Anti-Atlas Belt (Mesoproterozoic gap). However, this interpretation was challenged with the results of Youbi et al. (2013), El Bahat et al. (2013), Kouyaté et al. (2013), Söderlund et al. (2013), which all indicated important intraplate magmatic events at ca. 1.75, 1.65, and 1.38-1.41 Ga. See the text for more explanation. Note that this figure is the outdated correlation scheme for the Anti-Atlas Belt since it uses outdated chronology of the Anti-Atlas cover successions. Abbreviations: PI (XI), PII (XII), PII-III (XII-III) and PIII (XIII) are the classical stratigraphic symbols used on Anti-Atlas geological maps (Choubert, 1963). Adoud.- Adoudounien (or Adoudounian); Calc. Sup.- “Calcaires Supérieures” (Upper Limestones) ; Cambr.- Cambrian; HKCA- High-K calc-alkaline (granitoids); L. d. Vin - Lie de Vin (wine-coloured) ; Paleoproteroz.- Paleoproterozoic.

Fig. 3. Lithostratigraphic subdivision, sequence stratigraphy, and paleogeographic data for the lower Anti-Atlas Supergroup (modified after Bouougri and Saquaque, 2004). We use the name of the Ifrane-n-Taghatine Formation instead of the Taghdout Formation to ovoid confusion with the widely used name of the group - “the Taghdout Group” in the Zenaga Inlier. Abbreviations: systems tracts consist of (LST) lowstand system tracts, (TST) transgressive system tracts, and (HST) highstand system tracts. U1 to U5 are unconformities. DS1 to DS5 are depositional systems.

Fig. 4. Geology of the Zenaga Inlier (modified after Choubert, 1963; Ennih and Liégeois, 2001; Thomas et al., 2002; Kouyaté et al., 2013; Youbi et al., 2013). The Taghdout Group corresponds to

the lower Anti-Atlas Supergroup (Thomas et al., 2004). Inset shows a rose diagram that summarizes mafic dyke trends measured from the map and Google Earth; n is the number of measurements. The U-Pb ages obtained in this study are indicated with asterisks; other age constraints are from literature (Kouyaté et al., 2013; Youbi et al., 2013).

Fig. 5. Simplified geological map of the Bou Azer-El Graara Inlier showing the main lithotectonic units. The localities (Tachdamt and Bleida) mentioned in the text are indicated, as well as the location of samples used for U-Pb detrital geochronology (after Blein et al., 2014a). The Bleida Group corresponds to the lower Anti-Atlas Supergroup (Blein et al., 2014a)

Fig. 6. (A) General view of the unconformity between the Eburnean basement and the overlying quartzites of Oumoula Formation (O Fm.) of the lower Anti-Atlas Supergroup at Tizi n'Taghatine locality. The Eburnean basement (EB: gneiss and schists) is crosscut by pegmatite dyke (PE). The arrow indicates the road from Taliwine to Tazenakht. Geologists are Fida Medina, Maria Giuditta Fellin, Claudio Faccenna, and Riccardo Lanari; (B) View of the unconformity between the schists of the Bleida Formation (B Fm.) and the overlying volcanic rocks of the Ouarzazate Supergroup (OS); (C) View of the Taghdout sill (TS) crosscutting the mixed siliciclatic-carbonate succession of the Ifrane-n-Taghatine Formation (IT Fm.) in the Zenaga Inlier near the Taghdout Town. Note hornfels (h) at the baked margin of the sill. The Ifrane-n-Taghatine Formation is overlain by thick quartzites of Oumoula Formation (O Fm.); and (D) Detailed view of the upper contact between the Taghdout dolerite sill (TS) and limestones of the Ifrane-n-Taghatine Formation (IT Fm.) transformed into hornfels.

Fig. 7. Thin-section photomicrographs of the Great Taghdout sill. (A) coarse-grained dolerite in the centre of the sill with plagioclase (Pl) and clinopyroxene (Cpx) minerals and oxides (Ox), crossed nicols; (B) fine-grained, microlitic porphyric texture at the border of the sill with microlites (tiny

crystals) of plagioclase (Pl) and clinopyroxene (Cpx) minerals and oxides (Ox). Epidote (Ep) is filling vesicles; crossed nicols.

Fig. 8. Th/U ratios versus concordant U-Pb ages of igneous and detrital zircon grains of the lower Anti-Atlas Supergroup.

Fig. 9. Zircon U-Pb SHRIMP geochronology: (A) Wetherill concordia plots of U-Pb zircon data for the Taghdout sill (sample TA) of the Zenaga Inlier. (B) Weighted mean average $^{207}Pb/^{206}Pb$ age of analysis with low Th and U concentrations (spots 2.1, 7.1, and 13.1).

Fig. 10. (A) Total alkali vs. silica (TAS) diagram for the chemical classification and nomenclature (after Le Bas et al., 1986). Subalkaline vs. alkaline series boundary (dotted line) is from Irvine and Baragar (1971). (B) Ti vs. V variations in samples from the Zenaga, Agadir Melloul, Iguerda-Taïfast, and Tagragra of Akka inliers including four datasets reported by Mortaji (1989, unpublished thesis), Hafid (1999, unpublished thesis), Hafid et al., (2001) and El Aouli et al., (2010); diagram is after Shervais (1982). The studied samples TA1 (centre of the sill dated at 1676 ± 37 Ma; this work) and TA2 (border of the sill) and the 1.6 Ga dolerite dykes and sills from the Zenaga and Agadir Melloul inliers collected by Kouyaté et al., (2013) are also shown on this diagram.

Fig. 11. Primitive mantle-normalized trace element 'spidergram' for the dated mafic sill and dykes of the Zenaga and Agadir Melloul inliers. Primitive mantle values used for normalization are from Sun and McDonough (1989).

Fig; 12. Thin section photomicrographs of the sedimentary samples. (A) Metasiltstones of the Tasserda Formation: sample TG-15-1; purple, coarse-grained and quartz-rich metasiltstone with

quartz (Qz) and feldspar (Pl) embedded in a sericite-rich matrix (Mx); crossed nicols. (B) Quartzites of the Agoummy Formation: sample BA21, with quartz grains that are mostly subrounded. (C) Quartzites of the Tachdamt Formation: sample ALBL29, with a mineral assemblage comprised mainly of quartz (Qz) associated to a small amount of feldspars (Pl) with a matrix (Mx) of silt-sized quartz and mica minerals. (D) Metasandstone of the Bleida Formation: sample BA24, fine-grained, moderately sorted metasandstone with quartz (Qz), plagioclase (Pl), and lithic fragments in mica matrix (Mx).

Fig. 13. U-Pb ages for detrital zircon grains from samples TG-15-1 (metasiltstones of the Tasserda Formation) and BA21 (quartzites of the Agoummy Formation) of the lower Anti-Atlas Supergroup. (A) and (C) are concordia diagrams; (B) and (D) are combined binned frequency and probability density plots of detrital zircon grains. Abbreviations: Conc.-Concordance; Decay-const. errs.- Decay-constant errors

Fig. 14. U-Pb ages for detrital zircon grains from samples ALBL29 (quartzites of the Tachdamt Formation) and BA24 (metasandstone of the Bleida Formation) of the lower Anti-Atlas Supergroup. (A) and (C) are concordia diagrams; (B) and (D) are combined binned frequency and probability density plots of detrital zircon grains. Abbreviations: Conc.-Concordance; Decay-const. errs.- Decay-constant errors

Fig. 15. Paleomagnetically and geologically informed reconstruction of WAC, Amazonia, and Baltica cratons (SAMBA connection) along with Laurentia and Siberia in the core of the Nuna supercontinent (modified after Evans and Mitchell, 2011); additional ca. 1640-1680 Ma dyke swarms include the 1641 ± 8 Ma Nersa sill complex of Southern Siberia (U-Pb baddeleyite TIMs age; Metelkin et al, 2011; Ernst et al., 2016), 1635.0 ± 2.7 to 1622.1 ± 3.2 Ma Melville Bugt dykes of western Greenland (U-Pb baddeleyite TIMS age; Halls et al., 2011; Klausen and Nilsson, 2019),

1663 ± 8 Ma bimodal Narakay Volcanic Complex of Canada (U-Pb zircon TIMS age; Bowring and Ross, 1985), and 1642 ± 2 Ma dyke swarms of Häme, Sipoo, and Suomenniemi of the Fennoscandian Shield in southeast Finland (U-Pb ID-TIMS baddelleyite age; Vaasjoki et al., 1991; Salminen et al., 2017). Star locates mantle plume centre, proposed for the Melville Bugt swarm by Klausen and Nilsson (2019).

Fig. 16. Age compilation for detrital zircon grains from four samples collected from the lower Anti-Atlas Supergroup in the Zenaga and Bou Azzer El Graara inliers. Ages older than 1.7 Ga indicate the West African provenance (modified from Linnemann et al., 2010 and Abubaker et al., 2017). See the text for more explanation. Abbreviations: Conc.-Concordance

Fig. 17. Distribution of U-Pb ages for detrital zircon grains analyzed in this study from the lower Anti-Atlas Supergroup in the Zenaga and Bou Azzer El Graara inliers (all grouped together) and potential sources compiled from the literature. Gray stripes: detrital zircons; black stripes: zircons from magmatic rocks. Detrital zircon data sources: Pyrenees (Margalef et al., 2016); Lybia (Altumi et al., 2013); Algeria, Ahaggar (Linnemann et al., 2011); Meguma, Ganderia, and Avalonia detrital zircons (Fyffe et al., 2009; Gärtner et al., 2016; Henderson et al., 2016; Murphy et al., 2004a, 2004b; Waldron et al., 2009 and references therein); Anti-Atlas and Sardinia Cambrian (Avigad et al., 2012); Anti-Atlas Neoproterozoic (Abati et al., 2010; Karaoui et al., 2015). Anti-Atlas mafic rocks (Youbi et al., 2013 and references therein). Modified after Linnemann et al., (2011), Pratt et al., (2015), and Marzoli et al., (2017), and references therein. Abbreviations: ANS = Arabian–Nubian Shield; CAMP-Central Atlantic Magmatic Province; Camb.-Cambrian; Dev.- Devonian; Jur., Jurassic; Neoprot.- Neoproterozoic; Ord.- Ordovician; Sil.-Silurian

Fig. 18. A tentative correlation scheme of the lower Anti-Atlas Supergroup and its stratigraphic equivalents in the Anti-Atlas inliers. U1 to U8 are unconformities. U-Pb geochronology data are

from (1) this study, (2) Letsch (2018), (3) Youbi et al., (2018) and Bouougri et al., (2018; 2020), (4) Abati et al., (2010), (5) Walsh et al., (2012), (6) Thomas et al., (2002), (7) Soulaimani et al., (2013a), Hafid et al., (2013), Blein et al., (2014b), (8) Soulaimani et al., (2019), (9) Walsh et al., (2002), (10) Ikenne et al., (2017), (11) Aït Malek et al., (1998), (12) Youbi et al., (2019), (13) Benziane et al., (2016), and (14) Schulte et al., (2016).

Table captions

Table 1. Site location and summary of the data for the studied samples. The names of units and formations are sensu Bouougri and Saquaque (2004).

Table 2. Representative whole-rock major and trace element geochemical data for dykes and sills from the Zenaga, Agadir Melloul, Iguerda-Taïfast, and Tagragra of Akka inliers including the dated dykes, samples TA1 from the Zenaga Inlier (1676 ± 37 Ma; this work), DZ 36 (1640 ± 2 Ma and 1641 ± 3 Ma; Kouyaté et al., 2013) and DZ 40 (1656 ± 9 Ma; Kouyaté et al., 2013) from the Zenaga Inlier (Kouyaté et al, 2013), and AMHA069 (1654 ± 16 Ma; Kouyaté et al, 2013) from the Agadir Melloul Inlier. The geochemical data are from unpublished theses (Hafid, 1999; Mortaji, 1989) and published papers (Hafid et al., 2001; El Aouli et al., 2010; Youbi et al., 2013). Fe_2O_{3t}= total Fe expressed as Fe_2O_3. Loss-on-ignition (L.O.I.) determined by sample weight loss at 1000◦C.

Appendix: Supplementary data

Figure S1 of supplementary data**.** Cathodoluminescence (CL) images of zircon grains obtained from the sample TA 1 showing their internal texture, spots (yellow circles), and apparent ages in Ma (1σ error).

1143 **Figure S2** of supplementary data**.** Cathodoluminescence (CL) images of zircon grains obtained
1144 from the sample TG-15-1 (metasiltstone of the Tasserda Formation) of the lower Anti-Atlas
1145 Supergroup showing their internal texture, laser spots (yellow circles=concordant ages; red
1146 circles=discarded ages due to high discordance and/or U/Th/Pb contents), and apparent ages in Ma
1147 (1σ error).
1148
1149 **Figure S3** of supplementary data**.** Cathodoluminescence (CL) images of zircon grains obtained
1150 from the sample BA21 (quartzites of the Agoummy Formation) of the lower Anti-Atlas Supergroup
1151 showing their internal texture, laser spots (yellow circles=concordant ages; red circles= discarded
1152 ages due to high discordance and/or U/Th/Pb contents), and apparent ages in Ma (1σ error).
1153
1154 **Figure S4** of supplementary data**.** Cathodoluminescence (CL) images of zircon grains obtained
1155 from the sample ALBL29 (quartzites of the Tachdamt Formation) of the lower Anti-Atlas
1156 Supergroup showing their internal texture, laser spots (yellow circles=concordant ages; red circles=
1157 discarded ages due to high discordance and/or U/Th/Pb contents), and apparent ages in Ma (1σ
1158 error).
1159
1160 **Figure S5** of supplementary data**.** Cathodoluminescence (CL) images of zircon grains obtained
1161 from the sample BA24 (metasandstone of the Bleida Formation) of the lower Anti-Atlas
1162 Supergroup showing their internal texture, laser spots (yellow circles=concordant ages; red circles=
1163 discarded ages due to high discordance and/or U/Th/Pb contents), and apparent ages in Ma (1σ
1164 error).
1165
1166 **Table S1** of supplementary data. SHRIMP zircon U-Th-Pb data for the Taghdout Sill (Sample
1167 TA1).
1168

Table S2 of supplementary data. LA-ICP-MS zircon U-Th-Pb data for the sample TG-15-1 (metasiltstone of the Tasserda Formation) of the lower Anti-Atlas Supergroup.

Table S3 of supplementary data. SHRIMP zircon U-Th-Pb data for the sample BA21 (quartzites of the Agoummy Formation) of the lower Anti-Atlas Supergroup.

Table S4 of supplementary data**.** LA-ICP-MS zircon U-Th-Pb data for the sample ALBL29 (quartzites of the Tachdamt Formation) of the lower Anti-Atlas Supergroup.

Table S5 of Supplementary data**.** SHRIMP zircon U-Th-Pb data for the sample BA24 (metasandstone of the Bleida Formation) of the lower Anti-Atlas Supergroup.

References

Abati, J., Aghzer A.M., Gerdes A., Ennih N., 2010. Detrital zircon ages of Neoproterozoic sequences of the Moroccan Anti-Atlas belt. Precambrian Research, v. 181(1), p.115-128. Doi:10.1016/j.precamres.2010.05.018.

Abati, J., Aghzer, A. M., Gerdes, A., Ennih, N., 2012. Insights on the crustal evolution of the West African craton from Hf isotopes in detrital zircons from the Anti-Atlas belt. Precambrian Research, 212-213, 263–274. doi:10.1016/j.precamres.2012.06.005.

Abouchami, W., Boher, M., Michard, A. and Albarede, F., 1990. A Major 2.1 Ga event of mafic magmatism in West Africa: An early stage of crustal accretion. Journal of Geophysical Research, v. 95, p. 17605-17629. Doi:10.1029/jb095ib11p17605

Abubaker, A., Hofmann, M., Gärtner, A., Linnemann, U., Elicki, O., 2017. First U–Pb geochronology on detrital zircons from Early-Middle Cambrian strata of the Torgau-Doberlug

Syncline (eastern Germany) and palaeogeographic implications. International Journal of Earth Sciences (Geologische Rundschau), v. 106, p. 2445–2459. Doi:10.1007/s00531-016-1440-y

Admou, H., and Juteau, T., 1998. Découverte d'un système hydrothermal océanique fossile dans l'ophiolite antécambrienne de Khzama (massif du Siroua, Anti-Atlas marocain). Comptes Rendus de l'Académie Des Sciences - Series IIA - Earth and Planetary Science, 327(5), 335–340. doi:10.1016/s1251-8050(98)80052-9.

Ahmed, A., Arai, S., Abdelaziz, Y., Rahimi, A., 2005. Spinel composition as a petrogenetic indicator of the mantle section in the Neoproterozoic Bou Azzer ophiolite, Anti Atlas, Morocco. Precambrian Research, 138(3-4), 225–234. Doi:10.1016/j.precamres.2005.05.004

Aït Malek, H.A., Gasquet, D., Bertrand, J.M., Leterrier, J., 1998. Geochronologie U–Pb sur zircon de granitoïdes éburnéens et panafricains dans les boutonnières protérozoïques d'Igherm, du Kerdous et du Bas Draâ (Anti-Atlas occidental, Maroc). Comptes Rendus de l'Academie des Sciences, Serie II. Sciences de la Terre et des Planetes: v. 327 (12), p. 819–826. Doi:10.1016/s1251-8050(99)80056-1

Altumi, M.M., Elicki, O., Linnemann, U., Hofmann, M., Sagawe, A., Gärtner, A., 2013. U–Pb LA-ICP-MS detrital zircon ages from the Cambrian of Al Qarqaf Arch, central-western Libya: provenance of the West Gondwanan sand sea at the dawn of the early Palaeozoic. Journal of African Earth Sciences, v. 79, p. 74–97. Doi:10.1016/j.jafrearsci.2012.11.007

Alvaro, J. J., Pouclet, A., Ezzouhairi, H., Soulaimani, A., Bouougri, E. H., Imaz, A. G., Fekkak, A., 2014. Early Neoproterozoic rift-related magmatism in the Anti-Atlas margin of the West African craton, Morocco. Precambrian Research, v 255, 433–442. Doi:10.1016/j.precamres.2014.10.008

Andersson, U. B., Rutanen, H., Johansson, Å., Mansfeld, J., Rimša, A., 2007. Characterization of the Paleoproterozoic Mantle beneath the Fennoscandian Shield: Geochemistry and Isotope Geology (Nd, Sr) of ~ 1.8 Ga Mafic Plutonic Rocks from the Transscandinavian Igneous Belt in Southeast Sweden. International Geology Review, 49(7), 587–625. Doi:10.2747/0020-6814.49.7.587

1220 Armstrong, R. A., Master, S., Robb, L. J., 2005. Geochronology of the Nchanga Granite, and
1221 constraints on the maximum age of the Katanga Supergroup, Zambian Copperbelt. Journal of
1222 African Earth Sciences, 42(1-5), 32–40. doi:10.1016/j.jafrearsci.2005.08.012
1223 Avigad, D., Gerdes A., Morag, N., Bechstädt, T., 2012. Coupled U–Pb–Hf of detrital zircons of
1224 Cambrian sandstones from Morocco and Sardinia: Implications for provenance and
1225 Precambrian crustal evolution of North Africa. Gondwana Research, v. 21, p.690–703.
1226 Doi:10.1016/j.gr.2011.06.005
1227 Bahlburg, H., Vervoort, J.D., DuFrane, S.A., 2010. Plate tectonic significance of Middle Cambrian
1228 and Ordovician siliciclastic rocks of the Bavarian Facies, Armorican Terrane Assemblage,
1229 Germany: U–Pb and Hf isotope evidence from detrital zircons. Gondwana Research, v. 17,
1230 p.223–235. Doi:10.1016/j.gr.2009.11.007
1231 Baratoux, L., Metelka, V., Naba, S., Jessell, M. W., Grégoire, M., Ganne, J., 2011. Juvenile
1232 Paleoproterozoic crust evolution during the Eburnean orogeny (~2.2–2.0Ga), western Burkina
1233 Faso. Precambrian Research, 191(1-2), 18–45. Doi:10.1016/j.precamres.2011.08.010
1234 Baratoux, L., Söderlund, U., Ernst, R. E., De roever, E., Jessell, M. W., Kamo, S., Naba, S.,
1235 Perrouty, S., Metelka, V., Yatte, D., Grenholm, M., Diallo, D. P., Ndiaye, P. M., Dioh, E.,
1236 Cournède, C., Benoit, M., Baratoux, D., Youbi, N., Rousse S., Bendaoud, A., 2019. New U–
1237 Pb Baddeleyite Ages of Mafic Dyke Swarms of the West African and Amazonian Cratons:
1238 Implication for Their Configuration in Supercontinents Through Time. Springer Nature
1239 Singapore Pte Ltd. 2019 R. K. Srivastava et al. (eds.), Dyke Swarms of the World: A Modern
1240 Perspective, Springer Geology, p. 263-314, DOI https://doi.org/10.1007/978-981-13-1666-
1241 1_7.
1242 Barbey, P., Oberli, F., Burg, J-P., Nachit, H, Pons, J., Meier, M., 2004. The Palaeoproterozoic in
1243 western Anti-Atlas (Morocco): a clarification. Journal of African Earth Sciences, v. 39, p. 39–
1244 245. Doi:10.1016/j.jafrearsci.2004.07.044

1245 Beghin, J., Storme, J.-Y., Blanpied, C., Gueneli, N., Brocks, J. J., Poulton, S. W., Javaux, E. J.,
1246 2017. Microfossils from the late Mesoproterozoic-early Neoproterozoic Atar/El Mreïti Group,
1247 Taoudeni Basin, Mauritania, northwestern Africa. Precambrian Research, 291, 63–82.
1248 doi:10.1016/j.precamres.2017.01.009.
1249 Benan, C. A. A., Deynoux, M., 1998. Facies analysis and sequence stratigraphy of neoproterozoic
1250 Platform deposits in Adrar of Mauritania, Taoudeni basin, West Africa. Geologische Rundschau,
1251 87(3), 283–302. Doi:10.1007/s005310050210
1252 Benziane, F., Yazidi, A., Schulte, B., Boger, S., Stockhammer, S., Lehmann, A., Saadane, A.,
1253 Yazidi, M., 2016. Carte géologique du Maroc, feuille au 1/50 000 Tlata Al Akhçaç. Notes et
1254 Mém. Serv. Géol. Maroc- Rabat n° 543bis.
1255 Benziane, F., 2007. Lithostratigraphie et évolution géodynamique de l'Anti-Atlas (Maroc) du
1256 Paléoprotérozoïque au Néoprotérozoïque: exemples de la boutonnière de Tagragra de Tata et
1257 du Jbel Saghro. Ph.D. Univ. Savoie, France.
1258 Benziane, F., Yazidi, A., Saadane, A., Yazidi, M., El Fahssi, A., Stone, B.D., Walsh, G.J., Burton,
1259 W.C., Aleinikoff, J.N., Ejjaouani, H., Kalai, M., 2008. Carte géologique au1/50 000, Feuille
1260 Qalâat Mgouna. Notes et Mémoires du Service Géologique du Maroc n° 468, 1–139.
1261 Bertrand, H., Dostal, J., Dupuy, C., 1982. Geochemistry of early Mesozoic tholeiites from
1262 Morocco. Earth and Planetary Science Letters, 58(2), 225–239. Doi:10.1016/0012-
1263 821x(82)90196-0
1264 Black, L.P., Kamo, S.L., Allen, C.M., Davis, D.W., Aleinikoff, J.N., Valley J.W., Mundil R.,
1265 Campbell I.H., Korsch R.J., Williams I.S., Foudoulis C., 2004. Improved 206Pb/ 238U
1266 microprobe geochronology by the monitoring of a trace-element relatedmatrix effect:
1267 SHRIMP, ID-TIMS, ELA-ICP-MS and oxygen isotope documentation for a series of zircon
1268 standards. Chemical Geology 205, p. 115–140. Doi:10.1016/j.chemgeo.2004.01.003
1269 Blein, O., Baudin, T., Chèvremont, P., Soulaimani, A., Admou, H., Gasquet, P., Cocherie, A., Egal,
1270 E., Youbi, N., Razin, P., Bouabdelli, M., Gombert, P., 2014a. Geochronological constraints on

1271 the polycyclic magmatism in the Bou Azzer-El Graara inlier (Central Anti-Atlas Morocco).
1272 Journal of African Earth Sciences, v. 99, p.287–306. Doi:10.1016/j.jafrearsci.2014.04.021
1273 Blein, O., Baudin, T., Soulaimani, A., Cocherie, A., Chèvremont, P., Admou, H., Ouanaimi, H.,
1274 Hafi, A., Razin, P., Bouabdelli, M., and Roger, J., 2014b. New geochemical, geochronological
1275 and structural constraints on the Ediacaran evolution of the south Sirwa, Agadir-Melloul and
1276 Iguerda inliers, Anti-Atlas, Morocco. Journal of African Earth Sciences, v. 98, p. 47–71,
1277 https://doi.org/10.1016/j.jafrearsci.2014.06.019
1278 Block, K. A., Steiner, J. C., Puffer, J. H., Jones, K. M., Goldstein, S. L., 2015. Evolution of late
1279 stage differentiates in the Palisades Sill, New York and New Jersey. Lithos, 230, 121–132.
1280 doi:10.1016/j.lithos.2015.05.018
1281 Bodinier, J. L., Dupuy, C., Dostal, J., 1984. Geochemistry of Precambrian ophiolites from Bou
1282 Azzer, Morocco. Contributions to Mineralogy and Petrology, 87(1), 43–50. 87(1), 43–50.
1283 Doi:10.1007/bf00371401
1284 Bogdanova, S. V., Bingen, B., Gorbatschev, R., Kheraskova, T. N., Kozlov, V. I., Puchkov, V. N.,
1285 Volozh, Y. A., 2008. The East European Craton (Baltica) before and during the assembly of
1286 Rodinia. Precambrian Research, 160 (1-2), 23–45. Doi:10.1016/j.precamres.2007.04.024
1287 Bogdanova, S.V., Gorbatschev, R., Garetsky, R.G., 2016. Europe/East European Craton. Reference
1288 Module in Earth Systems and Environmental Sciences, Elsevier, pp. 1-18. Doi:10.1016/b978-0-
1289 12-409548-9.10020-x
1290 Boher, M., Abouchami, W., Michard, A., Albarede, F. and Arndt, N. T., 1992. Crustal growth in
1291 West Africa at 2.l Ga. Journal of Geophysical Research, v. 97, p. 345-369.
1292 Doi:10.1029/91jb01640
1293 Bouougri, E.H., Saquaque, A., 2004. Lithostratigraphic framework and correlation of the
1294 Neoproterozoic northern Western African Craton passive margin sequence (Siroua-Zenaga Bou
1295 Azzer El Graarara Inliers, Central Anti-Atlas, Morocco): an intergrated approach. Journal of
1296 African Earth Sciences, v. 39, p. 227–238. Doi:10.1016/j.jafrearsci.2004.07.045

1297 Bouougri, E. H., Ait Lahna, A., Tassinari, C. C. G., Basei, M. A. S., Youbi, N., Admou, H.,
1298 Maacha, L., 2020. Time constraints on Early Tonian Rifting and Cryogenian Arc terrane-
1299 continent convergence along the northern margin of the West African craton: Insights from
1300 SHRIMP and LA-ICP-MS zircon geochronology in the Pan-African Anti-Atlas belt (Morocco).
1301 Gondwana Research. Volume 85, p. 169-188. doi.org/10.1016/j.gr.2020.03.011

1302 Bowring, S. A., Ross, G. M., 1985. Geochronology of the Narakay Volcanic Complex: implications
1303 for the age of the Coppermine Homocline and Mackenzie igneous events. Canadian Journal of
1304 Earth Sciences, 22(5), 774–781. Doi:10.1139/e85-082

1305 Brabers, P. M., 1988. A plate tectonic model for the Panafrican Orogeny in the Anti-Atlas,
1306 Morocco. Lecture Notes in Earth Sciences, 61–80. Doi:10.1007/bfb0011586

1307 Bradley, D.C., O'Sullivan, P., Cosca, MA., Motts, HA., Horton, JD., Taylor, CD., Beaudoin, G.,
1308 Lee G.K., Ramezani, J., Bradley, D.B., Jones, J.V., Bowring, S., 2015. Synthesis of Geological,
1309 Structural, and Geochronologic Data (Phase V, Deliverable 53): Chapter A of Taylor CD (ed.),
1310 Second Projet de Renforcement Institutionnel du Secteur Minier de la République Islamique de
1311 Mauritanie (PRISM-II). U.S. Geological Survey Open-File Report 2013-12080-A, p. 328.
1312 https://doi.org/10.3133/ofr20131280A

1313 Brahimi, S., Liégeois, J.-P., Ghienne, J.-F., Munschy, M., Bourmatte, A., 2018. The Tuareg shield
1314 terranes revisited and extended towards the northern Gondwana margin: Magnetic and
1315 gravimetric constraints. Earth-Science Reviews, 185, 572–599.
1316 Doi:10.1016/j.earscirev.2018.07.002

1317 Cahen, L., Snelling, N.J., Delhal, J., Vail, J.R., 1984. The Geochronology and Evolution of Africa:
1318 Clarendon Press, Oxford, United Kingdom, p. 512.

1319 Chacko, T., De, S. K., Creaser, R. A., Muehlenbachs, K, 2000. Tectonic setting of the Taltson
1320 magmatic zone at 1.9–2.0 Ga: a granitoid-based perspective. Canadian Journal of Earth Sciences,
1321 37 (11), 1597–1609. Doi:10.1139/e00-029

1322 Charlot, R., 1976. The precambrian of the Anti-Atlas (Morocco): a geochronologic synthesis:
1323 Precambrian Research, v. 3, p. 273–299. Doi:10.1016/0301-9268(76)90013-9
1324 Charlot, R., 1982. Caracterisation des evenements eburneens et panafricains dans l'Anti-Atlas
1325 marocain; apport de la methode geochronologique Rb–Sr : Notes et Mémoires du Service
1326 Géologique du Maroc. v. 313, 106p.
1327 Choubert, G., 1962. Réflexions sur les parallélismes probables des formations quaternaires
1328 atlantiques du Maroc avec celles de la Méditerranée: Quaternaria, v. 5, p.137-175.
1329 Choubert, G., 1963. Histoire géologique de l'Anti-Atlas de l'archéen à l'aurore des temps primaries.
1330 Notes et Mémoires du Service Géologique du Maroc, v. 62, p. 350–352.
1331 Choubert, G., Faure-Muret, A., Dahmani, M., Mouatani, E.A., Horrenberger, J.C., Salem, M., 1992.
1332 Carte géologique du Maroc à 1/100 000 feuille Agadir Melloul. Notes et Mémoires n° 359.
1333 Ministère de l'Energie et des Mines, Rabat.
1334 Choubert, G., Termier, H., Termier, G., 1951. Les calcaires précambriens de Taghdout et leures
1335 organismes problématiques. Notes et Mémoires du Service géologique du Maroc 85 (5), 9-34.
1336 Christoffel, C. A., Connelly, J. N., Åhäll, K.-I., 1999. Timing and characterization of recurrent pre-
1337 Sveconorwegian metamorphism and deformation in the Varberg–Halmstad region of SW
1338 Sweden. Precambrian Research, 98(3-4), 173–195. Doi:10.1016/s0301-9268(99)00046-7
1339 Clauer, N., 1976. Grochimie isotopique du strontium des milieux sédimentaires. Application à la
1340 géochronologie du craton ouest-africain. Sciences géologiques, Strasbourg, v. 45, 256 p.
1341 Coish, R. A., and Sinton, C. W., 1992. Geochemistry of mafic dikes in the Adirondack Mountains:
1342 Implications for late Proterozoic continental rifting. Contributions to Mineralogy and Petrology,
1343 v. 110, p. 500–514. Doi:10.1007/bf00344084
1344 Corrigan, D., Hajnal, Z., Németh, B., Lucas, S. B., 2005. Tectonic framework of a Paleoproterozoic
1345 arc-continent to continent-continent collisional zone, Trans-Hudson Orogen, from geological and
1346 seismic reflection studies. Canadian Journal of Earth Sciences, 42 (4), 421–434.
1347 Doi:10.1139/e05-025

1348 Corrigan, D., Pehrsson, S., Wodicka, N., de Kemp, E., 2009. The Palaeoproterozoic Trans-Hudson
1349 Orogen: a prototype of modern accretionary processes. Geological Society, London, Special
1350 Publications, 327(1), 457–479. Doi:10.1144/sp327.19
1351 Cosca, M. A., Mezger, K., Essene, E. J., 1998. The Baltica-Laurentia Connection: Sveconorwegian
1352 (Grenvillian) Metamorphism, Cooling, and Unroofing in the Bamble Sector, Norway. The
1353 Journal of Geology, 106(5), 539–552. Doi:10.1086/516040
1354 Dalziel, I.W.D., 1991. Pacific margins of Laurentia and East Antarctica–Australia as a conjugate
1355 rift pair: evidence and implications for an Eocambrian supercontinent. Geology 19, p. 598–601.
1356 Doi:10.1130/0091-7613(1991)019<0598:pmolae>2.3.co;2
1357 Dalziel, I.W.D., 1997. Neoproterozoic–Paleozoic geography and tectonics: review, hypothesis and
1358 environmental speculation. Bulletin of the Geological Society of America, v. 109, p. 16–42.
1359 Doi:10.1130/0016-7606(1997)109<0016:onpgat>2.3.co;2
1360 Deynoux, M., Affaton, P., Trompette, R., Villeneuve, M., 2006. Pan-African tectonic evolution and
1361 glacial events registered in Neoproterozoic to Cambrian cratonic and foreland basins of West
1362 Africa. J. Afr. Earth Sci. 46, 397–426. Doi:10.1016/j.jafrearsci.2006.08.005
1363 Doblas, M., Lopez-Ruiz, J., Cebria, J.M., Youbi, N., Degroote, E., 2002. Mantle insulation beneath
1364 the West African Craton during the Precambrian-Cambrian transition. Geology 30, p. 839–842.
1365 Doi:10.1130/0091-7613(2002)030<0839:mibtwa>2.0.co;2
1366 Dorais, M.J., Harper, M., Larson, S., Nugroho, H., Richardson, P., Roosmawati, N., 2005. A
1367 comparison of Eastern North America and Coastal New England magma suites: implications for
1368 subcontinental mantle evolution and the broad terrane hypothesis. Canadian Journal of Earth
1369 Sciences, v. 42, p. 1571–1587. Doi:10.1139/e05-056
1370 Dupuy, C., and Dostal, J., 1984. Trace element geochemistry of some continental tholeiites. Earth
1371 and Planetary Science Letters, 67(1), 61–69. doi:10.1016/0012-821x(84)90038-4
1372 Egal, E, Thiéblemont, D., Lahondère, D., Guerrot, C., Adi Coseta, C., Iliescu, D., Delor, C.,
1373 Goujou, J-C., Lafon, JM., Tegyey, M., Diaby, S., Kolié, P., 2002. Late Eburnean granitization

and tectonics along the western and northwestern margin of the Archean Kénéma-Man domain (Guinea, West African Craton). Precambrian Research, v. 117, p.57–84. Doi:10.1016/s0301-9268(02)00060-8

El Aouli, E.H., Ikenne, M., Amaouain, H., 2010. Petrographic and geochemical characterization of Cryogenian mafic dykes of the Iguerda–Taïfast inlier (Central Anti-Atlas, Morocco). International Journal of Geomatics and Geosciences, v. 1, p. 355–371.

El Aouli, E.H., Ikenne, M., Beraaouz, E.H., Mortaji, A., 2004. Les roches basiques des boutonnières d'Agadir Melloul et d'Iguerda-Taïfast: témoins de l'histoire préorogénique de la chaîne panafricaine de l'Anti-Atlas (Maroc). Estudios Geologicos 60, p. 11–20. https://doi.org/10.3989/egeol.04601-269

El Bahat, A., Ikenne, M., Cousens, B., Söderlund, U., Ernst, R., Klausen, M., B., Youbi, N., 2017. New constraints on the geochronology and Sm-Nd isotopic characteristics of Bas-Drâa mafic dykes, Anti-Atlas of Morocco. Journal of African Earth Sciences, 127, 77-87. Doi:10.1016/j.jafrearsci.2016.09.003

El Bahat, A., Ikenne, M., Söderlund, U., Cousens, B., Youbi N., Ernst R., Soulaimani A., Janati M., Ahmid Hafid A., 2013. U–Pb baddeleyite ages and geochemistry of dolerite dykes in the Bas Drâa Inlier of the Anti-Atlas of Morocco: Newly identified 1380 Ma event in the West African Craton. Lithos, V. 174, p. 85–98. Doi:10.1016/j.lithos.2012.07.022

El Hadi, H., Simancas, J.F., Martínez-Poyatos, D., Azor, A., Tahiri, A., Montero, P.,Fanning, C.M., Bea, F., González-Lodeiro, F., 2010. Structural and geochronological constraints on the evolution of the Bou Azzer Neoproterozoic ophiolite (Anti-Atlas, Morocco). Precambrian Research, v. 182, p. 1–14. Doi:10.1016/j.precamres.2010.06.011

Ennih, N., and Liégeois, J. P., 2008. The boundaries of the West African craton, with special reference to the basement of the Moroccan metacratonic Anti-Atlas belt. Geological Society, London, Special Publications, v. 297(1), p. 1-17.

1399 Ennih, N., Liégeois, J. P., 2001. The Moroccan Anti-Atlas: the West Africain craton passive margin
1400 with limited pan-african activity. Implications for the northern limit of the craton. Precambrian
1401 Research, v. 112, p. 289-302. https://doi.org/10.1016/S0301-9268(01)00195-4
1402 Ernst, R.E,. Hamilton, M.A., Söderlund, U., Hanes, J.A., Gladkochub, D.P., Okrugin, A.V.,
1403 Kolotilina, T., Mekhonoshin, A.S. Bleeker, W., LeCheminant, A.N., Buchan, K.L.,
1404 Chamberlain, K.R., Didenko, A.N., 2016. Long-lived connection between southern Siberia and
1405 northern Laurentia in the Proterozoic. Nature Geoscience, v. 9, p. 464-469.
1406 Doi:10.1038/ngeo2700
1407 Ernst, R.E. 2014. Large Igneous Provinces. Cambridge University Press, 653 p.
1408 https://doi.org/10.1017/CBO9781139025300
1409 Ernst, R.E., and Buchan, K.L., 2001. Large mafic magmatic events through time and links to mantle
1410 plume heads: In: Ernst, R.E., Buchan, K.L. (Eds.), Mantle Plumes: Their Identification Through
1411 Time, Geological Society of America, Special Paper, v. 352, p. 483–575.
1412 https://doi.org/10.1130/0-8137-2352-3.483
1413 Ernst, R.E., and Youbi, N., 2017. How large igneous provinces affect global climate, sometimes
1414 cause mass extinctions, and represent natural markers in the geological record.:
1415 Palaeogeography, Palaeoclimatology, Palaeoecology, v. 478, p. 30–52.
1416 Doi:10.1016/j.palaeo.2017.03.014
1417 Evans, D.A.D. 2013. Reconstructing pre-Pangean supercontinents. Geological Society of America
1418 Bulletin, 125, 1735–1751. Doi:10.1130/b30950.1
1419 Evans, D.A.D., Li, Z.X., Murphy, J.B., 2016. Four-dimensional context of Earth's supercontinents.
1420 In: Li, Z.X., Evans, D.A.D., Murphy, J.B. (Eds.), Supercontinent Cycles Through Earth History.
1421 Geological Society, London, Special Publications, pp. 1–14. Doi:10.1144/sp424.12
1422 Evans, D.A.D., Mitchell, R.N., 2011. Assembly and breakup of the core of Paleoproterozoic–
1423 Mesoproterozoic supercontinent Nuna. Geology 39, p. 443–446. doi:10.1130/g31654.1

1424 Fairchild, I.J., Marshall, J.D., Bertrand-Sarfati, J., 1990. Stratigraphic shifts in carbon isotopes from
1425 Proterozoic stromatolitic carbonates (Mauritania): influence of primary mineralogy an
1426 diagenesis. Am. J. Sci. 290A:46–79

1427 Fekkak, A., Pouclet, A., Badra, L., 2002. The Pre-Pan-African rifting of Saghro (Anti-Atlas,
1428 Morocco): example of the middle Neoproterozoic Basin of Boumalne. Bulletin de la Société
1429 géologique de France, v. 173(1), p. 25–35. Doi:10.2113/173.1.25

1430 Fekkak, A., Pouclet, A., Ouguir, H., Ouazzani, H., Badra, L., Gasquet, D., 2001. Géochimie et
1431 signification géotectonique des volcanites du Cryogénien inférieur du Saghro (Anti-Atlas
1432 oriental, Maroc) / Geochemistry and geotectonic significance of Early Cryogenian volcanics of
1433 Saghro (Eastern Anti-Atlas, Morocco). Geodinamica Acta, 14(6), 373–385.
1434 doi:10.1080/09853111.2001.10510730.

1435 Fodor, R. V., 2009. Diorite Segregations in Gabbro: Geochemical Characteristics and Conditions
1436 for Origin Assessed at Diorite-Gabbro Contacts. The Journal of Geology, 117(2), 109–125.
1437 doi:10.1086/596506

1438 Friedl, G., Finger, F., McNaughton, NJ., Fletcher, IR., 2000. Deducing the ancestry of terranes:
1439 SHRIMP evidence for South America-derived Gondwana fragments in central Europe. Geology
1440 28, p.1035-1038. Doi:10.1130/0091-7613(2000)28<1035:dtaots>2.0.co;2

1441 Fyffe, L.L., Barr, S.M., Johnson, S.C., McLeod, M.J., McNicoll, V.J., Valverde-Vaquero, P., van
1442 Staal, C.R., White, C.E., 2009. Detrital zircon ages from Neoproterozoic and Early Paleozoic
1443 conglomerate and sandstone units of New Brunswick and coastal Maine: implications for the
1444 tectonic evolution of Ganderia. Atlantic Geology, v. 45, p. 110–144.
1445 Doi:10.4138/atlgeol.2009.006

1446 Gärtner, A., Villeneuve, M., Linnemann, U., El Archi, A., Bellon, H., 2013. An exotic terrane of
1447 Laurussian affinity in the Mauritanides and Souttoufides (Moroccan Sahara). Gondwana
1448 Research, v. 24, p. 687–699. Doi:10.1016/j.gr.2012.12.019

1449 Gärtner, A., Villeneuve, M., Linnemann, U., Gerdes, A., Youbi, N., Hofmann, M., 2016. Similar
1450 crustal evolution in the western units of the Adrar Souttouf Massif (Moroccan Sahara) and the
1451 Avalonian terranes: insights from Hf isotope data. Tectonophysics, v. 681, p. 305–317.
1452 Doi:10.1016/j.tecto.2015.11.030
1453 Gärtner, A., Youbi, N., Villeneuve, M., Linnemann, U., Sagawe, A., Hofmann, M., Zieger, J.,
1454 Mahmoudi, A., Boumehdi, M. A., 2018. Provenance of detrital zircon from siliciclastic rocks of
1455 the Sebkha Gezmayet unit of the Adrar Souttouf Massif (Moroccan Sahara) – Palaeogeographic
1456 implications. Comptes Rendus Geoscience. Doi:10.1016/j.crte.2018.06.004
1457 Gärtner, A., Youbi, N., Villeneuve, M., Sagawe, A., Hofmann, M., Mahmoudi, A., Boumehdi
1458 M.A., Linnemann U. 2017. The zircon evidence of temporally changing sediment transport—the
1459 NW Gondwana margin during Cambrian to Devonian time (Aoucert and Smara areas, Moroccan
1460 Sahara). International Journal of Earth Sciences 106 (8): 2747-2769. Doi:10.1007/s00531-017-
1461 1457-x
1462 Gasquet, D., Chevremont, P., Baudin, T., Chalot-Prat, F., Guerrot, C., Cocherie, A., Roger, J.,
1463 Hassenforder, B., Cheilletz, A., 2004. Polycyclic magmatism in the Tagragra and Kerdous-
1464 Tafeltast inliers (Western Anti-Atlas, Morocco). Journal of African Earth Sciences, v. 39, p.
1465 267–275. Doi:10.1016/j.jafrearsci.2004.07.062
1466 Gasquet, D., Ennih, N., Liégeois, J.-P., Soulaimani, A., Michard, A., 2008. The Pan-African belt,
1467 In: Michard, A., Saddiqi, O., Chalouan, A., Frizon de Lamotte, D. (Eds.), Continental Evolution:
1468 The Geology of Morocco. Lecture Notes in Earth Sciences 116, Springer-Verlag, Berlin
1469 Heidelberg, p. 33–64, Chapter 2. Doi:10.1007/978-3-540-77076-3_2
1470 Gasquet, D., Levresse, G., Cheilletz, A., Azizi-Samir, M.R., Mouttaqi A., 2005. Contribution to a
1471 geodynamic reconstruction of the Anti-Atlas (Morocco) during Pan-African times with the
1472 emphasis on inversion tectonics and metallogenic activity at the Precambrian-Cambrian
1473 transition. Precambrian Research, v. 140, p. 157–182. Doi:10.1016/j.precamres.2005.06.009

1474 Geyer, G., Landing, E., 2006. Ediacaran–Cambrian depositional environments and stratigraphy of
1475 the western Atlas regions. In: Geyer, G., Landing, E. (Eds.), Morocco 2006 – Ediacaran–
1476 Cambrian depositional environments and stratigraphy of the western Atlas regions. UCL
1477 Maghreb Petroleum Research Group, Infracambrian/Early Palaeozoic Field Guide Series 1 und
1478 Beringeria Special Issue 6, pp. 47–120.
1479 Geyer, G., Landing, E., 2020. Cambrian deposition in northwestern Africa: Relationship of Tamlelt
1480 massif (Moroccan–Algerian border region) succession to the Moroccan Meseta. Journal of
1481 African Earth Sciences, 103772. Doi:10.1016/j.jafrearsci.2020.103772
1482 Gladkochub, D.P., Pisarevsky, S.A., Donskaya, T.V., Ernst, R.E., Wingate, M.T.D., Söderlund, U.,
1483 Mazukabzov, A.M., Sklyarov, E.V., Hamilton, M.A., Hanesg, J.A., 2010. Proterozoic mafic
1484 magmatism in Siberian craton: an overview and implications for paleocontinental reconstruction.
1485 Precambrian Research 183, p. 660–668. Doi:10.1016/j.precamres.2010.02.023
1486 Grenholm, M., Jessell, M., Thébaud, N., 2019. A geodynamic model for the Paleoproterozoic (ca.
1487 2.27–1.96 Ga) Birimian Orogen of the southern West African Craton – Insights into an evolving
1488 accretionary-collisional orogenic system. Earth-Science Reviews.
1489 Doi:10.1016/j.earscirev.2019.02.006
1490 Hafid, A., 1999. Magmatisme basique filonien Néoproterozoique (Précambrien II inferieur) dans
1491 l'Anti-Atlas central et occidental. Minéralogie, géochimie, pétrogenèse et implication
1492 geodynamique. Unpublished Thèse de Doctorat d'Etat, Faculté des Sciences-Semlalia.
1493 Université Cadi Ayyad.
1494 Hafid, A., Sagon, J.P., Julivert, M., Arboleya, M.L., Saquaque, A., El Boukhari, A., Saidi, A., Soler,
1495 J.M.F., 2001. Neoproterozoic basic dykes of the Zenaga Inlier, central Anti-Atlas, Morocco:
1496 petrology, geochemistry and geodynamic significance. Journal of African Earth Sciences 32,
1497 707–721. Doi.org/10.1016/S0899-5362(02)00050-7
1498 Hafid, A., Blein, O., Admou, H., Soulaimani, A., Razin, P.H., Simon, B., Ouanaimi, H., El janati,
1499 M., Chevemont, P.H., Baudin, T., Bouabdelli, M., Abia, E.H., Beni Akhy, R., 2013. Notice

explicative carte géol. Maroc (1/50 000), feuille Assaragh, Notes et Mémoires Serv. Géol. Maroc, n°550, MEM/BRGM.

Halls, H.C., Hamilton, M., Denyszyn, S.W., 2011. The Melville Bugt dyke swarm of Greenland: A connection to the 1.5 - 1.6 Ga Fennoscandian rapakivi granite province?. In: Srivastava (ed.) Dyke Swarms: keys for Geodynamic Interpretation, p. 509-535. Doi:10.1007/978-3-642-12496-9_27

Hassenforder, B., 1987. La tectonique panafricaine et varisque de l'Anti-Atlas dans le massif de Kerdous (Maroc). Ph.D. thesis. Universite Strasbourg, Strasbourg, France, 249p.

Hefferan, K., et al. 2014. A reconsideration of Pan African orogenic cycle in the Anti-Atlas Mountains, Morocco. Journal of African Earth Sciences, v. 98, p. 34-46. Doi:10.1016/j.jafrearsci.2014.03.007

Henderson, B.J., Collins, W.J., Murphy, J.B., Gutierrez-Alonso, G., Hand, M., 2016. Gondwanan basement terranes of the Variscan–Appalachian orogen: Baltican, Saharan and West African hafnium isotopic fingerprints in Avalonia, Iberia and the Armorican Terranes. Tectonophysics, v. 681, 278–304. Doi:10.1016/j.tecto.2015.11.020

Hindermeyer, J., 1953. Le Précambrien III du Sarhro. Comptes Rendus Hebdomadaires des Séances de l'Académie des Sciences, 237 (17), 1024–1026.

Hodel, F., Macouin, M., Triantafyllou, A., Carlut, J., Berger, J., Rousse, S., Ennih, N., Trindade, R. I. F., 2017. Unusual massive magnetite veins and highly altered Cr-spinels as relics of a Cl-rich acidic hydrothermal event in Neoproterozoic serpentinites (Bou Azzer ophiolite, Anti-Atlas, Morocco). Precambrian Research, 300, 151–167. Doi:10.1016/j.precamres.2017.08.005

Hoffman, P. F., 1988. United Plates of America, the Birth of a Craton: Early Proterozoic Assembly and Growth of Laurentia. Annual Review of Earth and Planetary Sciences, 16 (1), 543–603. Doi:10.1146/annurev.ea.16.050188.002551

Hoffman, P.F., 1991. Did the breakout of Laurentia turn Gondwana inside out?. Science, v. 252, p. 1409–1412. Doi:10.1126/science.252.5011.1409

1526 Hoskin, P.W.O., Schaltegger, U., 2003. The composition of zircon and igneous and metamorphic
1527 petrogenesis. In: Hanchar JM, Hoskin PWO (eds) Zircon; Reviews in Mineralogy and
1528 Geochemistry, v. 53, p. 27–62. Doi:10.2113/0530027
1529 Ikenne, M., 1997. La boutonnière précambrienne du bas Draa (Anti-Atlas occidental, Maroc):
1530 caractérisation pétrologique et géochimique des roches magmatiques et métamorphiques et leurs
1531 relations avec la déformation. Ph.D. thesis. University of Agadir, 259p.
1532 Ikenne, M., Söderlund, U., Ernst, R.E., Pin, C., Youbi, N., El Aouli, E., Hafid, A., 2017. A c. 1710
1533 Ma mafic sill emplaced into a quartzite and calcareous series from Ighrem, Anti-Atlas –
1534 Morocco: Evidence that the Taghdout passive margin sedimentary group is nearly 1 Ga older
1535 than previously thought. Journal of African Earth Sciences, v. 127, p. 62-76.
1536 Doi:10.1016/j.jafrearsci.2016.08.020
1537 Inglis, J.D., Hefferan, K., Samson, S.D., Admou, H., Saquaque, A., 2016. Determining age of Pan-
1538 African metamorphism using Sm-Nd garnet-whole rock geochronology and phase equilibria
1539 modeling in the Tasriwine ophiolite, Sirwa, Anti-Atlas Morocco. Journal of African Earth
1540 Sciences. v. 127, p. 88–98. Doi:10.1016/j.jafrearsci.2016.06.021
1541 Inglis, J.D., MacLean, J.S., Samson, S.D., D'Lemos R.S., Admou, H., Hefferan, K., 2004. A precise
1542 U–Pb zircon age for the Bleïda granodiorite, Anti-Atlas, Morocco: implications for the timing
1543 of deformation and terrane assembly in the eastern Anti-Atlas. Journal of African Earth
1544 Sciences, v. 39, p.277–283. doi:10.1016/j.jafrearsci.2004.07.041
1545 Irvine, T.N. and Baragar, W.R.A., 1971. A guide to the chemical classification of the common
1546 volcanic rocks. Canadian Journal of Earth Science, 8, 523-548. https://doi.org/10.1139/e71-
1547 055
1548 Jackson, S. E., Pearson, N. J., Griffin, W. L., Belousova, E. A., 2004. The application of laser
1549 ablation-inductively coupled plasma-mass spectrometry to in situ U–Pb zircon geochronology.
1550 Chemical Geology, 211(1-2), 47–69. doi:10.1016/j.chemgeo.2004.06.017

1551 Jeannette, D., Benziane F., Yazidi A., 1981. Lithostratigraphie et datation du Proterozoique de la
1552 boutonniere d'Ifni (Anti-Atlas, Maroc). Precambrian Research; 14(3):363-378.
1553 Doi:10.1016/0301-9268(81)90045-0
1554 Jessell, M.W., Begg, G.C., Miller, M.S., 2016. The geophysical signatures of the west African
1555 craton. Precambrian Res. 274, 3–24. Doi:10.1016/j.precamres.2015.08.010
1556 Johansson, Å., 2009. Baltica, Amazonia and the SAMBA connection - 1000 million years of
1557 neighbourhood during the Proterozoic?. Precambrian Research, v. 175, p. 221–234.
1558 Doi:10.1016/j.precamres.2009.09.011
1559 Johansson, Å., 2014. From Rodinia to Gondwana with the 'SAMBA' model – A distant view from
1560 Baltica towards Amazonia and beyond. Precambrian Research 244, 226-235.
1561 Doi:10.1016/j.precamres.2013.10.012
1562 Kah, L. C., Bartley, J. K., Teal, D. A., 2012. Chemostratigraphy of the Late Mesoproterozoic Atar
1563 Group, Taoudeni Basin, Mauritania: Muted isotopic variability, facies correlation, and global
1564 isotopic trends. Precambrian Research, 200-203, 82–103.
1565 Doi:10.1016/j.precamres.2012.01.011
1566 Karaoui, B., Breitkreuz, C., Mahmoudi, A., Youbi, N., 2014. Physical volcanology, geochemistry
1567 and basin evolution of the Ediacaran volcano-sedimentary succession in the Bas Draâ Inlier
1568 (Ouarzazate Supergroup, Western Anti-Atlas, Morocco). Journal of African Earth Sciences. v.
1569 99(2), p. 307-331. Doi:10.1016/j.jafrearsci.2014.06.022
1570 Karaoui, B., Breitkreuz, C., Mahmoudi, A., Youbi, N., Hofmann, M., Gärtner, A., Linnemann, U.,
1571 2015. U-Pb zircon ages from volcanic and sedimentary rocks of the Ediacaran Bas Draa inlier
1572 (Anti-Atlas Morocco): chronostratigraphic and provenance implications. Precambrian Research.
1573 v. 263, p. 43-58. Doi:10.1016/j.precamres.2015.03.003
1574 Key, R.M., Loughlin, S.C., Horstwood, M.S.A., Gillespie, M., Pitfield, P.E.J., Henney, P.J.,
1575 Crowley, Q.G., Del Rio, M., 2008. Two Mesoarchaean terranes in the Reguibat shield of NW

Mauritania. In: Ennih, N., Liégeois, J.-P. (Eds.), Boundaries of the West African Craton, v. 297. Special Publication of the Geological Society, London, p. 33–52. Doi:10.1144/sp297.3

Klausen, M.B. Nilsson, M.K.M. 2019. The Melville Bugt Dyke Swarm across SE Greenland: A closer link to Mesoproterozoic AMCG-complexes. Volume 329, pages 88-107. Doi:10.1016/j.precamres.2018.06.001

Koffi, G., R-S., Kouamelan, A. N., Allialy, M. E., Coulibaly, Y., Peucat, J.-J., 2020. Re-evaluation of Leonian and Liberian events in the geodynamical evolution of the Man-Leo Shield (West African Craton). Precambrian Research, 105582. Doi:10.1016/j.precamres.2019.105582

Kouyaté, D., Söderlund, U., Youbi, N., Ernst, R., Hafid, A., Ikenne, M., Soulaimani, A., Bertrand, H., El Janati, M., Chaham, K.R., 2013. U–Pb baddeleyite and zircon ages of 2040 Ma, 1650 Ma and 885 Ma on dolerites in the West African Craton (Anti-Atlas Inlier): possible links to break-up of Precambrian supercontinents. Lithos, v. 174, p. 71–84. doi:10.1016/j.lithos.2012.04.028

Krasnobaev, A., Kozlov, V.I., Puchkov, V.N., Busharina, S.V., Sergeeva, N.D., Paderin I.P., 2013a. Zircon geochronology of the Mashak volcanic rocks and the problem of the age of the lower middle Riphean boundary (Southern Urals). Stratigraphy and Geological Correlation 21, 465–481. Doi:10.1134/s0869593813050055

Krasnobaev, A., Puchkov, V.N., Kozlov, V.I., Sergeeva, N.D., Busharina, S.V., Lepekhina E.N., 2013b. Zirconology of Navysh Volcanic Rocks of the Ai Suite and the Problem of the Age of the Lower Riphean Boundary in the Southern Urals. Doklady Earth Sciences 448, 185–190. Doi:10.1134/s1028334x13020050

Kuznetsov, A. B., Bekker, A., Ovchinnikova, G. V., Gorokhov, I. M., Vasilyeva, I. M., 2017. Unradiogenic strontium and moderate-amplitude carbon isotope variations in early Tonian seawater after the assembly of Rodinia and before the Bitter Springs Excursion. Precambrian Research, 298, 157–173. Doi:10.1016/j.precamres.2017.06.011

LE Bas, M. J., Maitre, R. W. L., Streckeisen, A., Zanettin, B., 1986. A Chemical Classification of Volcanic Rocks Based on the Total Alkali-Silica Diagram. Journal of Petrology, 27(3), 745–750. Doi:10.1093/petrology/27.3.745

Leblanc, M., 1975. Ophiolites précambriennes et gîtes arsénites de cobalt (Bou Azzer, Maroc). Ph.D. thesis, université. Paris VI, p. 329.

Leblanc, M., 1981. The late Proterozoic ophiolites of bou Azzer (Morocco): evidence for Pan-African plate tectonics. In: Kroner, A. (Ed.), Precambrian Plate Tectonics. Elsevier, Amsterdam, p. 435–451. Doi:10.1016/s0166-2635(08)70022-7

Leblanc, M., and Moussine-Pouchkine, A., 1994. Sedimentary and volcanic evolution of a Neoproterozoic continental margin (Bleida, Anti-Atlas, Morocco). Precambrian Research, 70(1-2), 25–44. doi:10.1016/0301-9268(94)90019-1.

Letsch, D., 2018. The Anti-Atlas belt (Morocco) during the Proterozoic – a sedimentary perspective. Ph.D. thesis, ETH Zurich, 201p. https://doi.org/10.3929/ethz-b-000296186

Li, Z. X., D. A. D. Evans, and G. P. Halverson. 2013. Neoproterozoic glaciations in a revised global palaeogeography from the breakup of Rodinia to the assembly of Gondwanaland. Sedimentary Geology, 294, 219-232. Doi:10.1016/j.sedgeo.2013.05.016

Liégeois, J.-P., Abdelsalam, M.G., Ennih, N., Ouabadi, A., 2013. Metacraton: nature, genesis and behavior. Gondwana Res. 23, 220–237. Doi:10.1016/j.gr.2012.02.016

Liégeois, J.-P.; Fekkak, A.; Bruguier, O.; Errami, E.; Ennih, N, 2006. The Lower Ediacaran (630–610 Ma) Saghro group: An orogenic transpressive basin development during the early metacratonic evolution of the Anti-Atlas (Morocco). In Proceedings of the IGCP485 4th Meeting, Algiers, Algeria, 2 September 2006; p. 57.

Linnemann, U., Gerdes, A., Drost, K., Buschmann, B., 2007. The continuum between Cadomian Orogenesis and opening of the Rheic Ocean: constraints from LA-ICP-MS U–Pb zircon dating and analysis of plate-tectonic setting (Saxo-Thuringian Zone, NE Bohemian massif, Germany). In: Linnemann, U., Nance, D., Kraft, P., Zulauf, G. (Eds.), The Evolution of the Rheic Ocean:

From Avalonian–Cadomian Active Margin to Alleghenian–Variscan Collision: Memoir of Geological Society of America, v. 423, p. 61–96. Doi:10.1130/2007.2423(03)

Linnemann, U., Hofmann, M., Romer, R.L., Gerdes, A., 2010. Transitional stages between the Cadomian and Variscan Orogenies: Basin development and tectonomagmatic evolution of the southern margin of the Rheic Ocean in the Saxo-Thuringian Zone (North Gondwana shelf). In: Linnemann U, Romer RL (eds) Pre-Mesozoic Geology of Saxo-Thuringia-From the Cadomian Active Margin to the Variscan Orogen. Schweizerbart Science Publishers, Stuttgart, pp 59–98.

Linnemann, U., McNaughton, N.J., Romer, R.L., Gehmlich, M., Drost, K., and Tonk, C., 2004. West African provenance for Saxo-Thuringia (Bohemian Massif): Did Armorica ever leave pre-Pangean Gondwana? U/Pb-SHRIMP zircon evidence and the Nd-isotopic record. International Journal of Earth Sciences, v. 93, p. 683–705. doi: 10.1007/s00531-004-0413-8.

Linnemann, U., Ouzegane, K., Drareni, A., Hofmann, M., Becker, S., Gärtner, A., Sagawe, A., 2011. Sands of West Gondwana: an archive of secular magmatism and plate interactions—a case study from the Cambro-Ordovician section of the Tassili Ouan Ahaggar (Algerian Sahara) using U–Pb LA-ICP-MS detrital zircon ages. Lithos, v. 123, p. 188–203. Doi:10.1016/j.lithos.2011.01.010

Lottaroli, F., Craig, J., Thusu, B., 2009. Neoproterozoic–Early Cambrian (Infracambrian) hydrocarbon prospectivity of North Africa: a synthesis. In: Craig, J., Thurow, J., Thusu, B., Whitham, A., Abutarruma, Y. (Eds.), Global Neoproterozoic Petroleum Systems: The Emerging Potential in North Africa. Vol. 326. Geological Society of London, Special Publication, pp. 137–156. Doi:10.1144/sp326.7

Ludwig, K.R., 2003. Isoplot 3. In: A Geochronological toolkit for Microsoft Excel: Berkeley Geochronology Centre Special Publication 1a.

Maloof, A., Schrag, D., Crowley, J., and Bowring, S., 2005. An expanded record of early Cambrian carbon cycling from the Anti-Atlas margin, Morocco. Canadian Journal of Earth Sciences, v. 42(12), p. 2195-2216. Doi:10.1139/e05-062

1652 Margalef, A., Castiñeiras, P., Casas, J.M., Navidad, M., Liesa, M., Linnemann, U., Hofmann, M.,
1653 Gärtner, A., 2016. Detrital zircon from the Ordovician rocks of the Pyrenees: geochronological
1654 constraints and provenance. Tectonophysics, v. 681, p. 121–134.
1655 Doi:10.1016/j.tecto.2016.03.015
1656 Marzoli, A., Bertrand, H., Knight, K., Cirilli, S., Buratti, N., Verati, C., Nomade, S., Renne, P. R.,
1657 Youbi, N., Martini, R., Allenbach, K., Neuwerth, R., Rapaille, C., Zaninetti, L., Bellieni, G.,
1658 2004. Synchrony of the Central Atlantic Magmatic province and the Triassic–Jurassic boundary
1659 climatic and biotic crisis. Geology, 32, 973–976. Doi:10.1130/g20652.1
1660 Marzoli, A., Bertrand, H., Youbi,N., Callegaro, S., Merle, R., Reisberg, L. Chiaradia, M., Brownlee,
1661 S., Jourdan, F., Zanetti, A., Davies, J. H F L, Cuppone, T., Mahmoudi, A., Medina, F. Renne,
1662 P.R., Bellieni, G., Crivellari, S. EL Hachimi, H., Bensalah,M.K., Meyzen,C.M., Tegner, C.,
1663 2019. The Central Atlantic Magmatic Province (CAMP) in Morocco. Journal of Petrology,
1664 Volume 60, Issue 5, May 2019, Pages 945–996. Doi:10.1093/petrology/egz021
1665 Marzoli, A., Davies, J.H.F.L., Youbi, N., Merle, R., Dal Corso, J., Dunkley, D.J., Fioretti, A.M.,
1666 Bellieni, G., Medina, F., Wotzlaw, J.-F., McHone, G., Font, E., Bensalah, M.K., 2017.
1667 Proterozoic to Mesozoic evolution of North-West Africa and Peri-Gondwana microplates:
1668 Detrital zircon ages from Morocco and Canada. Lithos, 278-281, 229-239. DOI:
1669 10.1016/j.lithos.2017.01.016. Doi:10.1016/j.lithos.2017.01.016
1670 Massironi, M., Moratti, G., Algouti, A., Benvenuti, M., Dal Piaz, G.V., Eddebbi, A., El Boukhari,
1671 A., Laftouhi, N., Ouanaimi, H., Schiavo, A., Taj-Eddine, K., Visonà, D., 2007. Carte géologique
1672 au 1/50 000, Feuille Boumalne. Not. Mém. Serv. Géol. Maroc 521, 80.
1673 McFarlane, H.B., Ailleres, L., Betts, P., Ganne, J., Baratoux, L., Jessell, M.W., Block S., 2019.
1674 Episodic collisional orogenesis and lower crust exhumation during the Palaeoproterozoic
1675 Eburnean Orogeny: Evidence from the Sefwi Greenstone Belt, West African Craton.
1676 Precambrian Research, 325, 88–110. DOI: 10.1016/j.precamres.2019.02.012.

1677 Merdith, A. S., Williams, S. E., Müller, R. D., Collins, A. S., 2017. Kinematic constraints on the
1678 Rodinia to Gondwana transition. Precambrian Research, 299, 132–150.
1679 Doi:10.1016/j.precamres.2017.07.013
1680 Metelkin, D.V., Ernst, R.E., Hamilton, M.A., 2011. A ca. 1640 Ma mafic magmatic event in
1681 southern Siberia, and links with northern Laurentia. Geological Society of America Annual
1682 Meeting, abstract, Minneapolis, USA.
1683 Michard, A., Saddiqi, O., Chalouan, A. Frizon de La Motte, D. (Eds.) 2008. Continental Evolution:
1684 the Geology of Morocco. Springer-Verlag Berlin Heidelberg, p. 404 p. Doi:10.1007/978-3-540-
1685 77076-3
1686 Michard, A., Soulaimani, A., Ouanaimi, H., Raddid, Y., Aït Brahim, L., Rjimati, E. ., Baidder, L.,
1687 Saddiqi, O., 2017. Saghro Group in the Ougnat Massif (Morocco), an evidence for a continuous
1688 Cadomian basin along the northern West African Craton. Comptes Rendus Geoscience, v.
1689 349(2), p. 81-90. Doi:10.1016/j.crte.2017.01.001
1690 Möller, A., O'Brien, P.J., Kennedy, A., Kröner, A., 2003. Linking growth episodes of zircon and
1691 metamorphic textures to zircon chemistry: an example from the ultrahigh-temperature granulites
1692 of Rogaland (SW Norway). Geological Society, London, Special Publications, v. 220, p. 65-81.
1693 Doi:10.1144/gsl.sp.2003.220.01.04
1694 Mortaji, A. 1989. La boutonniere prébcambrienne de Tagragra d'Akka (Anti-Atlas Occidental,
1695 Maroc), Pérologie et géochimie des granitoides. filons basiques et métamorphites associées.
1696 Thése 3éme Cycle, Université Nancy I, 211 p.
1697 Moussine-Pouchkine, A., and Bertrand-Sarfati, J., 1978. Le Gourma; un aulacogene du Precambrien
1698 superieur?. Bulletin de la Société Géologique de France ; S7-XX (6): 851–855.
1699 Doi:10.2113/gssgfbull.s7-xx.6.851
1700 Murphy, J.B., Fernández-Suárez, J., Keppie, J.D., Jeffries, T.E., 2004a. Contiguous rather than
1701 discrete Paleozoic histories for the Avalon and Meguma terranes based on detrital zircon data.
1702 Geology, v. 32, 585–588. Doi:10.1130/g20351.1

1703 Murphy, J.B., Fernández-Suárez, J., Keppie, J.D., Jeffries, T.E., 2004b. Lithogeochemical and Sm–
1704 Nd and U–Pb isotope data from the Silurian–Lower Devonian Arisaig Group clastic rocks,
1705 Avalon terrane, Nova Scotia: a record of terrane accretion during the Appalachian–Caledonide
1706 orogen. Geological Society of America Bulletin, v. 116, p. 1183–1201. Doi:10.1130/b25423.1
1707 Naidoo, D. D., Bloomer, S. H., Saquaque, A., Hefferan, K., 1991. Geochemistry and significance of
1708 metavolcanic rocks from the Bou Azzer-El Graara ophiolite (Morocco). Precambrian Research,
1709 53(1-2), 79–97. Doi:10.1016/0301-9268(91)90006-v
1710 Nance, RD., Murphy, JB., 1994. Contrasting basement isotopic signatures and the palinspastic
1711 restoration of peripheral orogens: example from the Neoproterozoic Avalonian-Cadomian belt.
1712 Geology, v. 22(7), p.617–620. Doi:10.1130/0091-7613(1994)022<0617:cbisat>2.3.co;2
1713 Nicoll, G., Straathof, G., Tait, J., Lo K., Ousmane, N., El Moctar Dahmada, M., Berndt, J., Key, R.,
1714 2010. Provenance analysis and tectonic setting of the Neoproterozoic sediments within the
1715 Taoudeni Basin, Northern Mauritania. Geophys Res Abstr 12:EGU2010-7094-2.
1716 O'Connor, E.A., Barnes, R.P., Beddoe-Stephens, B., Fletcher, T., Gillespie, M.R., Hawkins, M.P.,
1717 Loughlin, S.C., Smith, M., Smith, R.A., Waters, C.N., Williams, M., 2010. Geology of the Drâa,
1718 Kerdous, and Boumalne Districts, Anti Atlas, Morocco. Keyworth, Nottingham British
1719 Geological Survey, p. 324.
1720 Ouguir, H., Macaudière, J., Dagallier, G., 1996. Le Protérozoïque supérieur d'Imiter,Saghro
1721 oriental, Maroc : un contexte géodynamique d'arrière-arc. Journal of African Earth Sciences, v.
1722 22, p.173–189. Doi:10.1016/0899-5362(96)00002-4
1723 Pearce, J. A., and Cann, J. R., 1973. Tectonic setting of basic volcanic rocks determined using trace
1724 element analyses. Earth and Planetary Science Letters, 19(2), 290–300. Doi:10.1016/0012-
1725 821x(73)90129-5
1726 Pehrsson, S. J., Berman, R. G., Eglington, B., Rainbird, R., 2013. Two Neoarchean supercontinents
1727 revisited: The case for a Rae family of cratons. Precambrian Research, 232, 27–43.
1728 Doi:10.1016/j.precamres.2013.02.005

1729 Pratt, J.R., Barbeau Jr., D.L., Garver, J.I., Emran, A., Izykowski, T.M., 2015. Detrital zircon
1730 geochronology of Mesozoic sediments in the Rif and Middle Atlas Belts of Morocco:
1731 provenance constraints and refinement of the West African signature. Journal of Geology, v.
1732 123, p. 177–200. Doi:10.1086/681218
1733 Puchkov, V.N., Krasnobaev, A.A., Sergeeva, N.D., 2014. The New Data on Stratigraphy of the
1734 Riphean Stratotype in the Southern Urals, Russia. Journal of Geoscience and Environment
1735 Protection, v. 2, p. 108-116. DOI: 10.4236/gep.2014.23015
1736 Rainbird, R., Cawood, P.A., and Gehrels, G., 2012. The Great Grenvillian Sedimentation Episode:
1737 Record of Supercontinent Rodinia's Assembly. In Busby, C., and Azor, A., eds., Recent
1738 Advances in the Tectonics of Sedimentary Basins: Blackwell Publishing Ltd., p. 583 601.
1739 Rainbird, R.H., McNicoll, V.J., Theraiault, R.J., Heaman, L.M., Abbott, J.G., Long, D.G.F.,
1740 Thorkelson, D.J., 1997. Pan-continental river systems draining Grenville orogen recorded by U-
1741 Pb and Sm-Nd geochronology of Neoproterozoic quartz arenites and mudrock, northwestern
1742 Canada. Journal of Geology, v. 105, p. 1e10. Doi:10.1086/606144
1743 Rainbird, R.H., Young, G.M., 2009. Colossal rivers, massive mountains and supercontinents. Earth
1744 54, 52-61.
1745 Rino, S., Kon, Y., Sato, W., Maruyama, S., Santosh, M., Zhao, D., 2008. The Grenvillian and Pan-
1746 African Orogenies: World's largest orogenies through geologic time, and their implications on
1747 the origin of the superplume. Gondwana Research, v. 14, p. 51–72.
1748 Doi:10.1016/j.gr.2008.01.001
1749 Rocci, G., Bronner, G., Deschamps, M., 1991. Crystalline Basement of the West African Craton. In:
1750 Dallmeyer, R.D., Lécorché, J.P. (Eds.), the West African Orogens and Circum-Atlantic
1751 Correlatives: Springer Verlag, Berlin, p. 31–61. Doi:10.1007/978-3-642-84153-8_3
1752 Rooney, A.D., Selby, D., Houzay, J.-P., Renne, P.R., 2010. Re–Os geochronology of a
1753 Mesoproterozoic sedimentary succession, Taoudeni basin, Mauritania: implications for basin

1754 wide correlations and re–Os organic-rich sediments systematics. Earth Planet. Sci. Lett. 289,
1755 486–496. Doi:10.1016/j.epsl.2009.11.039
1756 Sadowski, G.R., Bettencourt, J.S., 1996. Mesoproterozoic tectonic correlations between eastern
1757 Laurentia and the western border of the Amazon craton. Precambrian Research, v. 76, 213-227.
1758 Doi:10.1016/0301-9268(95)00026-7
1759 Salminen, J., Klein, R., Veikkolainen, T., Mertanen, S., Mänttäri, I., 2017. Mesoproterozoic
1760 geomagnetic reversal asymmetry in light of new paleomagnetic and geochronological data for
1761 the Häme dyke swarm, Finland: Implications for the Nuna supercontinent. Precambrian
1762 Research, 288, 1–22. Doi:10.1016/j.precamres.2016.11.003
1763 Samson, S.D., Inglis, J.D., D'Lemos, R.S., Admou, H., Blichert-Toft, J., Hefferan, K., 2004.,
1764 Geochronological, geochemical, and Nd–Hf isotopic constraints on the origin of Neoproterozoic
1765 plagiogranites in the Tasriwine ophiolite, Anti-Atlas orogen, Morocco: . Precambrian Research,
1766 v. 135, p. 133–147. Doi:10.1016/j.precamres.2004.08.003
1767 Santos, J.O.S., Hartmann, L.A., Gaudette, H.E., Groves, D.I., Mcnaughton, N.J., and Fletcher, I.R.,
1768 2000. A new understanding of the provinces of the Amazon craton based on integration of field
1769 mapping and U-Pb and Sm-Nd geochronology. Gondwana Research, v. 3, no. 4, p.453–488.
1770 Doi:10.1016/s1342-937x(05)70755-3
1771 Santos, J.O.S., Rizzotto, G.J., Potter, P.E., McNaughton, N.J., Matos, R.S., Hartmann, L.A.,
1772 Chemale Jr., F., Quadros, M.E.S., 2008. Age and autochthonous evolution of the Sunsás Orogen
1773 in West Amazon Craton based on mapping and U–Pb geochronology. Precambrian Research
1774 165, 120–152. Doi:10.1016/j.precamres.2008.06.009
1775 Saquaque, A., Admou, H., Karson, J., Hefferan, K., Reuber, I., 1989. Precambrian accretionary
1776 tectonics in the Bou Azzer-El Graara region, Anti-Atlas, Morocco. Geology, 17(12), 1107.
1777 Doi:10.1130/0091-7613(1989)017<1107:patitb>2.3.co;2

1778 Schiavo, A., Taj-Eddine, K., Algouti, A., Benvenuti, M., Dal Piaz, G.V., Eddebbi, A., El Boukhari,
1779 A., Laftouhi, N., Massironi, M., Moratti, G., Ouanaimi, H., Pasquarè, G., Visonà, D., 2007.
1780 Carte géologique au 1/50 000, Feuille Imtir. Not. Mém. Serv. Géol. Maroc 518, 96.
1781 Schofield, D.I., Horstwood, M.S.A., Pitfield, P.E.J., Crowley, Q.G., Wilkinson, A.F., Sidaty,
1782 H.C.O, 2006. Timing and kinematics of Eburnean tectonics in the central Reguibat Shield.
1783 Mauritania: Journal of the Geological Society, v. 163, p.549–560. Doi:10.1144/0016-764905-
1784 097
1785 Schulte B., Benziane F., Yazidi A., Boger S., Stockhammer S., Lehmann A., Saadane A., Yazidi
1786 M., 2016. Carte géologique du Maroc, feuille au 1/50 000 Arbaa Sahel. Notes et Mém. Serv.
1787 Géol. Maroc- Rabat n° 543bis.
1788 Shervais, J.W., 1982. Ti–V plots and the petrogenesis of modern and ophiolitic lavas. Earth and
1789 Planetary Science Letters, v. 59, p. 101–118. Doi:10.1016/0012-821x(82)90120-0
1790 Shields, G. A., Deynoux, M., Strauss, H., Paquet, H., Nahon, D., 2007. Barite-bearing cap
1791 dolostones of the Taoudéni Basin, northwest Africa: Sedimentary and isotopic evidence for
1792 methane seepage after a Neoproterozoic glaciation. Precambrian Research, 153(3-4), 209–235.
1793 Doi:10.1016/j.precamres.2006.11.011
1794 Shumlyanskyy, L., Hawkesworth, C., Dhuime, B., Billström, K., Claesson, S., Storey, C., 2015.
1795 207Pb/206Pb ages and Hf isotope composition of zircons from sedimentary rocks of the
1796 Ukrainian shield: Crustal growth of the south-western part of East European craton from
1797 Archaean to Neoproterozoic. Precambrian Research, 260, 39–54.
1798 Doi:10.1016/j.precamres.2015.01.007
1799 Sircombe, K.N., 2004. AgeDisplay: an EXCEL workbook to evaluate and display univariate
1800 geochronological data using binned frequency histograms and probability density distributions.
1801 Computational Geosciences, v. 30, p. 21–31. Doi:10.1016/j.cageo.2003.09.006
1802 Söderlund, U., Ibanez-Mejia, M., El Bahat, A., Ernst, R.E., Ikenne, M., Soulaimani, A., Youbi, N.,
1803 Cousens, B., El Janati, M., Hafid, A., 2013. Reply to Comment on “U–Pb baddeleyite ages and

geochemistry of dolerite dykes in the Bas Drâa inlier of the Anti-Atlas of Morocco: Newly identified 1380 Ma event in the West African Craton" by André Michard and Dominique Gasquet: Lithos, v. 174, p.101–108. Doi:10.1016/j.lithos.2013.04.003

Soulaimani, A., Ouanaimi, H., Michard, A., Montero, P., Bea, F., Corsini, M., Molina, J. F., Rjimatif, E. C., Saddiqi, O., Hefferan, K., 2019. Quartzite crests in Paleoproterozoic granites (Anti-Atlas, Morocco); a hint to Pan-African deformation of the West African Craton margin. Journal of African Earth Sciences, 157, 103501. Doi:10.1016/j.jafrearsci.2019.05.009

Soulaimani, A., Ouanaimi, H., Saddiqi, O., Baidder, L., Michard, A., 2018. The Anti-Atlas Pan-African Belt (Morocco): Overview and pending questions. Comptes Rendus Geoscience. 350, 279-288. Doi:10.1016/j.crte.2018.07.002

Soulaimani, A., Blein, O., Chèvremont, P., Ouanaimi, H., Hafid, A., Admou, H., Baudin, T., Bouabdelli, M., Razin, P.H., Abia, E.H., Beni Akhy, R., 2013a. Notice explicative carte géol. Maroc (1/50 000), feuille Agadir Melloul, Notes et Mémoires Serv. Géol. Maroc, n°549, MEM/BRGM.

Spencer, C.J., Kirkland, C.L., Taylor, R.J.M., 2016. Strategies towards statistically robust interpretation of in situ U-Pb zircon geochronology. Geoscience Frontiers 7, 581–589. doi.org/10.1016/j.gsf.2015.11.006

Stacey, J. S., and Kramers, J. D., 1975. Approximation of terrestrial lead isotope evolution by a two stage model. Earth and Planetary Science Letters, 26(2), 207–221. doi:10.1016/0012 821x(75)90088-6.

Straathof, G.B., 2011. Neoproterozoic Low Latitude Glaciations: An African Perspective. Ph.D. thesis, University of Edinburgh, 285p.

Sun, S.S., and McDonough, W.F., 1989. Chemical and isotopic systematics of oceanic basalts; implications for mantle composition and processes. In: Magmatism in the ocean basins. Saunders, A.D. and Norry, M.J. (Editors), Geological Society of London, London, v. 42, p. 313-345. Doi:10.1144/gsl.sp.1989.042.01.19

1830 Tapsoba, B., Lo, C.-H., Wenmenga, U., Iizuka, Y., Chung, S.-L., Shellnutt, G., 2018. Chemical and
1831 Sr-Nd compositions and $^{40}Ar/^{39}Ar$ ages of NW-trending dolerite dikes of Burkina Faso:
1832 Evidence for a Mesoproterozoic magmatism in the West African Craton. Geoscience Frontiers.
1833 doi:10.1016/j.gsf.2017.12.015
1834 Tassinari, C.C.G, Macambira, M.J., 1999. Geochronological provinces of the Amazonian Craton.
1835 International Union of Geological Sciences, v. 22, p. 174–182.
1836 https://doi.org/10.18814/epiiugs/1999/v22i3/004
1837 Tassinari, C.C.G., Bettencourt, J.S., Geraldes, M.C., Macambira, M.J.B., Lafon, J.M., Cordani, U.,
1838 Milani, E.J., Thomaz Filho, A., and Campos, D.A., 2000. The Amazonian Craton, in Cordani,
1839 U.G., Milani, E.J., Thomaz Filho, A., and Campos, D.A., eds., Tectonic evolution of South
1840 America: Rio de Janeiro, 31st International Geological Congress, p.41–95.
1841 Tegner, C., Michelis, S.A.T, Mcdonald, I., Brown, E.L., Youbi, N., Callegaro, S., Lindström, S.,
1842 Marzoli, A., 2019. Mantle Dynamics of the Central Atlantic Magmatic Province (CAMP):
1843 Constraints from Platinum Group, Gold and Lithophile Elements in Flood Basalts of Morocco.
1844 Journal of Petrology. Doi:10.1093/petrology/egz041
1845 Thiéblemont, D., 2016. An updated geological map of Africa at 1/10 000 000 scale. In: Presented at
1846 the 35th International Geological Congress: IGC 2016. https://hal-brgm.archives-
1847 ouvertes.fr/hal-01326139
1848 Thiéblemont, D., Goujou, J.C., Egal, E., Cocherie, A., Delor, C., Lafon, J.M., Fanning, C.M., 2004.
1849 Archean evolution of the Leo Rise and its Eburnean reworking. Journal of African Earth
1850 Sciences, v. 39, p. 97–104. Doi:10.1016/j.jafrearsci.2004.07.059
1851 Thomas, R. J., Chevakier, L. P., Gresse, P. G., Harmer, R. E., Eglington, B. M., Armstrong, R. A.,
1852 De Beer, C. H., Martini, J. E. J., De Kock, G. S., Macey, P. H., and Ingram, B. A., 2002.
1853 Precambrian evolution of the Sirwa Window, Anti-Atlas Orogen, Morocco: Precambrian
1854 Research, v. 118, p. 1-57. Doi:10.1016/s0301-9268(02)00075-x

1855 Thomas, R.J., Fekkak, A., Ennih, N., Errami, E., Loughlin, S.C., Gresse, P.G., Chevakier, L.P. and
1856 Liegeois J.P., 2004. A new lithostratigraphic framework for the Anti-Atlas Orogen, Morocco.
1857 Journal of African Earth Sciences, v. 39, p. 217-226. Doi:10.1016/j.jafrearsci.2004.07.046
1858 Thompson, R.N., Dickin, A.P., Gibson, I.L., Morrison, M.A., 1982. Elemental fingerprints of
1859 isotopic contamination of Hebridean Palaeocene mantle-derived magmas by Archaean sial.
1860 Contributions to Mineralogy and Petrology, v. 79, p. 159–168. Doi:10.1007/bf01132885
1861 Toummite, A., Liégeois, J.P., Gasquet, D., Bruguier, O., Beraaouz, E.H., Ikenne, M., 2013. Field,
1862 geochemistry and Sr-Nd isotopes of the pan-African granitoids from the Tifnoute Valley (Sirwa,
1863 anti-atlas, Morocco): a post-collisional event in a metacratonic setting. Mineral. Petrol. 107,
1864 739–763. Doi:10.1007/s00710-012-0245-3
1865 Triantafyllou, A., 2015. Evolution géodynamique d'un arc insulaire néoprotérozoïque de l'Anti -
1866 Atlas marocain : caractérisation des processus de croissance intra-océanique et d'accrétion. PhD
1867 thesis. Université de Nantes, Nantes, France, 390 p.
1868 Triantafyllou, A., Berger, J., Baele, J.M., Bruguier, O., Diot, H., Ennih, N., Monnier, C., Plissart,
1869 G., Vandycke, S., Watlet, A., 2018. Intra-oceanic arc growth driven by magmatic and tectonic
1870 processes recorded in the Neoproterozoic Bougmane Arc complex (Anti-Atlas, Morocco).
1871 Precambrian Res. 304, 39–63. Doi:10.1016/j.precamres.2017.10.022
1872 Triantafyllou, A., Berger, J., Baele, J.-M., Diot H., Ennih, N., Plissart, G., Monnier, C., Watlet, A.,
1873 Bruguier, O., Spagna, P., Vandycke S., 2016. The Tachakoucht-Iriri-Tourtit arc complex
1874 (Moroccan Anti-Atlas): Neoproterozoic records of polyphased subduction-accretion dynamics
1875 during the Pan-African orogeny. Journal of Geodynamics, v. 98, p.81–103.
1876 Doi:10.1016/j.jog.2015.07.004
1877 Triantafyllou, A., Berger, J., Baele, J.-M., Mattielli, N., Ducea, M. N., Sterckx, S., Samson, S.,
1878 Florent Hodel, F., Ennih, N., 2020. Episodic magmatism during the growth of a
1879 Neoproterozoic oceanic arc (Anti-Atlas, Morocco). Precambrian Research, 105610.
1880 Doi:10.1016/j.precamres.2020.105610

1881 Triantafyllou, A., Hodel, F., Berger, J., Macouin, M., Baele, J.M., Mattielli, N., Monnier, C., Ducea
1882 Mihai, N., Poujol, M., Langlade, J., Trindade, R. I. F., 2019. The Bou azzer and Sirwa ophiolites
1883 (Anti-Atlas, Morocco): insight into polyphased subduction-accretion dynamics during
1884 Neoproterozoic times. GSA Annual Meeting, Phoenix, Arizona, USA. Doi:
1885 10.1130/abs/2019AM-336212
1886 Tuduri, J., Chauvet, A., Barbanson, L., Labriki, M., Dubois, M., Trapy, P.-H., Lahfid, A., Poujol,
1887 M., Melleton, J., Badra, L., Ennaciri, A., Maacha, L., 2018. Structural control, magmatic-
1888 hydrothermal evolution and formation of hornfels-hosted, intrusion-related gold deposits: Insight
1889 from the Thaghassa deposit in Eastern Anti-Atlas, Morocco. Ore Geology Reviews, 97, 171–
1890 198. doi:10.1016/j.oregeorev.2018.04.023
1891 Vaasjoki, M., Tapani Rämö, O., Sakko, M., 1991. New U-Pb ages from the Wiborg rapakivi area:
1892 constraints on the temporal evolution of the rapakivi granite-anorthosite-diabase dyke
1893 association of southeastern Finland. Precambrian Research, 51(1-4), 227–243.
1894 Doi:10.1016/0301-9268(91)90102-g
1895 Villeneuve, M., 2005. Paleozoic basins in West Africa and the Mauritanide thrust belt. Journal of
1896 African Earth Sciences, 43(1-3), 166–195. Doi:10.1016/j.jafrearsci.2005.07.012
1897 Waldron, J.W.F., White, C.E., Barr, S.M., Simonetti, A., Heaman, L.M., 2009. Provenance of the
1898 Meguma terrane, Nova Scotia: rifted margin of early Paleozoic Gondwana. Canadian Journal
1899 of Earth Sciences, v. 46, p. 1–8. Doi:10.1139/e09-004
1900 Walsh, G.J., Aleinikoff, J.N., Benziane, F., Yazidi, A., Armstrong, T.R., 2002. U-Pb zircon
1901 geochronology of the Paleoproterozic Tagragra de Tata inlier and its Neoproterozoic cover,
1902 western Anti-Atlas, Morocco. Precambrian Research, v. 117, p. 1–20. Doi:10.1016/s0301-
1903 9268(02)00044-x
1904 Walsh, G.J., Benziane, F., Aleinikoff, J.N., Harisson, R.W., Yazidi, A., Burton, W.C., Quick, J.E.,
1905 Saadane, A., 2012. Neoproterozoic tectonic evolution of the Jebel Saghro and Bou Azer-El

1906 Graara inliers, eastern and central Anti-Atlas, Morocco. Precambrian Research, v. 216–219, p.
1907 23–62. Doi:10.1016/j.precamres.2012.06.010
1908 Wang, C., Zhang, J.-H., Li, M., Li, R.-S., Peng, Y., 2015. Generation of ca. 900–870Ma bimodal
1909 rifting volcanism along the southwestern margin of the Tarim Craton and its implications for the
1910 Tarim–North China connection in the early Neoproterozoic. Journal of Asian Earth Sciences,
1911 113, 610–625. doi:10.1016/j.jseaes.2015.08.002
1912 Weil, A.B., Van der Voo, R., MacNiocall, C., Meert, J.G., 1998. The Proterozoic supercontinent
1913 Rodinia: paleomagnetically derived reconstructions for 1100–800 Ma. Earth Planet: Science
1914 Letters, v. 154, p. 13–24. Doi:10.1016/s0012-821x(97)00127-1
1915 Williams, I.S., 1998. U-Th-Pb geochronology by ion microprobe. In: McKibben, M.A., Shanks,
1916 W.C., Riley, W.I. (Eds.), Applications of Microanalytical Techniques to Understanding
1917 Mineralising Processes. Reviews in Economic Geology, v.7, p. 1–35.
1918 https://doi.org/10.5382/Rev.07.01
1919 Willner, A.P., Barr, S.M., Gerdes, A., Massonne, H.-J., White, C.E., 2013. Origin and evolution of
1920 Avalonia: evidence from U–Pb and Lu–Hf isotopes in zircon from the Mira terrane, Canada, and
1921 the Stavelot–Venn Massif, Belgium. Journal of the Geological Society of London: v. 170, p.
1922 769–784. Doi:10.1144/jgs2012-152
1923 Winchester, J. A., and Floyd, P. A., 1977. Geochemical discrimination of different magma series
1924 and their differentiation products using immobile elements. Chemical Geology, 20, 325–343.
1925 doi:10.1016/0009-2541(77)90057-2
1926 Youbi N., Söderlund U., Ernst R. E., Ait Malek M., Barzouk A., Ait Lahna A., Palassia M., Gong
1927 Z., Evans D., Wen B., Jing X-Q., Boumehdi M. A., Ikenne M., Bensalah M. K., Admou H.,
1928 Bajddi A., Maacha L, 2019. Ca. 1.65 Ga mafic sills emplaced into the quartzite of jbel Lkest
1929 from Kerdous Inlier, Anti-Atlas, West African craton, Morocco: additional evidence that the
1930 basal part of Taghdout group is nearly 1 Ga older than previously thought. The 7 International
1931 Science Conference Abstracts. Tomsk: p.165.

1932 Youbi, N., Bouougri, El H., Ait Lahna, A., Kouyaté, D., Tassinari, C.C.G., Admou, H., Mata, J.,
1933 Boumehdi, M.A., Bensalah, M.K., Basei, M., A., S., Sato., K., Ernst, R.E., Söderlund, U., Chaib,
1934 L., Bairouk L., Gärtner, A., Linnemann, U., Ikenne M., Bodinier, J-L., 2018. A grande província
1935 ígnea de Iguerda-Taifast (ca. 885 Ma) no Anti-Atlas (Marrocos-Cratão Oeste africano): os
1936 enxames de diques máficos de Ifzwane e os vulcanitos máficos do grupo Tizi n'Taghatine. X
1937 Congresso National de geologia, Acçores, Portugal, Vulcânica, v.2, p.21.
1938 Youbi, N., Ernst, R.E., Söderlund, U., Boumehdi, M.A., Ait Lahna, A., Tasssinari, C.C.G., El
1939 Moume, W., Bensalah, M.K., 2020. The Central Iapetus magmatic province: An updated review
1940 and link with the ca. 580 Ma Gaskiers glaciation. In: Thierry Adatte; David P.G. Bond; Gerta
1941 Keller (Editors). Mass Extinctions, Volcanism, and Impacts: New Developments. Geological
1942 Society of America Special Papers, Volume 544. Published: December 31, 2019 DOI:
1943 https://doi.org/10.1130/2020.2544(02)
1944 Youbi, N., Kouyaté, D., Söderlund, U., Ernst, RE., Soulaimani, A., Hafid, A., Ikenne, M., El Bahat,
1945 A., Bertrand, H., Chaham, KR., Ben Abbou, M., Mortaji, A., El Ghorfi, M., Zouhair, M., El
1946 Janati, M., 2013. The 1750 Ma Magmatic Event of the West African Craton (Anti-Atlas,
1947 Morocco). Precambrian Research, v. 236, p.106–123. Doi:10.1016/j.precamres.2013.07.003
1948 Youbi, N., Martins, L. T., Munhá, J. M., Ibouh, H., Madeira, J., Ait Chayeb, H., El Boukhari, A.,
1949 2003. The Late Triassic-Early Jurassic Volcanism of Morocco and Portugal in the Framework of
1950 the Central Atlantic Magmatic province: An Overview. In: Hames, W. E., Machone, J. G.,
1951 Renne, P. R., Ruppel, C. (Eds.) The Central Atlantic Magmatic Province: Insights from
1952 Fragments of Pangea. American Geophysical Union Geophysical Monograph Series, 136, 179-
1953 207. Doi:10.1029/136gm010
1954 Zhang, C.-L., Ye, X.-T., Ernst, R. E., Zhong, Y., Zhang, J., Li, H.-K., Long, X.-P., 2019. Revisiting
1955 the Precambrian evolution of the Southwestern Tarim terrane: implications for its role in
1956 Precambrian supercontinents. Precambrian Research. Doi:10.1016/j.precamres.2019.01.018
1957

Table 1. Site location and summary of the data for the studied samples. The names of units and formations are sensu Bouougri and Saquaque (2004).

Sample ID	Coordinates (GPS WGS84)	Inlier/ Subinlier	Lithology	Units/Formations/Suites	Methodes/ Mineral	Number of spots	U-Pb zircon Age (Ma)
BA24	N 30°23'7.90", W 6°30'33.40"	Bou Azzer El Graara/Bleida	Fine-grained sandstone	Upper Unit/Bleida Formation	SHRIMPII/Zircon	44 spots	1855 ± 6.5 - 977 ± 10*
ALBL29	N 30°20'19.28", W 6°24'48.70"	Bou Azzer El Graara/Bleida	Medium to coarse-grained quartzite	Middle Unit/Tachdamt Formation	LA-ICP-MS/Zircon	96 spots	1060 ± 5.5 - 930 ± 12*
BA21	N 30°29'11.40", W 6°52'44.00"	Bou Azzer El Graara/Tachdamt	Medium-grained quartzite	Lower Unit/Agoummy Formation	SHRIMPII/Zircon	55 spots	1818 ± 6.4*
TA1	N 30°36'43.6", W 7°17'13.4"	Zenaga	Coarse-grained to a fine-grained microlitic porphyric dolerite	Ifzwane Suite	SHRIMPII/Zircon	18 spots	1676 ± 37**
TG-15-1	N 30°35'11.76", W 7°20'06.92"	Zenaga	Purple coarse-grained and quartz rich metasiltstone	Lower Unit/Tasserda Formation	LA-ICP-MS/Zircon	99 spots	2049.3 ± 4.6*

* U-Pb detrital zircon, maximum depositional age

** U-Pb age emplacement

SHRIMPII: Sensitive High Resolution Ion Microprobe

LA-ICP-MS: Laser Ablation Inductively Coupled Plasma Mass Spectrometry

ID: Identification

GPS WGS84: The Global Positioning System (GPS) uses the World Geodetic System (WGS84) as its reference coordinate system.

Table 1. Site location and data summary of the investigated samples. The names of Units and Formations are sensu Bouougri and Saquaque (2004).

Sample ID	Coordinates (GPS WGS84)	Inlier/ Subinlier	Lithology	Units/Formations/Suites	Methodes/ Mineral	Number of spots	U-Pb zircon Age (Ma)
BA 24	N 30°23'7.90", W 6°30'33.40"	Bou Azzer El Graara/Bleida	Fine-grained sandstone	Upper Unit/Bleida Formation	SHRIMPII/ Zircon	44 spots	1957 ± 63*
ALBL29	N 30°20'19.28", W 6°24'48.70"	Bou Azzer El Graara/Bleida	Medium to coarse-grained quartzarenite	Middle Unit/Tachdamt Formation	LA-ICP-MS/Zircon	96 spots	1060 ± 5.5*
BA 21	N 30°29'11.40", W 6°52'44.00"	Bou Azzer El Graara/Tachdamt	Medium-grained quartzarenite	Lower Unit/Agoummy Formation	SHRIMPII/ Zircon	54 spots	1818 ± 6.4*
TA 1	N 30°36'43.6", W 7°17'13.4"	Zenaga	Coarse-grained to a fine-grained microlitic porphyric doleritie	Ifzwane Suite	SHRIMPII/ Zircon	18 spots	1639 ± 34 **
TG-15-1	N 30°35'11.76", W 7°20'06.92"	Zenaga	Purple coarse-grained and quartz rich siltstone	Lower Unit/Tassarda Formation	LA-ICP-MS/Zircon	99 spots	2047 ± 9.7*

* U-Pb detrital zircon, maximum depositional age

** U-Pb age emplacement

SHRIMPII: Sensitive High Resolution Ion Microprobe

LA-ICP-MS: Laser Ablation Inductively Coupled Plasma Mass Spectrometry

ID: Identification

GPS WGS84: The Global Positioning System (GPS) uses the World Geodetic System (WGS84) as its reference coordinate system.

Table 2. Representative whole-rock major and trace element geochemical data for dykes and sills from the Zenaga, Agadir Melloul, Iguerda-Taïfast, and Tagragra of Akka inliers including the dated dykes, samples TA1 from the Zenaga Inlier (1676 ± 37 Ma; this work), DZ 36 (1640 ± 2 Ma and 1641 ± 3 Ma; Kouyaté et al., 2013) and DZ 40 (1656 ± 9 Ma; Kouyaté et al., 2013) from the Zenaga Inlier (Kouyaté et al, 2013), and AMHA069 (1654 ± 16 Ma; Kouyaté et al, 2013) from the Agadir Melloul Inlier. The geochemical data are from unpublished theses (Hafid, 1999; Mortaji, 1989) and published papers (Hafid et al., 2001; El Aouli et al., 2010; Youbi et al., 2013). Fe2O3t= total Fe expressed as Fe2O3. Loss-on-ignition (L.O.I.) determined by sample weight loss at 1000◦C.

Sample	TA1	TA2	DZ36	DZ40	AMHA69	ZEN-4	ZEN-13	ZEN-1	ZEN-11	IT-5	IT-7	IT-12	IT-13	NC40	NC379	NC314aMor	NC 361
Inlier	Zenaga	Zenaga	Zenaga	Zenaga	Agadir Melloul	Zenaga	Zenaga	Zenaga	Zenaga	Iguerda-Taïfast	Iguerda-Taïfast	Iguerda-Taïfast	Iguerda-Taïfast	Tagragra of Akka	Tagragra of Akka	Tagragra of Akka	Tagragra of Akka
Latitude N	30°36'43.6"	30°36'43.7"															
Longitude W	7°17'13.4"	7°17'13.3"															
Orientation	N45°	N45°	N125°	N140°		N170°	N125°	N85°	N170°		N00°	N30°	N45°	N50°-N110°	N50°-N110°	N30°-N160°	N30°-N160°
Ages (Ma)	1676 ± 37		1640 ± 2/ 1641 ± 3	1656 ± 9	1654 ± 16												
Reference	(this work)	(this work)	Kouyaté (2013)	Kouyaté (2013)	Kouyaté (2013)	Hafid (1999)	Hafid (1999)	Hafid (1999)	Hafid (1999)	Hafid (1999)	Hafid (1999)	Hafid (1999)	Hafid (1999)	Mortaji (1989)	Mortaji (1989)	Mortaji (1989)	Mortaji (1989)
SiO2	49.31	49.73	50.66	50.84	45.78	48.56	49.71	48.38	48.30	49.12	49.98	49.00	47.98	50.85	47.58	44.35	49.18
TiO2	1.64	1.58	0.85	0.73	0.79	2.66	2.09	1.98	1.64	2.05	2.52	2.17	2.06	0.91	1.93	2.86	2.99
Al2O3	13.79	13.48	14.55	14.61	13.73	13.58	14.08	13.97	13.97	13.50	13.67	13.06	13.20	14.72	13.62	15.25	12.75
Fe2O3t	14.51	14.35	10.27	9.78	9.50	14.43	14.83	13.71	13.16	15.17	15.02	14.87	15.54	12.60	15.63	16.53	16.06
MnO	0.23	0.23	0.16	0.18	0.25	0.17	0.19	0.16	0.20	0.26	0.17	0.23	0.26	0.19	0.20	0.18	0.12
MgO	6.34	6.68	7.31	7.55	9.87	6.61	5.76	6.55	7.73	5.28	5.24	5.91	6.24	6.69	6.29	5.95	5.21
CaO	6.70	6.20	10.01	11.27	12.18	8.71	8.51	10.18	10.34	8.52	6.98	10.04	8.40	7.22	8.82	7.16	4.36
Na2O	3.26	4.06	2.17	1.94	2.49	2.40	2.59	1.86	2.10	2.46	2.45	1.91	2.73	3.36	2.04	2.58	2.63
K2O	0.96	0.32	0.74	0.62	0.29	0.54	0.78	0.32	0.64	1.15	1.79	0.36	0.95	0.14	0.77	1.04	1.31
P2O5	0.14	0.19	0.07	0.08	0.06	0.24	0.33	0.18	0.15	0.43	0.36	0.19	0.17	0.14	0.24	0.69	0.50
L.O.I.	2.47	3.04	2.48	2.38	4.37	2.35	2.18	2.67	2.02	1.46	1.73	2.07	1.99	3.67	2.69	3.80	5.00
Total	99.34	99.84	99.49	100.25	99.68	100.25	101.05	99.96	100.25	99.40	99.91	99.81	99.52	100.49	99.81	100.39	100.11
V	343.24	317.91	240.00	233.70	223.00	326.90	317.14	306.30	332.92	290.97	339.52	400.00	413.57	278.00	367.00	189.00	367.00
Cr	18.95	18.83	307.70	410.10	802.70	189.80	96.76	197.10	181.59	114.14	126.86	113.12	180.31	139.00	114.00	180.00	118.00
Co	51.53	54.75	46.00	44.67	57.36	43.13	50.47	40.43	55.85	44.43	46.07	44.10	43.62	57.00	54.00	46.00	46.00
Ni	39.42	37.22	143.00	185.20	178.30	117.00	69.71	94.16	121.74	44.20	64.28	79.64	92.72	55.00	95.00	109.00	65.00
Zn	126.00	158.84	90.36	92.06	228.20	150.20	152.60	119.80	161.27	131.25	129.48	134.44	155.27		116.00	153.00	62.00
Rb	35.95	8.84	26.89	20.34	10.88	16.85	20.90	8.44	19.70	63.40	68.05	24.02	45.85	10.00	43.00	29.00	81.00
Sr	192.75	220.51	215.20	196.60	191.10	391.10	410.50	269.90	256.15	372.90	370.30	253.56	200.55	593.00	185.00	247.00	120.00
Y	23.11	23.50	16.27	14.16	12.11	28.80	30.91	27.12	22.87	37.00	28.97	29.81	28.79	19.46	30.85	41.74	26.22
Zr	88.44	93.50	69.43	56.11	40.35	151.90	123.40	87.81	75.23	142.31	178.72	111.29	108.45		122.00	293.00	167.00
Nb	6.80	7.02	4.56	3.64	2.99	13.10	7.60	4.62	3.77	8.57	15.77	7.74	8.29		10.00	36.00	20.00
Ba	238.53	148.42	146.60	342.30	43.29	169.70	482.90	70.51	113.54	762.92	700.14	224.48	425.88	103.00	274.00	528.00	418.00

La	8.50	9.31	9.45	7.77	3.82	18.75	25.71	8.90	8.06	26.09	30.90	7.84	8.38	10.47	9.79	31.79	18.87
Ce	20.35	22.54	20.54	16.79	8.92	50.90	63.10	23.08	19.89	59.41	70.09	21.36	21.78	27.83	28.15	70.15	45.07
Pr	2.87	3.24	2.51	2.06	1.24	5.75	6.45	3.18	2.75	7.76	8.92	3.23	3.28				
Nd	13.34	15.24	11.26	9.54	6.45	25.95	26.89	14.22	12.43	33.49	37.03	16.27	15.26	13.43	17.19	40.17	27.38
Sm	3.65	4.05	2.74	2.29	1.84	6.44	6.11	4.55	3.81	7.32	7.46	4.56	4.44	3.60	5.26	8.75	7.06
Eu	1.36	1.31	0.87	0.78	0.68	2.21	2.07	1.56	1.31	1.96	2.42	1.68	1.53	1.01	1.52	1.87	2.32
Gd	3.98	4.24	2.81	2.42	2.11	6.61	6.10	4.47	3.55	6.89	7.19	5.96	5.53	3.40	5.49	7.93	6.94
Tb	0.66	0.69	0.47	0.39	0.35	1.07	0.99	0.84	0.67	1.06	1.05	0.96	0.93				
Dy	4.27	4.38	2.87	2.44	2.14	5.68	5.75	5.02	4.05	6.69	5.91	5.58	5.70	3.35	5.65	7.94	5.55
Ho	0.89	0.93	0.57	0.49	0.43	1.11	1.16	1.03	0.83	1.41	1.18	1.13	1.19				
Er	2.38	2.41	1.61	1.39	1.19	2.68	3.00	2.66	2.24	3.66	2.99	3.04	3.08	1.99	2.97	4.35	2.55
Tm	0.34	0.34	0.24	0.21	0.18	0.37	0.44	0.39	0.32	0.56	0.42	0.45	0.46				
Yb	2.21	2.26	1.62	1.38	1.14	2.39	2.70	2.45	1.88	3.34	2.53	2.68	2.77	2.01	2.82	4.12	2.04
Lu	0.34	0.36	0.25	0.22	0.18	0.35	0.39	0.36	0.29	0.51	0.37	0.40	0.42	0.37	0.46	0.67	0.36
Cu	279.90	20.75	67.27	60.43	193.30	22.64	61.31	68.13	10.68	73.30	20.24	200.74	18.26	15.00	148.00	33.00	18.00
U	0.28	0.32	0.53	0.41	0.14	0.54	0.47	0.24	0.25	0.40	1.65	0.18	0.21				
Th	0.81	0.92	1.69	1.33	0.37	1.77	2.42	0.89	0.79	1.70	3.65	0.64	0.80				
Ta	0.51	0.54	0.36	0.28	0.23	0.82	0.24	0.19	0.20	0.48	1.00	0.59	0.59				
Hf	2.45	2.65	2.00	1.61	1.16	3.86	3.03	2.29	1.95	3.99	4.92	3.36	3.29				
Sc	48.93	48.88				32.09	41.73	39.63	48.49	38.97	28.38	38.58	41.10		45.00	35.00	30.00
Ga	20.82	19.25	16.88	15.52	13.62	21.02	21.94	18.46	19.54	21.78	22.31	19.06	18.76				
Pb	4.00	4.47	8.16	16.85	8.78	7.07	9.65	5.42	5.55	8.50	6.98	5.52	5.90				
Cs	0.87	0.45	1.17	0.65	0.30	1.05	1.15	0.73	1.21	7.09	1.39	1.41	2.00				

Sample	Inlier	Latitude N	Logitude W	Orientation	Ages (Ma)	Reference	SiO2	TiO2	Al2O3	Fe2O3t	MnO	MgO	CaO	Na2O	K2O	P2O5	L.O.I.	Total	V	Cr	Co	Ni	Zn	Rb	Sr	Y	Zr	Nb	Ba	La	Ce	Pr	Nd	Sm	Eu	Gd	Tb	Dy	Ho	Er	Tm	Yb	Lu	Cu	U	Th	Ta	Hf	Sc	Ga	Pb	Cs
TA1	Zenaga	30°36'43.6"	7°17'13.4"	N45°	1639 ± 34 Ma	(this work)	49.31	1.64	13.79	14.51	0.23	6.34	6.70	3.26	0.96	0.14	2.47	99.34	343.24	18.95	51.53	39.42	126.00	35.95	192.75	23.11	88.44	6.80	238.53	8.50	20.35	2.87	13.34	3.65	1.36	3.98	0.66	4.27	0.89	2.38	0.34	2.21	0.34	279.90	0.28	0.81	0.51	2.45	48.93	20.82	4.00	0.87
TA2	Zenaga	30°36'43.7"	7°17'13.3"	N30°		(this work)	49.73	1.58	13.48	14.35	0.23	6.68	6.20	4.06	0.32	0.19	3.04	99.84	317.91	18.83	54.75	37.22	158.84	8.84	220.51	23.50	93.50	7.02	148.42	9.31	22.54	3.24	15.24	4.05	1.31	4.24	0.69	4.38	0.93	2.41	0.34	2.26	0.36	20.75	0.32	0.92	0.54	2.65	48.88	19.25	4.47	0.45
DZ36	Zenaga			N125°	1640 ± 2 Ma/ 1641 ± 3 Ma	Kouyaté (2013)	50.7	0.85	14.55	10.27	0.16	7.31	10	2.17	0.74	0.07	2.48	99.49	240	307.7	46	143	90.36	26.9	215.2	16.3	69.43	4.56	146.6	9.45	20.5	2.51	11.3	2.74	0.87	2.81	0.47	2.87	0.57	1.61	0.24	1.62	0.25	67.27	0.53	1.69	0.36	2		16.9	8.1606	1.17
DZ40	Zenaga			N140°	1656 ± 9 Ma	Kouyaté (2013)	50.8	0.73	14.61	9.78	0.18	7.55	11.3	1.94	0.62	0.08	2.38	100.3	233.7	410.1	44.7	185.2	92.06	20.3	196.6	14.2	56.11	3.64	342.3	7.77	16.8	2.06	9.54	2.29	0.78	2.42	0.39	2.44	0.49	1.39	0.21	1.38	0.22	60.43	0.41	1.33	0.28	1.61		15.5	16.847	0.65
AMHA69	Agadir Melloul				1654 ± 16 Ma	Kouyaté (2013)	45.8	0.79	13.73	9.5	0.25	9.87	12.2	2.49	0.29	0.06	4.37	99.68	223	802.7	57.4	178.3	228.2	10.9	191.1	12.1	40.35	2.99	43.29	3.82	8.92	1.24	6.45	1.84	0.68	2.11	0.35	2.14	0.43	1.19	0.18	1.14	0.18	193.3	0.14	0.37	0.23	1.16		13.6	8.7784	0.3
ZEN-4	Zenaga			N170°		Hafid (1999)	48.6	2.66	13.58	14.43	0.17	6.61	8.71	2.4	0.54	0.24	2.35	100.3	326.9	189.8	43.1	117	150.2	16.9	391.1	28.8	151.9	13.1	169.7	18.8	50.9	5.75	26	6.44	2.21	6.61	1.07	5.68	1.11	2.68	0.37	2.39	0.35	22.64	0.54	1.77	0.82	3.86	32.1	21	7.07	1.05
ZEN-13	Zenaga			N125°		Hafid (1999)	49.7	2.09	14.08	14.83	0.19	5.76	8.51	2.59	0.78	0.33	2.18	101.1	317.1	96.76	50.5	69.71	152.6	20.9	410.5	30.9	123.4	7.6	482.9	25.7	63.1	6.45	26.9	6.11	2.07	6.1	0.99	5.75	1.16	3	0.44	2.7	0.39	61.31	0.47	2.42	0.24	3.03	41.7	21.9	9.65	1.15
ZEN-1	Zenaga			N85°		Hafid (1999)	48.4	1.98	13.97	13.71	0.16	6.55	10.2	1.86	0.32	0.18	2.67	99.96	306.3	197.1	40.4	94.16	119.8	8.44	269.9	27.1	87.81	4.62	70.51	8.9	23.1	3.18	14.2	4.55	1.56	4.47	0.84	5.02	1.03	2.66	0.39	2.45	0.36	68.13	0.24	0.89	0.19	2.29	39.6	18.5	5.42	0.73
ZEN-11	Zenaga			N170°		Hafid (1999)	48.3	1.64	13.97	13.16	0.2	7.73	10.3	2.1	0.64	0.15	2.02	100.3	332.9	181.6	55.9	121.7	161.3	19.7	256.2	22.9	75.23	3.77	113.5	8.06	19.9	2.75	12.4	3.81	1.31	3.55	0.67	4.05	0.83	2.24	0.32	1.88	0.29	10.68	0.25	0.79	0.2	1.95	48.5	19.5	5.55	1.21
IT-5	Iguerda-Taïfast					Hafid (1999)	49.1	2.05	13.5	15.17	0.26	5.28	8.52	2.46	1.15	0.428	1.46	99.4	291	114.1	44.4	44.2	131.3	63.4	372.9	37	142.3	8.57	762.9	26.1	59.4	7.76	33.5	7.32	1.96	6.89	1.06	6.69	1.41	3.66	0.56	3.34	0.51	73.3	0.4	1.7	0.48	3.99	39	21.8	8.5	7.09
IT-7	Iguerda-Taïfast			N00°		Hafid (1999)	50	2.52	13.67	15.02	0.17	5.24	6.98	2.45	1.79	0.362	1.73	99.91	339.5	126.9	46.1	64.28	129.5	68.1	370.3	29	178.7	15.8	700.1	30.9	70.1	8.92	37	7.46	2.42	7.19	1.05	5.91	1.18	2.99	0.42	2.53	0.37	20.24	1.65	3.65	1	4.92	28.4	22.3	6.98	1.39
IT-12	Iguerda-Taïfast			N30°		Hafid (1999)	49	2.17	13.06	14.87	0.23	5.91	10	1.91	0.36	0.189	2.07	99.81	400	113.1	44.1	79.64	134.4	24	253.6	29.8	111.3	7.74	224.5	7.84	21.4	3.23	16.3	4.56	1.68	5.96	0.96	5.58	1.13	3.04	0.45	2.68	0.4	200.7	0.18	0.64	0.59	3.36	38.6	19.1	5.52	1.41
IT-13	Iguerda-Taïfast			N45°		Hafid (1999)	48	2.06	13.2	15.54	0.26	6.24	8.4	2.73	0.95	0.174	1.99	99.52	413.6	180.3	43.6	92.72	155.3	45.9	200.6	28.8	108.5	8.29	425.9	8.38	21.8	3.28	15.3	4.44	1.53	5.53	0.93	5.7	1.19	3.08	0.46	2.77	0.42	18.26	0.21	0.8	0.59	3.29	41.1	18.8	5.9	2
NC40	Tagragra of Akka			N50°-N110°		Mortaji (1989)	50.9	0.91	14.72	12.6	0.19	6.69	7.22	3.36	0.14	0.14	3.67	100.5	278	139	57	55		10	593	19.5			103	10.5	27.8		13.4	3.6	1.01	3.4		3.35		1.99		2.01	0.37	15								
NC379	Tagragra of Akka			N50°-N110°		Mortaji (1989)	47.6	1.93	13.62	15.63	0.2	6.29	8.82	2.04	0.77	0.24	2.69	99.81	367	114	54	95	116	43	185	30.9	122	10	274	9.79	28.2		17.2	5.26	1.52	5.49		5.65		2.97		2.82	0.46	148					45			
NC314aMor	Tagragra of Akka			N30°-N160°		Mortaji (1989)	44.4	2.86	15.25	16.53	0.18	5.95	7.16	2.58	1.04	0.69	3.8	100.4	189	180	46	109	153	29	247	41.7	293	36	528	31.8	70.2		40.2	8.75	1.87	7.93		7.94		4.35		4.12	0.67	33					35			
NC 361	Tagragra of Akka			N30°-N160°		Mortaji (1989)	49.2	2.99	12.75	16.06	0.12	5.21	4.36	2.63	1.31	0.5	5	100.1	367	118	46	65	62	81	120	26.2	167	20	418	18.9	45.1		27.4	7.06	2.32	6.94		5.55		2.55		2.04	0.36	18					30			

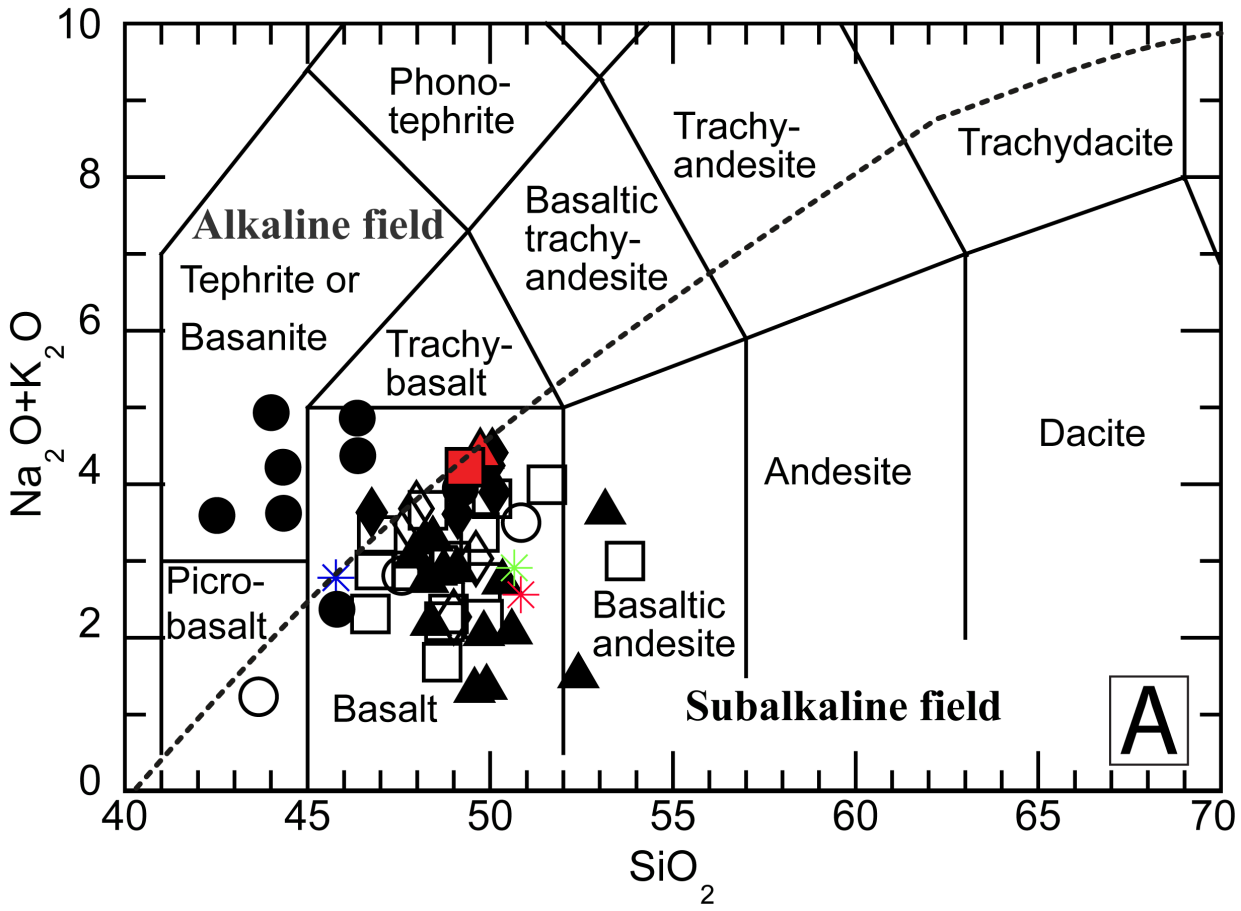
Phono-
tephrite
Trachy-
andesite
Trachydacite
Alkaline field
Tephrite or
Basanite
Basaltic
trachy-
andesite
Trachy-
basalt
Dacite
Andesite
Picro-
basalt
Basaltic
andesite
Basalt
Subalkaline field
A
Na2O+K2O
SiO2
0
2
4
6
8
10
40
45
50
55
60
65
70

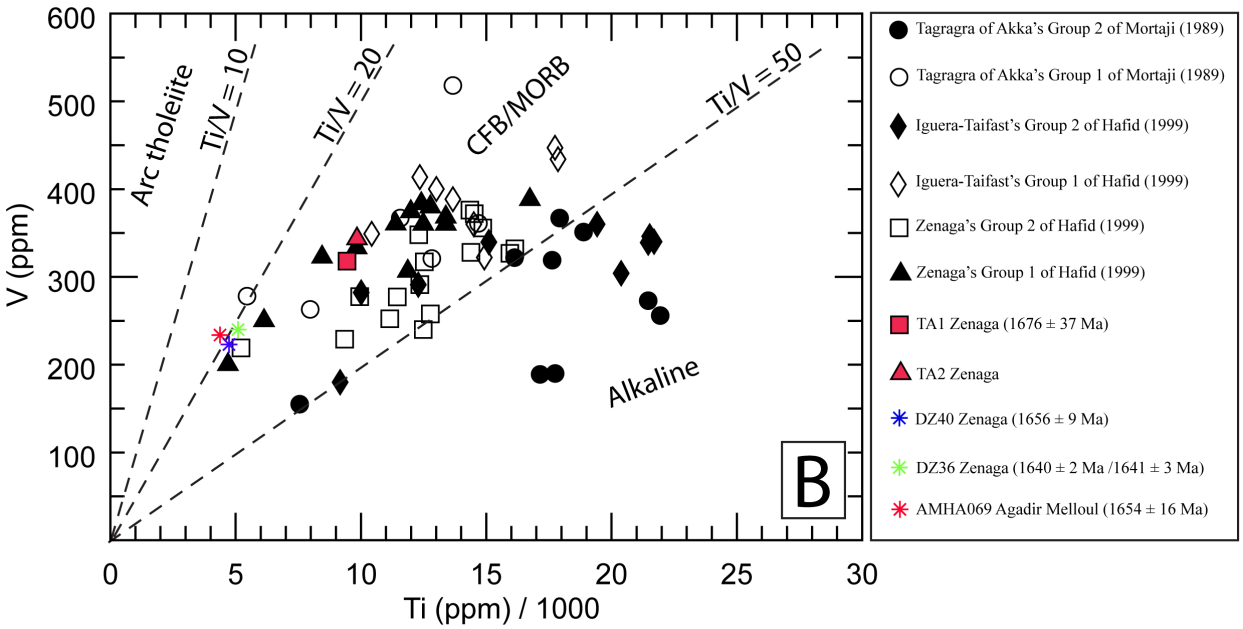

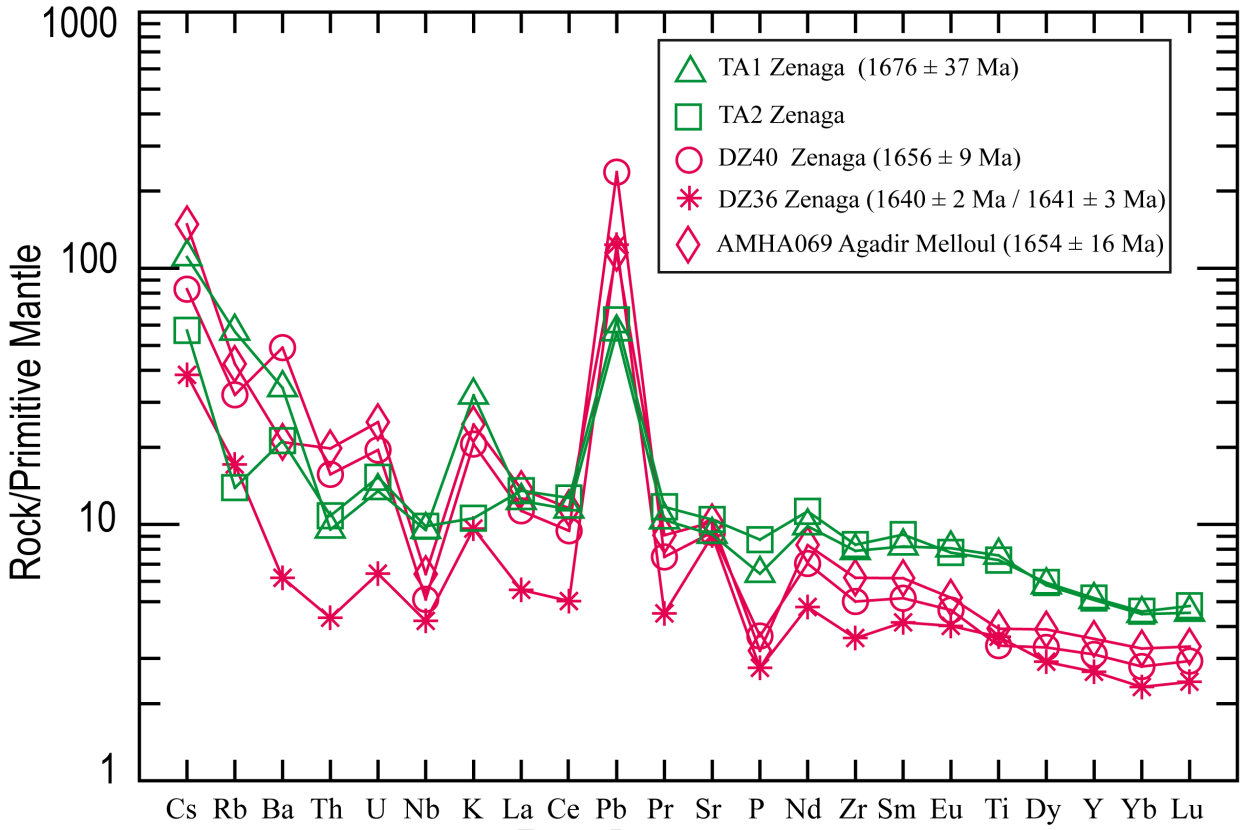
1000
100
10
1
Rock/Primitive Mantle
TA1 Zenaga (1676 ± 37 Ma)
TA2 Zenaga
DZ40 Zenaga (1656 ± 9 Ma)
DZ36 Zenaga (1640 ± 2 Ma / 1641 ± 3 Ma)
AMHA069 Agadir Melloul (1654 ± 16 Ma)
Cs Rb Ba Th U Nb K La Ce Pb Pr Sr P Nd Zr Sm Eu Ti Dy Y Yb Lu

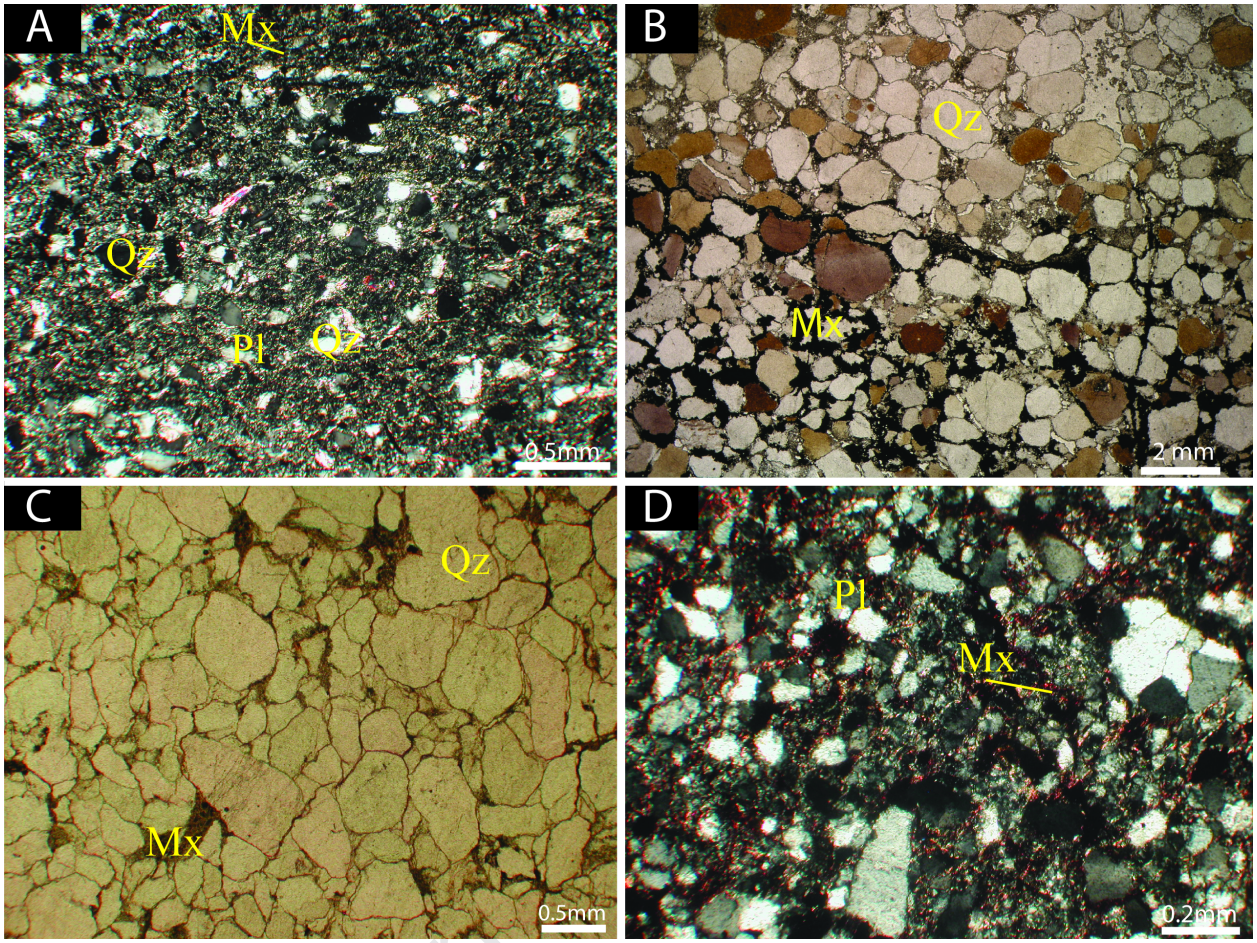

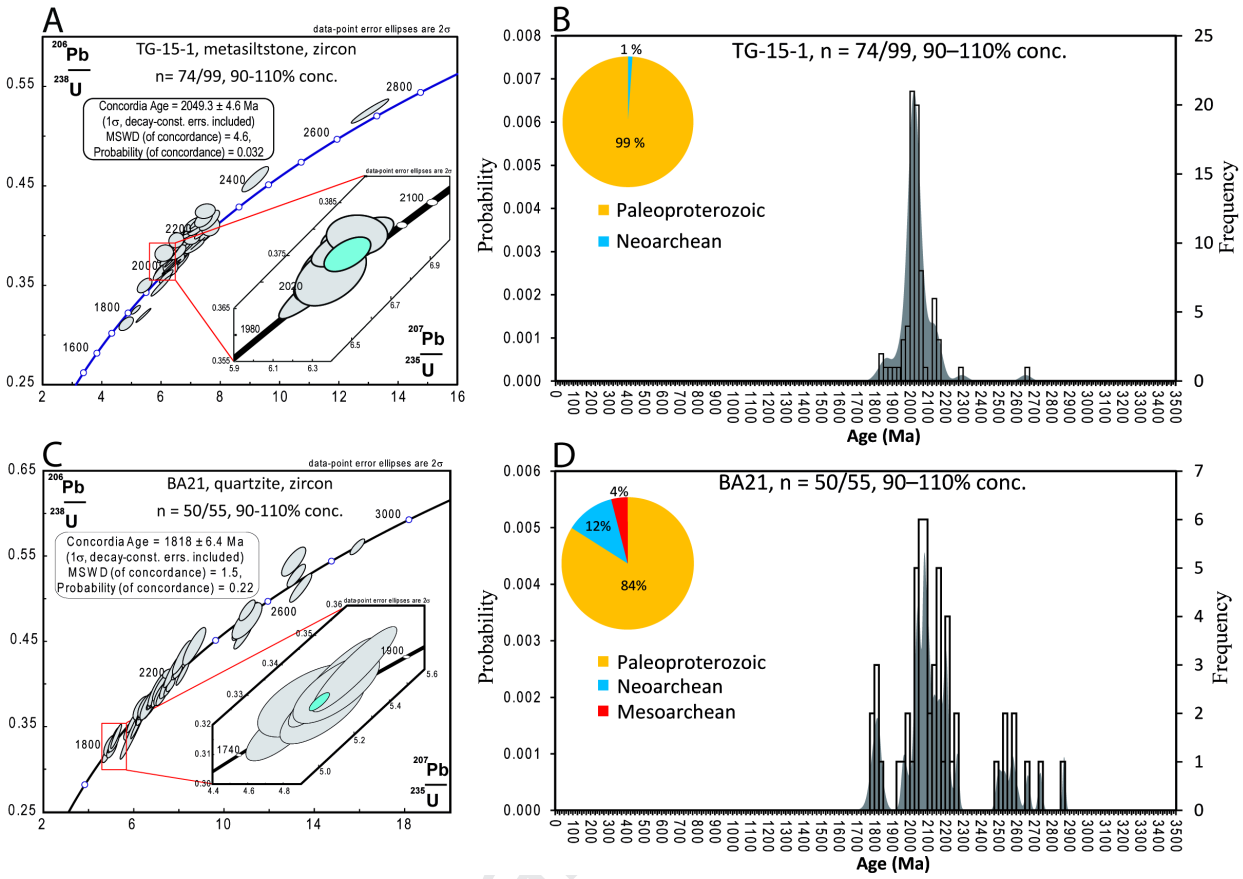
A
data-point error ellipses are 2σ
TG-15-1, metasiltstone, zircon
n= 74/99, 90-110% conc.
Concordia Age = 2049.3 ± 4.6 Ma
(1σ, decay-const. errs. included)
MSWD (of concordance) = 4.6,
Probability (of concordance) = 0.032
B
TG-15-1, n = 74/99, 90–110% conc.
1 %
99 %
Paleoproterozoic
Neoarchean
Probability
Frequency
Age (Ma)
C
data-point error ellipses are 2σ
BA21, quartzite, zircon
n = 50/55, 90-110% conc.
Concordia Age = 1818 ± 6.4 Ma
(1σ, decay-const. errs. included)
MSWD (of concordance) = 1.5,
Probability (of concordance) = 0.22
D
BA21, n = 50/55, 90–110% conc.
4%
12%
84%
Paleoproterozoic
Neoarchean
Mesoarchean
Probability
Frequency
Age (Ma)

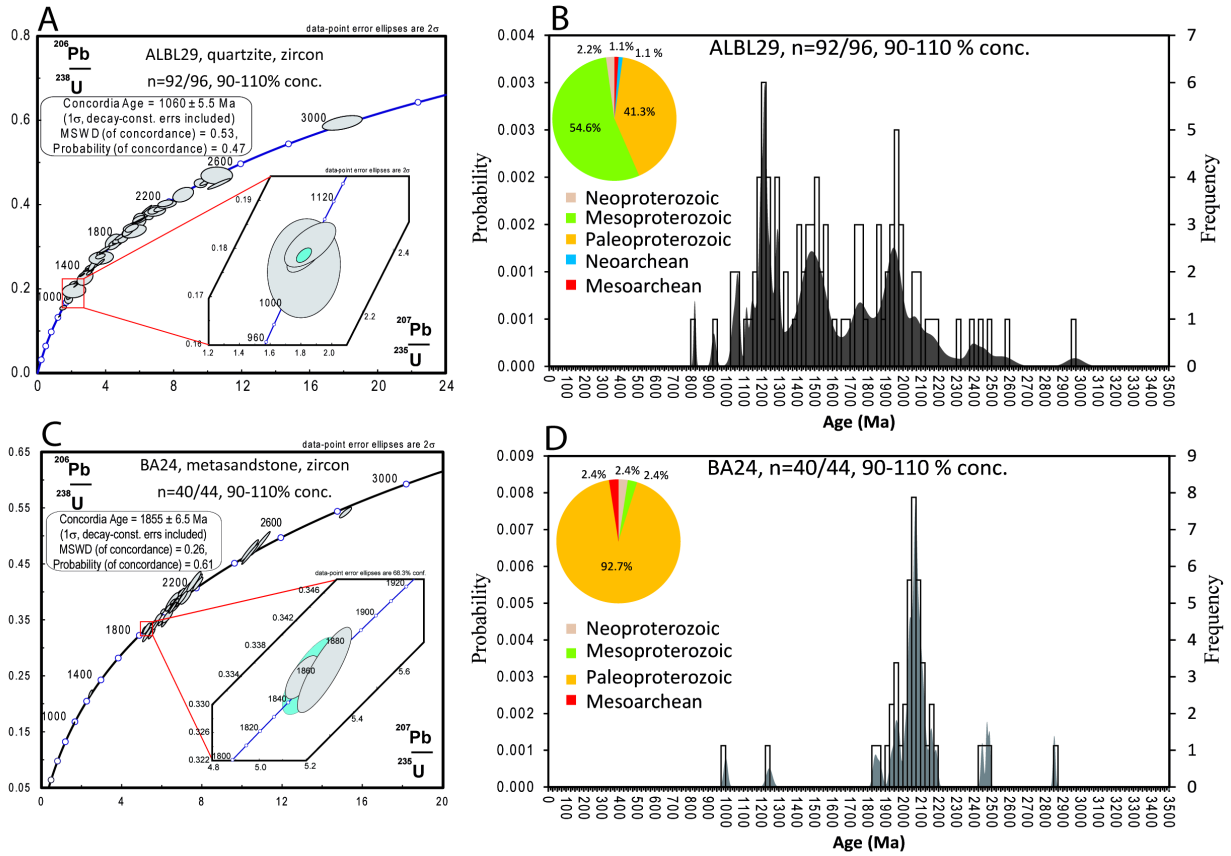
A
data-point error ellipses are 2σ
ALBL29, quartzite, zircon
n=92/96, 90-110% conc.
Concordia Age = 1060 ± 5.5 Ma
(1σ, decay-const. errs included)
MSWD (of concordance) = 0.53,
Probability (of concordance) = 0.47
B
ALBL29, n=92/96, 90-110 % conc.
2.2%
1.1%
1.1 %
54.6%
41.3%
Neoproterozoic
Mesoproterozoic
Paleoproterozoic
Neoarchean
Mesoarchean
Probability
Frequency
Age (Ma)
C
data-point error ellipses are 2σ
BA24, metasandstone, zircon
n=40/44, 90-110% conc.
Concordia Age = 1855 ± 6.5 Ma
(1σ, decay-const. errs included)
MSWD (of concordance) = 0.26,
Probability (of concordance) = 0.61
D
BA24, n=40/44, 90-110 % conc.
2.4%
2.4%
2.4%
92.7%
Neoproterozoic
Mesoproterozoic
Paleoproterozoic
Mesoarchean
Probability
Frequency
Age (Ma)

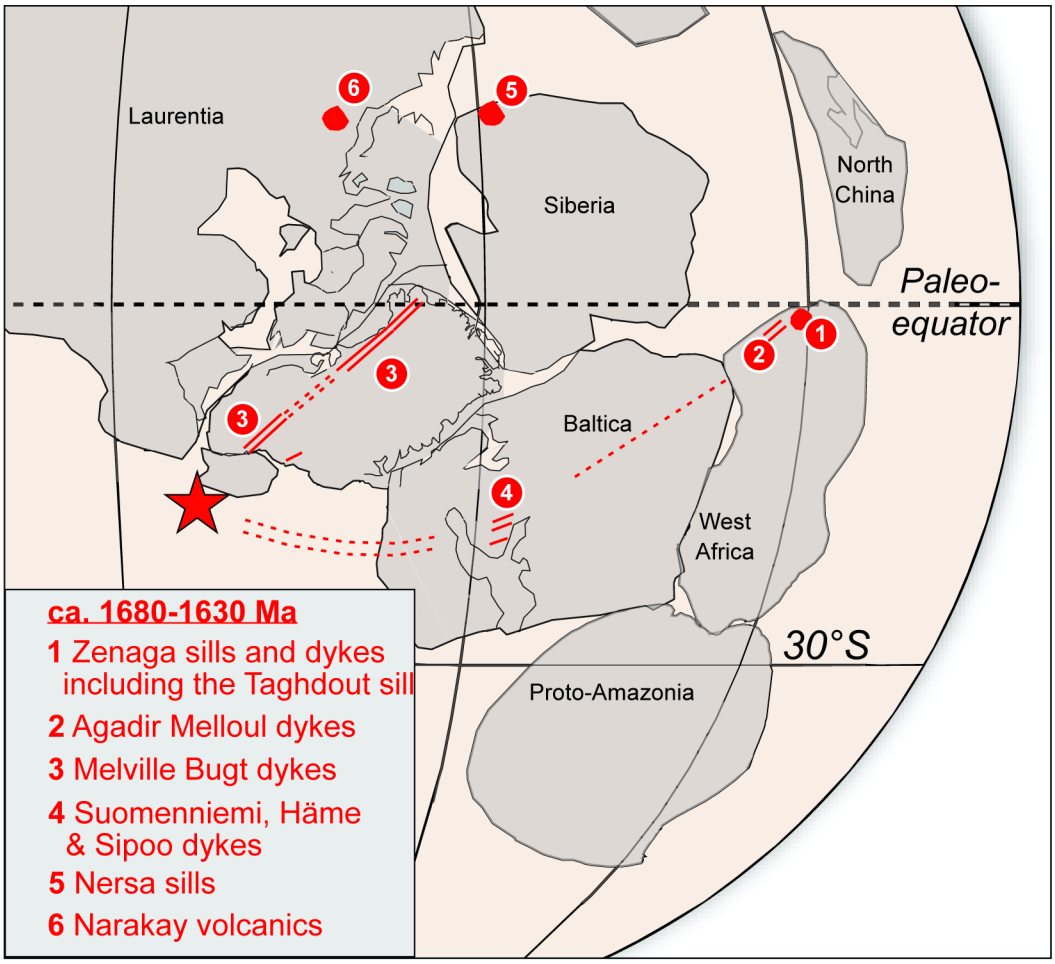
Laurentia
Siberia
North China
Paleo-equator
Baltica
West Africa
30°S
Proto-Amazonia
ca. 1680-1630 Ma
1 Zenaga sills and dykes including the Taghdout sill
2 Agadir Melloul dykes
3 Melville Bugt dykes
4 Suomenniemi, Häme & Sipoo dykes
5 Nersa sills
6 Narakay volcanics

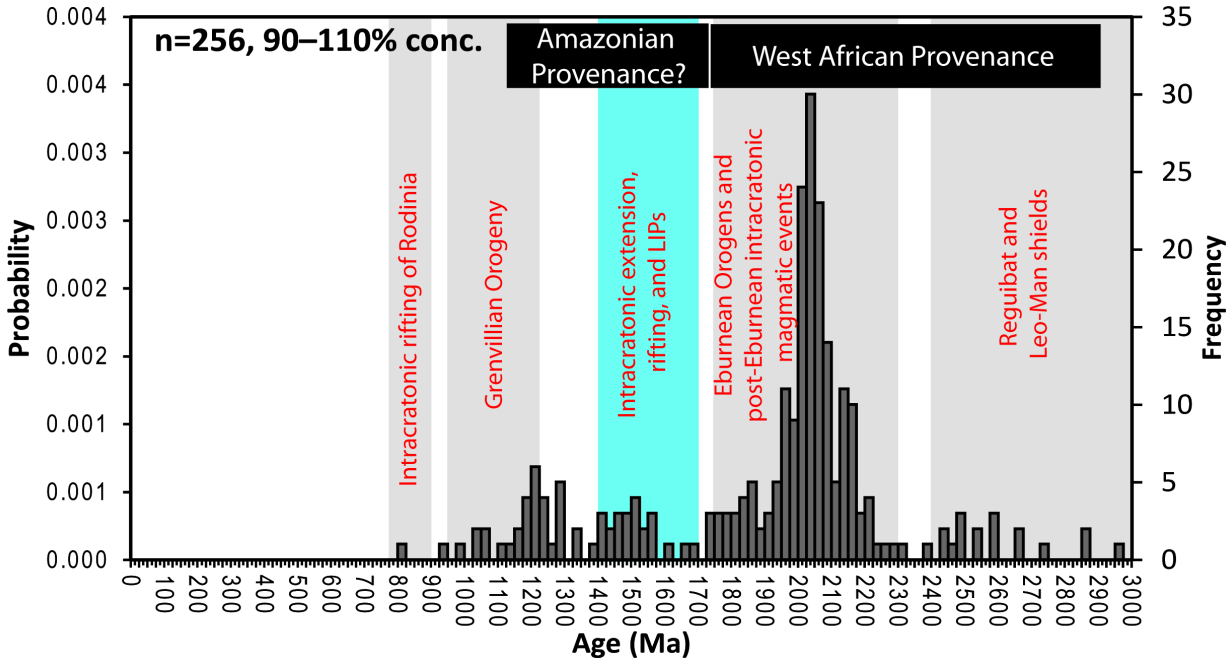

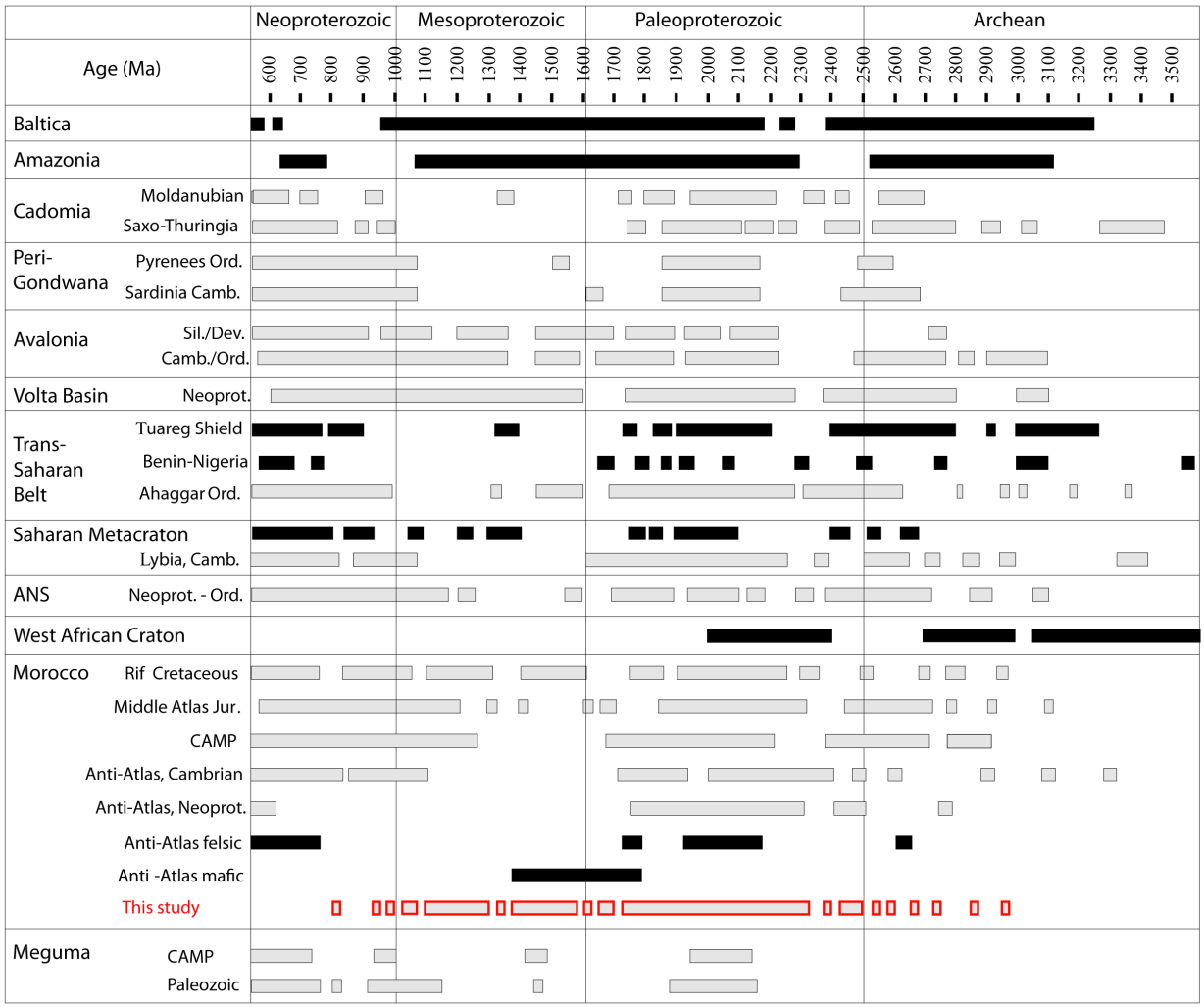
Neoproterozoic
Mesoproterozoic
Paleoproterozoic
Archean
Age (Ma)
600
700
800
900
1000
1100
1200
1300
1400
1500
1600
1700
1800
1900
2000
2100
2200
2300
2400
2500
2600
2700
2800
2900
3000
3100
3200
3300
3400
3500
Baltica
Amazonia
Cadomia
Moldanubian
Saxo-Thuringia
Peri-Gondwana
Pyrenees Ord.
Sardinia Camb.
Avalonia
Sil./Dev.
Camb./Ord.
Volta Basin
Neoprot.
Trans-Saharan Belt
Tuareg Shield
Benin-Nigeria
Ahaggar Ord.
Saharan Metacraton
Lybia, Camb.
ANS
Neoprot. - Ord.
West African Craton
Morocco
Rif Cretaceous
Middle Atlas Jur.
CAMP
Anti-Atlas, Cambrian
Anti-Atlas, Neoprot.
Anti-Atlas felsic
Anti -Atlas mafic
This study
Meguma
CAMP
Paleozoic

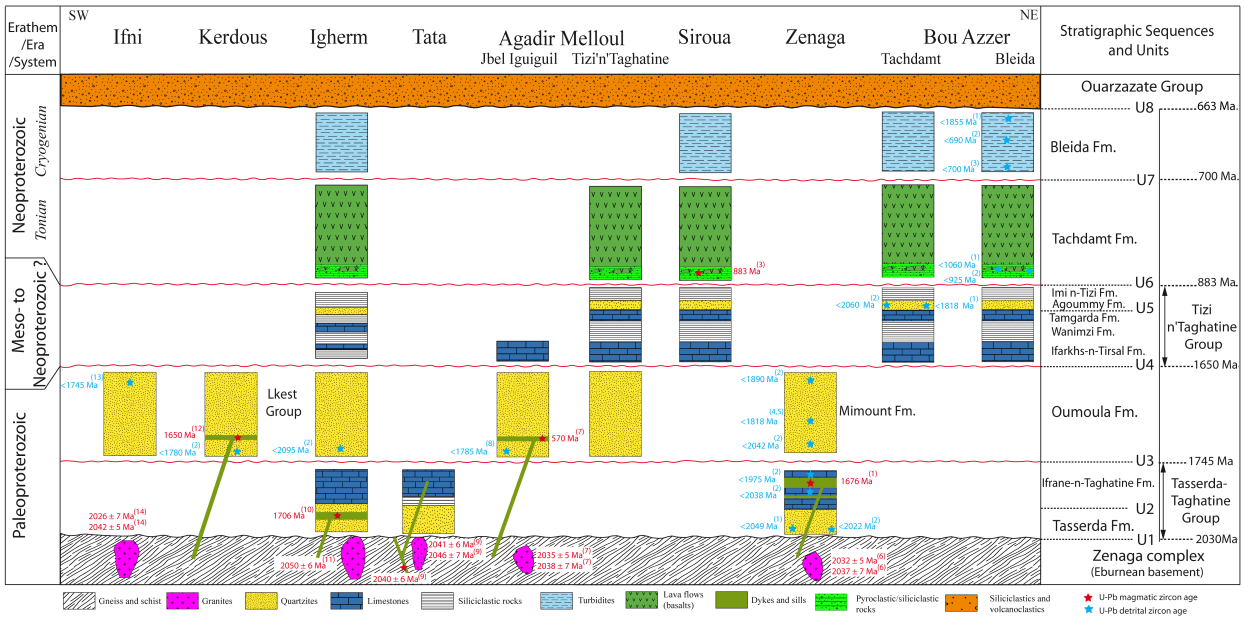

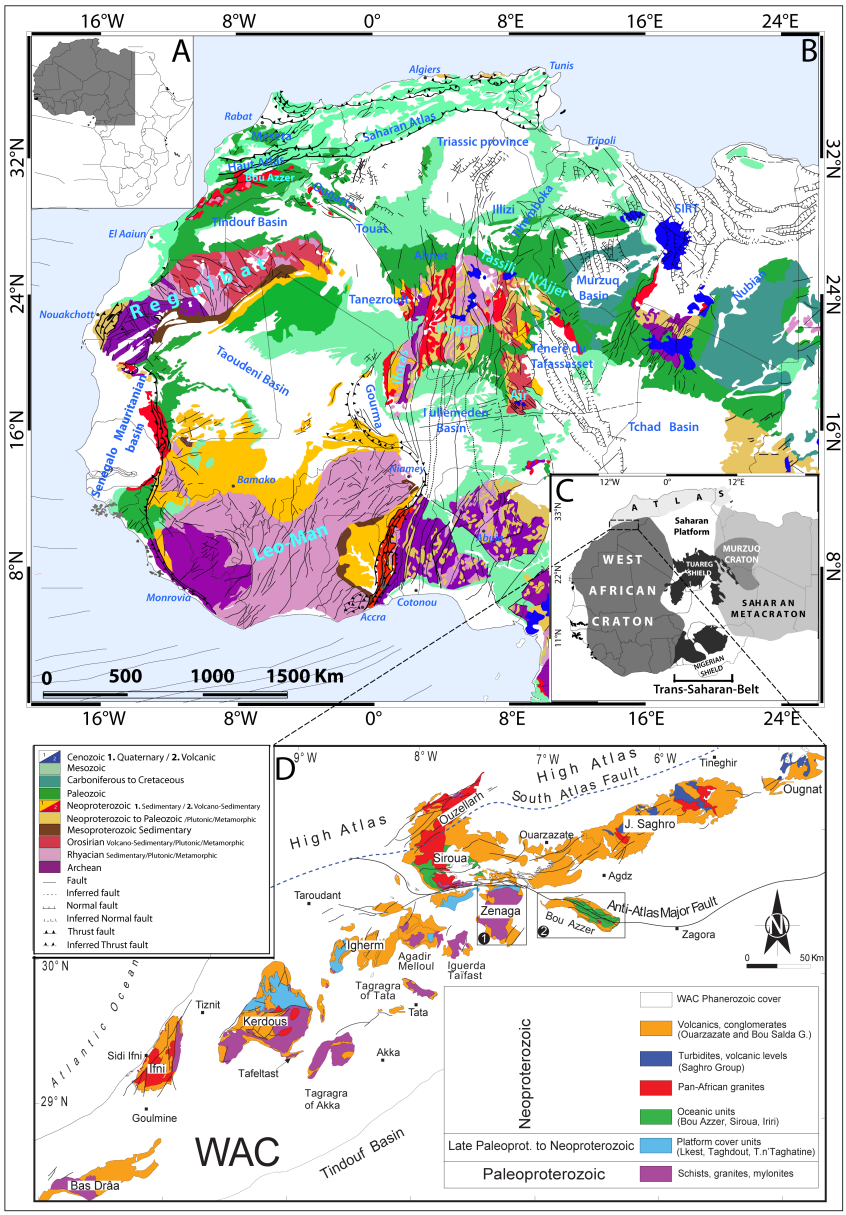
A
B
C
D
16°W
8°W
0°
8°E
16°E
24°E
32°N
24°N
16°N
8°N
33°N
16°N
8°N
Algiers
Tunis
Rabat
Tripoli
Saharan Atlas
Triassic province
Tindouf Basin
El Aaiun
Touat
Illizi
Murzuq Basin
SIRT
Nubia
Nouakchott
Tanezrouft
Taoudeni Basin
Tchad Basin
Bamako
Monrovia
Accra
Cotonou
Tamanrasset
Yafassasset
Senegalo Mauritanian basin
Volta basin
Iullemeden Basin
Gourma
Niamey
0 500 1000 1500 Km
Saharan Platform
WEST AFRICAN CRATON
TUAREG SHIELD
MURZUQ CRATON
SAHARAN METACRATON
NIGERIAN SHIELD
Trans-Saharan-Belt
Cenozoic 1. Quaternary / 2. Volcanic
Mesozoic
Carboniferous to Cretaceous
Paleozoic
Neoproterozoic 1. Sedimentary / 2. Volcano-Sedimentary
Neoproterozoic to Paleozoic /Plutonic/Metamorphic
Mesoproterozoic Sedimentary
Orosirian Volcano-Sedimentary/Plutonic/Metamorphic
Rhyacian Sedimentary/Plutonic/Metamorphic
Archean
Fault
Inferred fault
Normal fault
Inferred Normal fault
Thrust fault
Inferred Thrust fault
High Atlas
South Atlas Fault
Tineghir
Ougnat
J. Saghro
Ouarzazate
Agdz
Ouzellarn
Siroua
Taroudant
Zenaga
Bou Azzer
Anti-Atlas Major Fault
Zagora
Igherm
Agadir Melloul
Iguerda Taifast
Tagragra of Tata
Tata
Akka
Tagragra of Akka
Tafeltast
Kerdous
Tiznit
Sidi Ifni
Ifni
Goulmine
Bas Drâa
Atlantic Ocean
30° N
29° N
WAC
Tindouf Basin
0 50 Km
Neoproterozoic
WAC Phanerozoic cover
Volcanics, conglomerates (Ouarzazate and Bou Salda G.)
Turbidites, volcanic levels (Saghro Group)
Pan-African granites
Oceanic units (Bou Azzer, Siroua, Iriri)
Late Paleoprot. to Neoproterozoic
Platform cover units (Lkest, Taghdout, T.n'Taghatine)
Paleoproterozoic
Schists, granites, mylonites

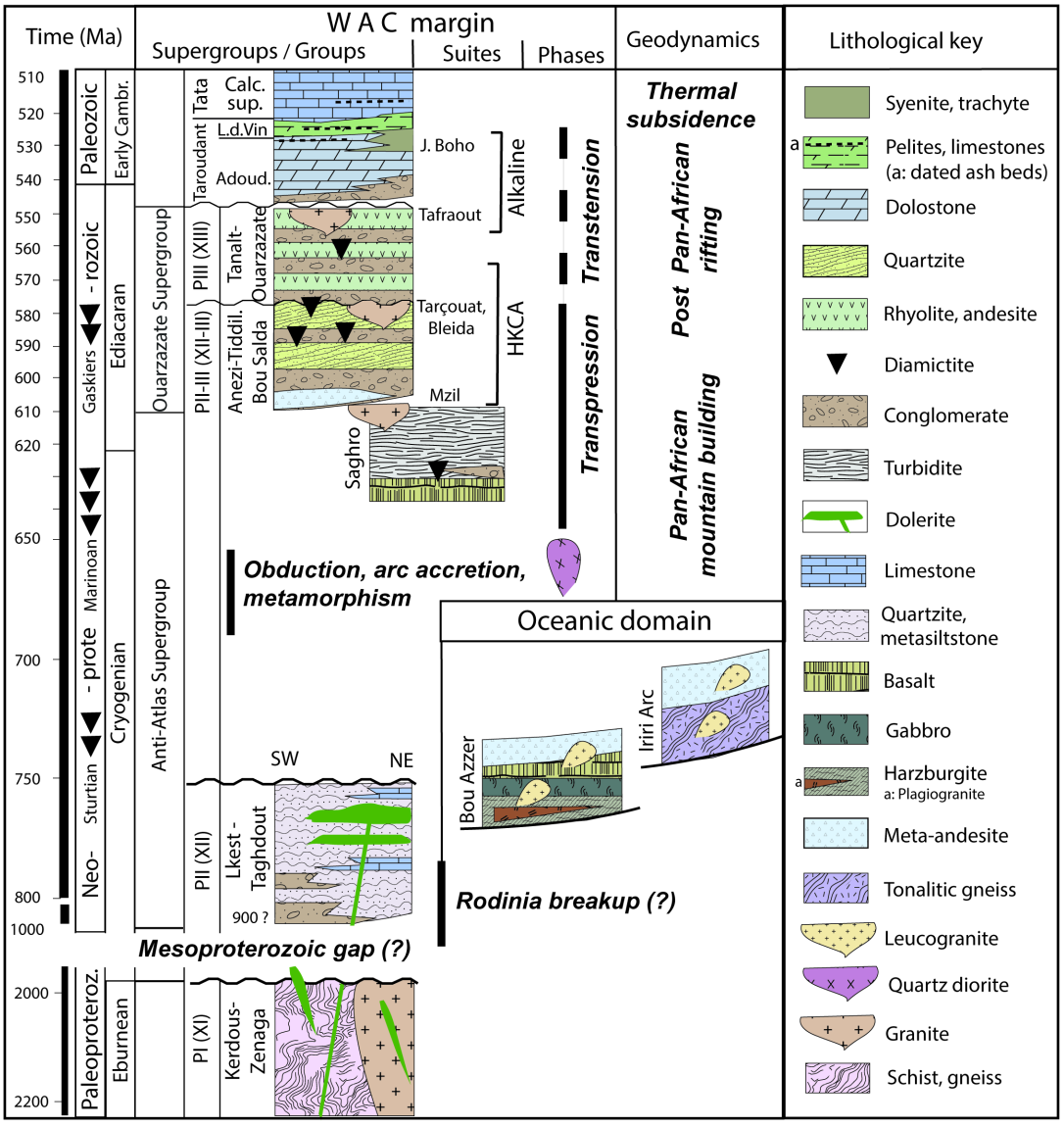
Time (Ma)
W A C margin
Supergroups / Groups
Suites
Phases
Geodynamics
Lithological key
Paleozoic
Early Cambr.
- rozoic
Ediacaran
Gaskiers
Marinoan
- prote
Cryogenian
Sturtian
Neo-
Paleoproteroz.
Eburnean
Ouarzazate Supergroup
Anti-Atlas Supergroup
Taroudant
Tata
Tanalt-Ouarzazate
Anezi-Tiddil.
Bou Salda
Lkest - Taghdout
Kerdous-Zenaga
PIII (XIII)
PII-III (XII-III)
PII (XII)
PI (XI)
Calc. sup.
L.d.Vin
Adoud.
J. Boho
Tafraout
Alkaline
Tarçouat, Bleida
HKCA
Mzil
Saghro
Obduction, arc accretion, metamorphism
Transpression
Transtension
Thermal subsidence
Post Pan-African rifting
Pan-African mountain building
Oceanic domain
Iriri Arc
Bou Azzer
SW
NE
900 ?
Rodinia breakup (?)
Mesoproterozoic gap (?)
Syenite, trachyte
Pelites, limestones (a: dated ash beds)
Dolostone
Quartzite
Rhyolite, andesite
Diamictite
Conglomerate
Turbidite
Dolerite
Limestone
Quartzite, metasiltstone
Basalt
Gabbro
Harzburgite
a: Plagiogranite
Meta-andesite
Tonalitic gneiss
Leucogranite
Quartz diorite
Granite
Schist, gneiss

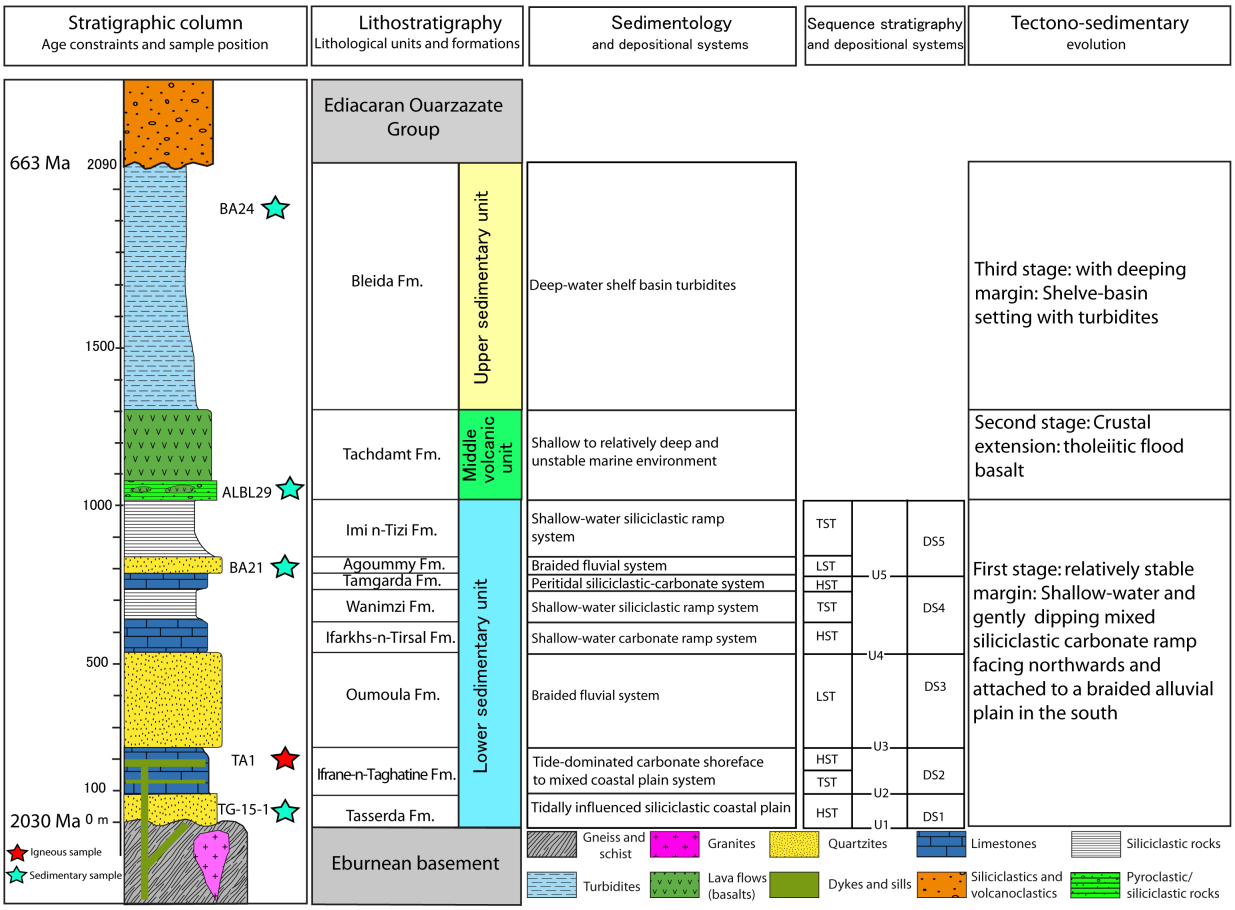

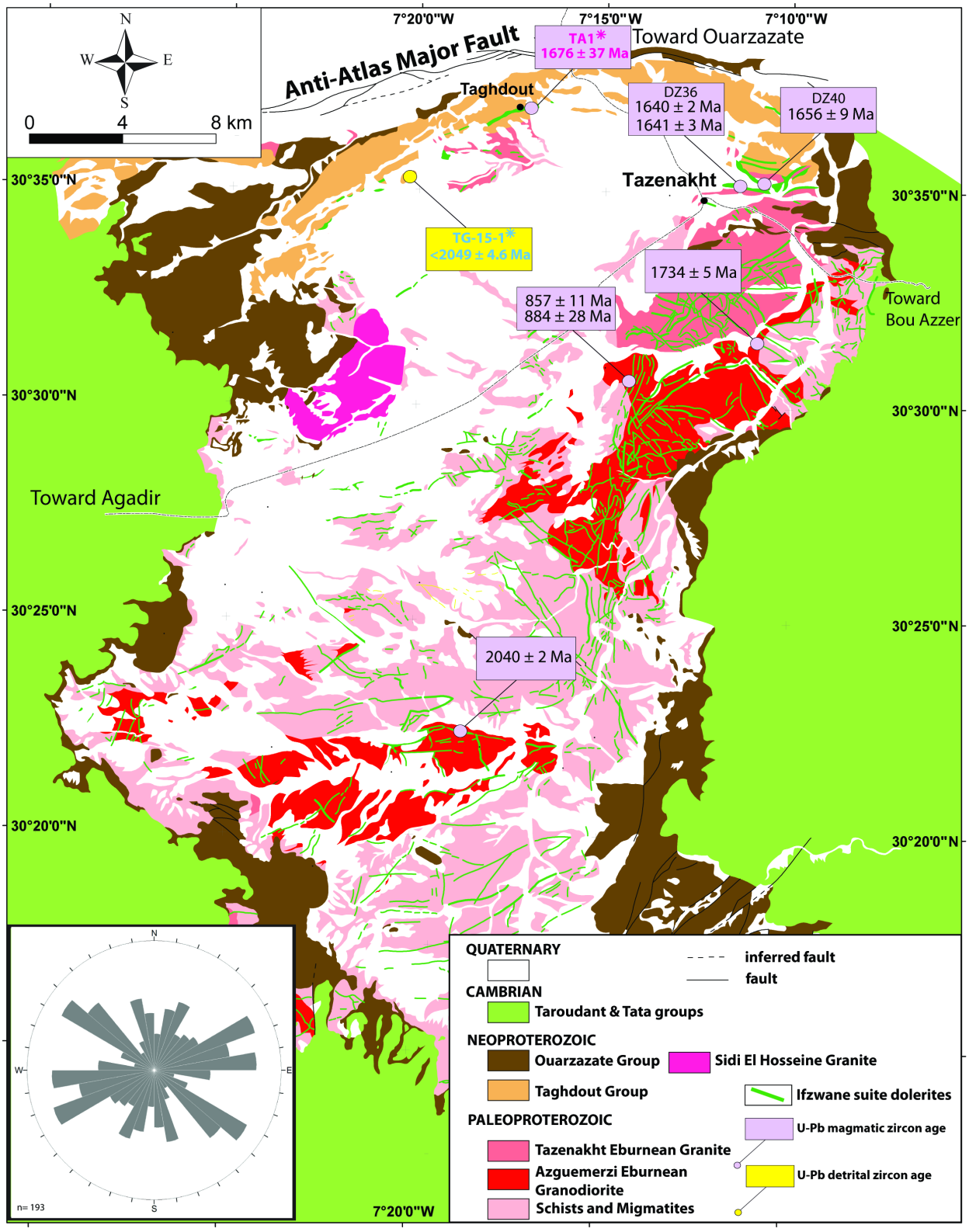
N
W
E
S
0
4
8 km
7°20'0"W
7°15'0"W
7°10'0"W
30°35'0"N
30°30'0"N
30°25'0"N
30°20'0"N
Anti-Atlas Major Fault
TA1*
1676 ± 37 Ma
Toward Ouarzazate
Taghdout
DZ36
1640 ± 2 Ma
1641 ± 3 Ma
DZ40
1656 ± 9 Ma
Tazenakht
TG-15-1*
<2049 ± 4.6 Ma
1734 ± 5 Ma
857 ± 11 Ma
884 ± 28 Ma
Toward
Bou Azzer
Toward Agadir
2040 ± 2 Ma
n= 193
QUATERNARY
CAMBRIAN
Taroudant & Tata groups
NEOPROTEROZOIC
Ouarzazate Group
Sidi El Hosseine Granite
Taghdout Group
Ifzwane suite dolerites
PALEOPROTEROZOIC
Tazenakht Eburnean Granite
Azguemerzi Eburnean Granodiorite
Schists and Migmatites
inferred fault
fault
U-Pb magmatic zircon age
U-Pb detrital zircon age

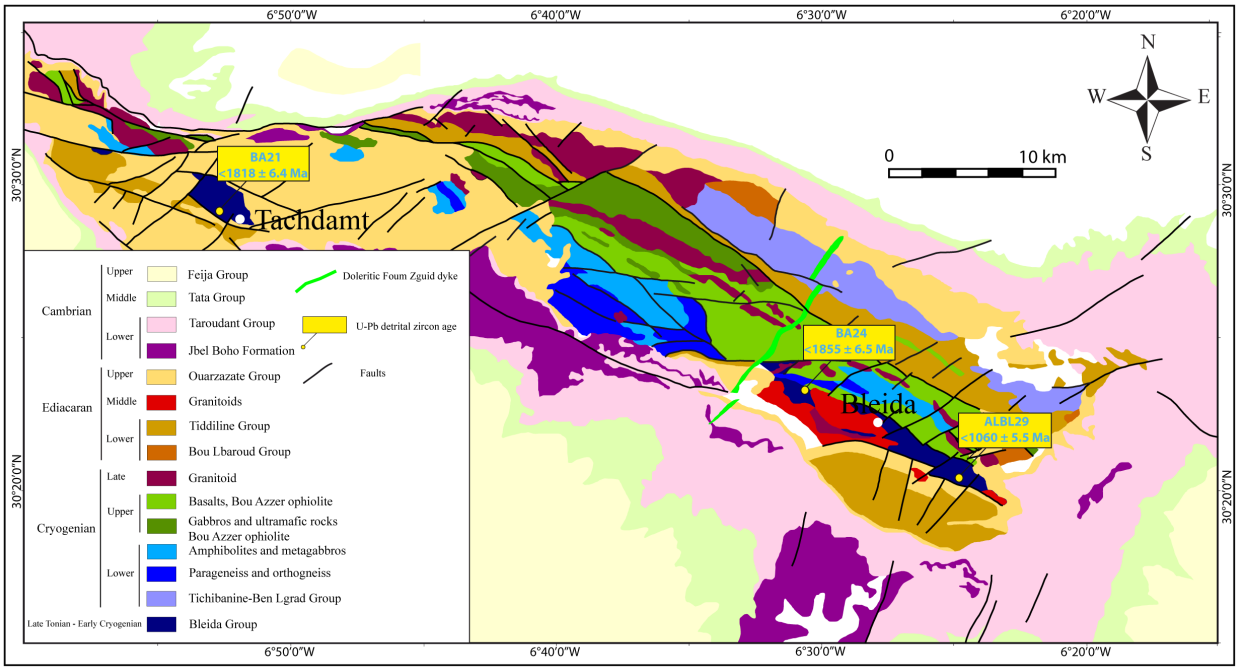

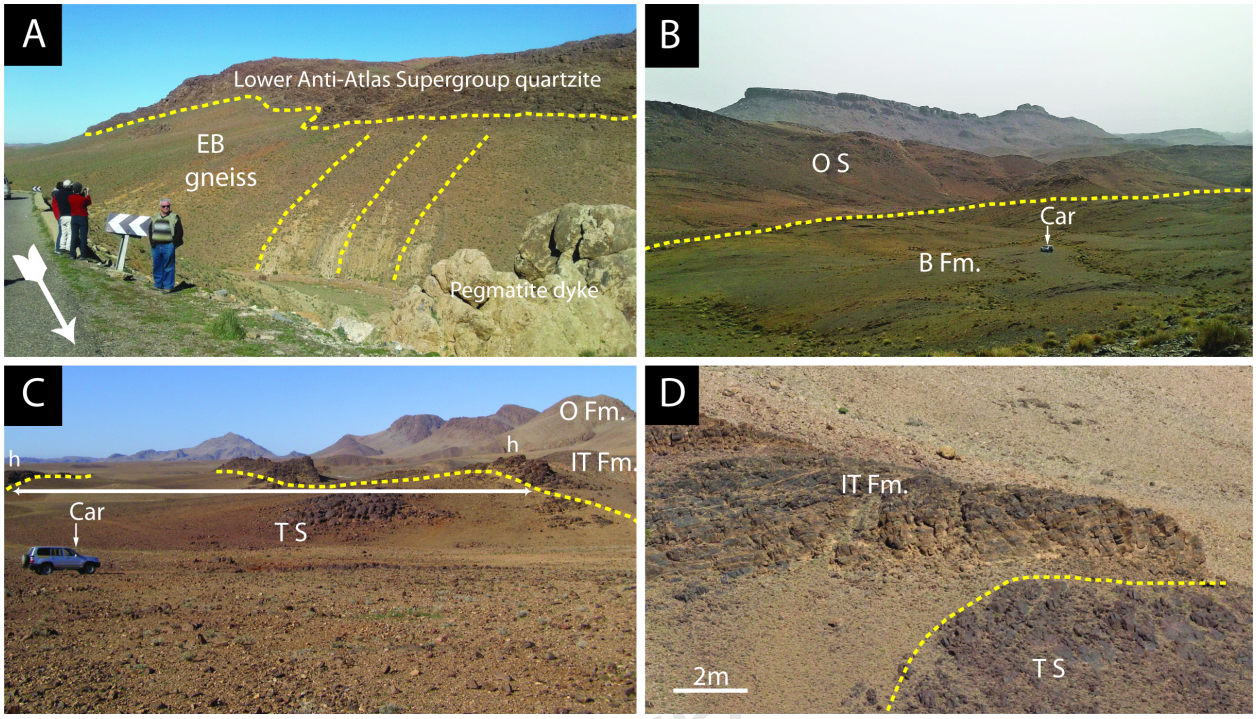
A
Lower Anti-Atlas Supergroup quartzite
EB
gneiss
Pegmatite dyke
B
O S
Car
B Fm.
C
O Fm.
h
h
IT Fm.
Car
T S
D
IT Fm.
2m
T S

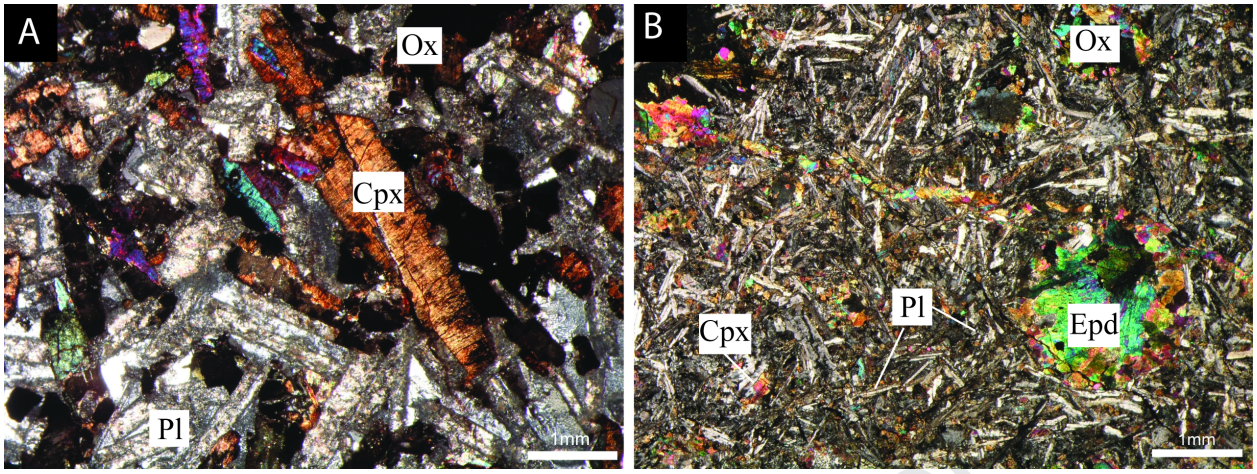

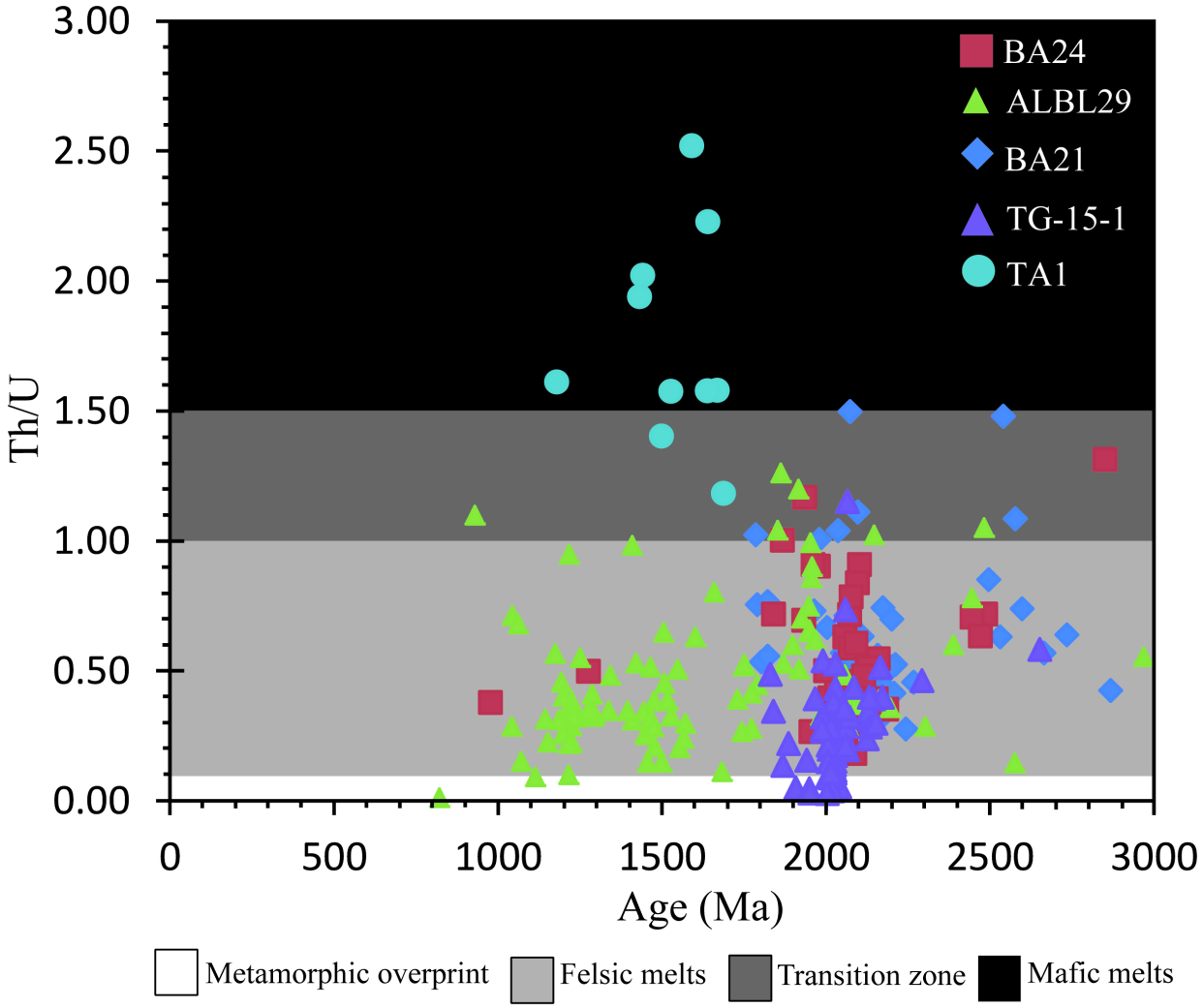
3.00
2.50
2.00
1.50
1.00
0.50
0.00
Th/U
0
500
1000
1500
2000
2500
3000
Age (Ma)
BA24
ALBL29
BA21
TG-15-1
TA1
Metamorphic overprint
Felsic melts
Transition zone
Mafic melts

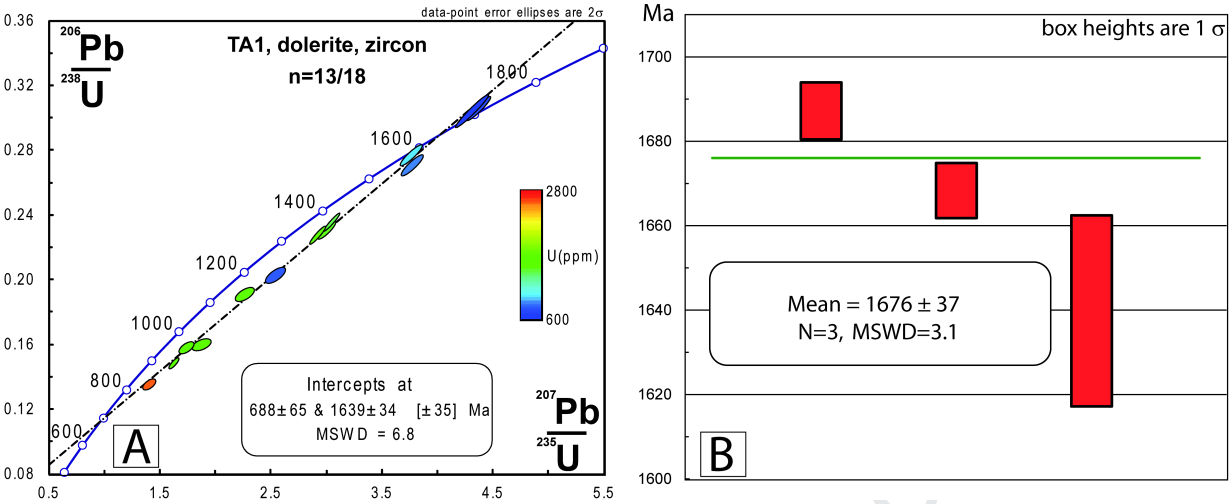

Highlights

►The Taghdout mafic sill of the Ifzwane Suite yielded an age of 1676 ± 37 Ma

►The maximum depositional age of the lower Anti-Atlas Supergroup ranges from 2049 Ma (bottom) to 700 Ma (top) and the provenance is mainly from the WAC

►A new 5-part lithostratigraphic framework for the Proterozoic lower Anti-Atlas Supergroup of the Anti-Atlas Belt is proposed

►The 1650-1640 Ma Zenaga and 885-883 Ma Iguerda-Taïfast LIPs provide important stratigraphic constraints

► Correlation between the lower Anti-Atlas Supergroup and the Taoudeni Basin succession in Mauritania

Declaration of interests

☒ The authors declare that they have no known competing financial interests or personal relationships that could have appeared to influence the work reported in this paper.

☐The authors declare the following financial interests/personal relationships which may be considered as potential competing interests: